



National Library
of Canada

Bibliothèque nationale
du Canada

Canadian Theses Service

Services des thèses canadiennes

Ottawa, Canada
K1A 0N4

CANADIAN THESES

THÈSES CANADIENNES

NOTICE

The quality of this microfiche is heavily dependent upon the quality of the original thesis submitted for microfilming. Every effort has been made to ensure the highest quality of reproduction possible.

If pages are missing, contact the university which granted the degree.

Some pages may have indistinct print especially if the original pages were typed with a poor typewriter ribbon or if the university sent us an inferior photocopy.

Previously copyrighted materials (journal articles, published tests, etc.) are not filmed.

Reproduction in full or in part of this film is governed by the Canadian Copyright Act, R.S.C. 1970, c. C-30.

**THIS DISSERTATION
HAS BEEN MICROFILMED
EXACTLY AS RECEIVED**

AVIS

La qualité de cette microfiche dépend grandement de la qualité de la thèse soumise au microfilmage. Nous avons tout fait pour assurer une qualité supérieure de reproduction.

S'il manque des pages, veuillez communiquer avec l'université qui a conféré le grade.

La qualité d'impression de certaines pages peut laisser à désirer, surtout si les pages originales ont été dactylographiées à l'aide d'un ruban usé ou si l'université nous a fait parvenir une photocopie de qualité inférieure.

Les documents qui font déjà l'objet d'un droit d'auteur (articles de revue, examens publiés, etc.) ne sont pas microfilmés.

La reproduction, même partielle, de ce microfilm est soumise à la Loi canadienne sur le droit d'auteur, SRC 1970, c. C-30.

**LA THÈSE A ÉTÉ
MICROFILMÉE TELLE QUE
NOUS L'AVONS REÇUE**

THE UNIVERSITY OF ALBERTA

RADIOFREQUENCY HEATING OF LOW-CONDUCTIVITY MATERIALS WITH A
SEMI-CYLINDRICAL SOLENOID

by

DAVID CHARLES ELLINGER

(C)

A THESIS

SUBMITTED TO THE FACULTY OF GRADUATE STUDIES AND RESEARCH
IN PARTIAL FULFILMENT OF THE REQUIREMENTS FOR THE DEGREE
OF MASTER OF SCIENCE

DEPARTMENT OF ELECTRICAL ENGINEERING

EDMONTON, ALBERTA

SPRING 1987

Permission has been granted to the National Library of Canada to microfilm this thesis and to lend or sell copies of the film.

The author (copyright owner) has reserved other publication rights, and neither the thesis nor extensive extracts from it may be printed or otherwise reproduced without his/her written permission.

L'autorisation a été accordée à la Bibliothèque nationale du Canada de microfilmer cette thèse et de prêter ou de vendre des exemplaires du film.

L'auteur (titulaire du droit d'auteur) se réserve les autres droits de publication; ni la thèse ni de longs extraits de celle-ci ne doivent être imprimés ou autrement reproduits sans son autorisation écrite.

ISBN 0-315-37738-0

THE UNIVERSITY OF ALBERTA

RELEASE FORM

NAME OF AUTHOR DAVID CHARLES ELLINGER
TITLE OF THESIS RADIOFREQUENCY HEATING OF
LOW-CONDUCTIVITY MATERIALS WITH A
SEMI-CYLINDRICAL SOLENOID
DEGREE FOR WHICH THESIS WAS PRESENTED MASTER OF SCIENCE
YEAR THIS DEGREE GRANTED SPRING 1987

Permission is hereby granted to THE UNIVERSITY OF ALBERTA LIBRARY to reproduce single copies of this thesis and to lend or sell such copies for private, scholarly or scientific research purposes only.

The author reserves other publication rights, and neither the thesis nor extensive extracts from it may be printed or otherwise reproduced without the author's written permission.

(SIGNED) *D. Ellinger*

PERMANENT ADDRESS:

#107...10635-83 AVENUE
EDMONTON...ALBERTA
T6E 2E3

DATED NOVEMBER 22, 1986

THE UNIVERSITY OF ALBERTA
FACULTY OF GRADUATE STUDIES AND RESEARCH

The undersigned certify that they have read, and recommend to the Faculty of Graduate Studies and Research, for acceptance, a thesis entitled RADIOFREQUENCY HEATING OF LOW-CONDUCTIVITY MATERIALS WITH A SEMI-CYLINDRICAL SOLENOID submitted by DAVID CHARLES ELLINGER in partial fulfilment of the requirements for the degree of MASTER OF SCIENCE in ELECTRICAL ENGINEERING.

.....*F.H. Korms*.....
Supervisor

.....*M. D.*.....
Supervisor

.....*D. G. Hughes*.....
.....*J. J. Wandulak*.....
.....

Date.....November.....14.....1986.....

Abstract

The finite-length solenoidal coil has shown considerable promise as an applicator for electromagnetic heating at radio frequencies. The geometry of the device limits its use to rather specialized situations, however, because it requires that the target material be placed in the interior of the solenoid. The properties of a semi-cylindrical solenoid, having a semicircular cross-section, are studied. Here the material to be heated lies outside the coil and adjacent to its flat side. This device places no restrictions upon the physical dimensions of the object to be heated.

In the configuration studied, the coil is insulated from the adjacent material by a thin dielectric. The effects of balanced versus unbalanced coil excitation on the heating distribution generated are investigated at various frequencies, both above and below self-resonance. The coupling efficiency of the coil as a function of the conductivity of the adjacent material is examined for four modes of operation. An equivalent circuit model developed by previous researchers is examined. Two nonperturbing dipole probes are designed and constructed. The electric field distribution generated by the coil within the adjacent material is measured for four modes of operation.

Conclusions are drawn regarding the applicability of the coil to radio-frequency heating of biological and earth-type materials.

Acknowledgements

I would like to express my sincere appreciation to the following:

Professors F.S. Chute and F.E. Vermeulen of the Department of Electrical Engineering, University of Alberta, for introducing me to this topic and providing support, advice, and encouragement.

Jim Fearn, Research technician in the Applied Electromagnetics Laboratory, Department of Electrical Engineering, University of Alberta, for his valuable advice and assistance with the experimental work.

Professor J.A. Plambeck of the Department of Chemistry, University of Alberta, for helpful discussions on the measurement of the conductivity of electrolytes.

Dr. R.G. McPherson and Dr. A.D. Hiebert, for many helpful suggestions regarding all aspects of the project.

My family and friends, for their support and encouragement.

The Natural Sciences and Engineering Research Council of Canada and the Government of the Province of Alberta for their financial support.

Table of Contents

Chapter	Page
Abstract	iv
Acknowledgements	v
List of Tables	ix
List of Figures	xi
List of Plates	xiv
List of Symbols and Abbreviations	xv
1. Introduction and Review of Literature	1
1.1 Electromagnetic Heating	1
1.2 Radiofrequency Heating with Solenoidal Coils	3
1.3 The Semi-Cylindrical Solenoid	4
1.4 Related Research	6
1.5 Discussion of Chapters and Appendices that Follow	11
2. Coil Excitation	13
2.1 Current Distribution on Solenoidal Coils	13
2.2 Demonstration of Heating Patterns	17
2.2.1 Procedure	17
2.2.2 Results	21
2.2.3 Discussion	24
3. Efficiency	30
3.1 Measurement of Input Resistance	30
3.1.1 Procedure	31
3.1.2 Results	35
3.1.3 Discussion	40
3.2 Estimation of Efficiency	40
3.3 Equivalent Circuit Models	43

3.3.1	Low Frequency Case	45
3.3.2	Self-Resonant Cases	50
4.	Distribution of Heating	51
4.1	Electric Field Distributions	51
4.1.1	Procedure	52
4.1.2	Results	53
4.1.3	Discussion	53
4.2	Conservative Electric Field Vector	66
4.3	Power Dissipation	67
5.	Summary	77
5.1	Review	77
5.2	Conclusions	78
5.3	Further Research	81
	Bibliography	82
	Appendix A: Loss Mechanisms	86
A.1	Energy Dissipation in an Electromagnetic Field ...	86
A.2	Loss Mechanisms in Aqueous Sodium Chloride	87
A.2.1	Joule Heating	87
A.2.2	Dielectric Losses	88
	Appendix B: Theory and Design of an Electric Field Probe .	94
B.1	Theory of the Dipole Probe	94
B.1.1	The Cylindrical Dipole	94
B.1.2	Detection	96
B.1.3	Transmission	99
B.1.4	Modulation	100
B.2	Design and Construction of the Dipole Probe	101
B.2.1	Transmission Line	103
B.2.2	Dipole and Detector	104

B.2.3 Instrumentation 107
B.2.4 Testing 108
Appendix C: Tabulated Data 112

List of Tables

Table		page
A.1	Dielectric Properties of Water	91
C.1	Input Resistance and Resonant Frequency of the Semi-Cylindrical Solenoid versus Target Material Conductivity: Low-Frequency Case.....	112
C.2	Input Conductance and Resonant Frequency of the Semi-Cylindrical Solenoid versus Target Material Conductivity: One-Half Wavelength Self-Resonant Case	114
C.3	Input Conductance and Resonant Frequency of the Semi-Cylindrical Solenoid versus Target Material Conductivity: One Wavelength Self-Resonant Case ..	115
C.4	Input Resistance and Resonant Frequency of the Semi-Cylindrical Solenoid versus Target Material Conductivity: Two Wavelength Self-Resonant Case ..	116
C.5(a)	Electric Field Strength: 1.0 MHz, X-component....	118
C.5(b)	Electric Field Strength: 1.0 MHz, Y-component....	119
C.5(c)	Electric Field Strength: 1.0 MHz, Z-component....	120
C.6(a)	Electric Field Strength: 6.3 MHz, X-component....	121
C.6(b)	Electric Field Strength: 6.3 MHz, Y-component....	122
C.6(c)	Electric Field Strength: 6.3 MHz, Z-component....	123
C.7(a)	Electric Field Strength: 12.8 MHz, X-component...	124
C.7(b)	Electric Field Strength: 12.8 MHz, Y-component...	125

C.7(c) Electric Field Strength: 12.8 MHz, Z-component...126

C.8(a) Electric Field Strength: 27.3 MHz, X-component...127

C.8(b) Electric Field Strength: 27.3 MHz, Y-component...128

C.8(c) Electric Field Strength: 27.3 MHz, Z-component...129

List of Figures

Figure		page
1.1	Positioning of the Coil and Definition of Coordinate System.....	6
2.1	Distributions of Current and Potential on an Infinite Solenoid.....	16
2.2	Balancing and Matching Network	20
2.3	Ideal Distributions of Current and Potential on a Finite Solenoid.....	28
3.1	Conductivity Measurement Cell	32
3.2	Input Resistance and Resonant Frequency of the Semi-Cylindrical Solenoid: Balanced Low-Frequency Case	36
3.3	Input Resistance and Resonant Frequency of the Semi-Cylindrical Solenoid: : One-Half Wavelength Balanced Self-Resonant Case.....	37
3.4	Input Resistance and Resonant Frequency of the Semi-Cylindrical Solenoid: One Wavelength Balanced Self-Resonant Case.....	38
3.5	Input Resistance and Resonant Frequency of the Semi-Cylindrical Solenoid: Two Wavelength Balanced Self-Resonant Case.....	39
3.6	Heating Efficiency of the Semi-Cylindrical Solenoid: Four Cases.....	44
3.7	Low-Frequency Equivalent Circuit	46
3.8	Low-Frequency Equivalent Circuit Component Values versus Target Material Conductivity	48

4.1	Relative Electric Field Strength: 1.0 MHz, X-component.....	54
4.2	Relative Electric Field Strength: 1.0 MHz, Y-component.....	55
4.3	Relative Electric Field Strength: 1.0 MHz, Z-component.....	56
4.4	Relative Electric Field Strength: 6.3 MHz, X-component.....	57
4.5	Relative Electric Field Strength: 6.3 MHz, Y-component.....	58
4.6	Relative Electric Field Strength: 6.3 MHz, Z-component.....	59
4.7	Relative Electric Field Strength: 12.8 MHz, X-component.....	60
4.8	Relative Electric Field Strength: 12.8 MHz, Y-component.....	61
4.9	Relative Electric Field Strength: 12.8 MHz, Z-component.....	62
4.10	Relative Electric Field Strength: 27.3 MHz, X-component.....	63
4.11	Relative Electric Field Strength: 27.3 MHz, Y-component.....	64
4.12	Relative Electric Field Strength: 27.3 MHz, Z-component.....	65
4.13	Conservative Electric Field: 1.0 MHz.....	68
4.14	Conservative Electric Field: 6.3 MHz.....	69
4.15	Conservative Electric Field: 12.8 MHz.....	70

4.16	Conservative Electric Field: 27.3 MHz.....	71
4.17	Relative Power Dissipation: 1.0 MHz.....	72
4.18	Relative Power Dissipation: 6.3 MHz.....	73
4.19	Relative Power Dissipation: 12.8 MHz.....	74
4.20	Relative Power Dissipation: 27.3 MHz.....	75
5.1	Balancing and Matching Network	80
A.1	Dielectric Properties of Aqueous NaCl at 25°C.....	93
B.1	Bare and Insulated Dipoles	95
B.2	Equivalent Circuit of a Detector Diode.....	98
B.3	Resistive Transmission Line	103
B.4	Lowpass Filter.....	105
B.5	Equivalent Circuit of a Probe	106
B.6	Buffer Circuit Schematic	109

List of Plates

Plate		page
1.1	The Semi-Cylindrical Solenoidal Coil.....	5
2.1	Heating Pattern Generated at 1 MHz by Balanced Excitation.....	21
2.2	Heating Pattern Generated at 10 MHz by Balanced Excitation.....	22
2.3	Heating Pattern Generated at 35.1 MHz by Balanced Excitation.....	22
2.4	Heating Pattern Generated at 1 MHz by Unbalanced Excitation.....	23
2.5	Heating Pattern Generated at 10 MHz by Unbalanced Excitation.....	23
2.6	Heating Pattern Generated at 35.1 MHz by Unbalanced Excitation.....	24
B.1	Completed Probes	102

List of Symbols and Abbreviations

a	dipole radius
AWG	american wire guage
b	radius of insulating sheath
B	magnetic flux density vector
BALUN	balanced to unbalanced transformer
c	distributed shunt capacitance of resistive transmission line
C	capacitance
C_c	equivalent capacitance of the insulating gap between the coil and the target material
C_e	capacitance representing the energy stored in the nonconservative electric field of the coil
C_j	junction capacitance of detector diode
C_{LP}	lowpass network capacitance
C_s	coaxial capacitance of insulating sheath
C_2	capacitance representing the energy stored in the conservative electric field of the coil
d	inside diameter of test cell
ds, dv	surface element vector, volume element

D	electric flux density vector
E	activation energy
$E, E(r), E(r,t)$	electric field vector
E^*	complex conjugate of E
E_x, E_y, E_z	x, y, and z components of E
f	cyclic frequency
f_c	cutoff frequency of probe
$f(V)$	detector diode V-I characteristic
G	conductance
G_{IN}	measured value of coil input conductance
h	dipole height
h_e	effective height of dipole
h_i	height of insulating sheath
H	magnetic field vector
H^*	complex conjugate of H
I, I_c, I_d	current, conduction current, displacement current
I_{sc}	short-circuit current
ISM	Industrial, Scientific, and Medical

J	current density vector
JFET	junction field-effect transistor
k	Boltzmann's constant
k_e, k_z	proportionality constants for R_e, R_z
$k_0(\omega)$	wave number of resistive transmission line
l'	dimension of test cell
L	length of the coil winding
L_0	inductance representing the energy stored in the magnetic field of the coil
O.D.	outside diameter
P, P_{IND}, P_0	electric polarization vector, induced component, orientational component
\bar{P}	time-average power
\bar{P}_d	time-average power absorbed by detector diode
PTFE	polytetrafluoroethylene (Teflon)
PVC	polyvinylchloride
Q	quality factor
r'	distributed series resistance of resistive transmission line
R_a, R_a^m	equivalent circuit component, its minimum value

R_{oe}	parallel combination of R_a and R_e
R_e	resistance representing energy dissipated by the nonconservative electric field of the coil
R_{IN}	measured value of coil input resistance
R_j	junction resistance of detector diode
R_{LP}	resistance of lowpass network
R_s	series resistance of diode semiconductor material
R_v	diode video resistance
R_w	resistance representing ohmic losses in the coil winding
R_z	resistance representing energy dissipated by the conservative electric field of the coil
RF	radiofrequency
s	length of resistive transmission line
SWR	standing-wave ratio
t	time
T	temperature
V	potential
V_{cc} , V_{ee}	d.c. supply voltages
V_{LF}	low-frequency voltage

V_m	voltage generated at input of measuring instrument
V_{oc}	open-circuit voltage
X_c, X_z	reactances of C_c and C_z
Y	detector admittance
Y_{bare}, Y_d, Y_{ins}	dipole admittances
Z_m	input impedance of measuring instrument
α	attenuation constant
β	phase constant
β_d	diode current sensitivity
γ_d	diode voltage sensitivity
$\delta i, \delta v$	increments of current and voltage
$\epsilon, \epsilon', \epsilon''$	permittivity, real part, imaginary part
ϵ_0	free space permittivity
ϵ_i	permittivity of insulating sheath
$\epsilon_s, \epsilon_\infty$	static permittivity, high frequency permittivity
$\bar{\epsilon}$	real effective permittivity
ϵ_w	permittivity of pure water
η	charge carrier density

$\eta_{LF}(\hat{\sigma})$, $\eta_{\lambda/2}(\hat{\sigma})$, heating efficiency of the coil in the low-frequency case, one-half wavelength case, and two wavelength case
 $\eta_{2\lambda}(\hat{\sigma})$

κ modulation level ($0 \leq \kappa \leq 1$)

λ wavelength

μ , μ' , μ'' permeability, real part, imaginary part

ξ charge per charge carrier

σ , σ' , σ'' conductivity, real part, imaginary part

$\hat{\sigma}$, $\hat{\sigma}^m$ real effective conductivity, value of $\hat{\sigma}$ at which R_0 reaches R_0^m

σ_{LF} low-frequency conductivity

τ , τ_0 dipole relaxation time

τ_v dipole relaxation time of pure water

v charge carrier mobility

ω angular frequency

ω_0 , ω_c , ω_m carrier frequency, cutoff frequency, modulation frequency

Chapter 1

Introduction and Review of Literature

In this chapter, electromagnetic heating is discussed and the subject matter is introduced. Relevant work conducted by previous researchers is reviewed, and the contents of the thesis are outlined.

1.1 Electromagnetic Heating

The industrial use of electrical heating has grown steadily since the turn of the century. The variety of techniques presently in use is extremely diverse, and includes direct and indirect resistance heating, electric arc and plasma heating, and electromagnetic heating.

Electromagnetic heating involves exposing the target material (the material to be heated) to a time-varying electromagnetic field. In homogeneous nonmagnetic materials, two heating mechanisms are significant. These are: Joule heating, due to resistive losses generated by currents induced in materials with nonzero d.c. conductivity; and dielectric heating, due to high-frequency relaxation phenomena in materials containing polar molecules. In heterogeneous substances, most notably biological tissues, the effects of interfacial (Maxwell-Wagner) polarization may also contribute to dielectric heating. Interfacial polarization is caused by the buildup of charge carriers at the interfaces between constituent materials.

At low frequencies (below approximately 100 MHz), where the dimensions of the system are much less than a wavelength, the target material is placed within the near-fields of the applicator. This has traditionally been referred to as induction heating.

Induction heating was first developed to heat metals at powerline frequencies by Faraday induction: The material to be heated is submerged in a time-varying magnetic field, which causes "eddy" currents to flow and heat to be generated. By this method metallic components are heated quickly, uniformly, and efficiently. Applications include melting, through-heating, soldering, brazing, and welding. At higher frequencies the currents induced are confined to flow near the surface of the object. This allows metallic components to be surface-hardened. Increased operating frequencies also make it possible to efficiently heat materials of lower conductivity. Applications include the processing of semiconductor materials, welding of plastics, acceleration of setting times for glues and adhesives, drying of wood, paper, and textile products, and the therapeutic heating of biological tissues (Hulls 1982, Sterzer *et al* 1980).

At still higher frequencies (above approximately 1000 MHz), where the dimensions of the system are comparable to a wavelength, an electromagnetic field is radiated from an antenna and propagates through free space to the target material. This technique is commonly referred to as microwave heating.

Microwave heating is generally used to heat substances containing polar molecules, in which the dominant loss mechanism is dielectric relaxation¹. It is not particularly effective for heating metals and other good conductors, because most of the incident power is reflected from the surface of these materials. Presently, the largest use of microwave heating is for domestic and commercial food preparation. Industrial applications include the acceleration of setting times for glues and adhesives, drying lumber, and moisture levelling in food, paper, and textile products (Cheremisinoff *et al* 1985, Metaxas and Meredith 1983). Microwave heating is also used for therapeutic heating of biological tissues (Sterzer *et al* 1980).

1.2 Radiofrequency Heating with Solenoidal Coils

The solenoidal coil will induce heating when the material to be heated is placed in the interior of the excited coil. The time-varying axial magnetic field in this region generates a non-conservative² circumferential electric field. A conservative axial electric field is also generated, which is larger than the circumferential electric field by a factor equal to the cotangent of the pitch angle of the solenoid (Chute, Vermeulen, and Cervenak 1981, pp. 21). Both of these field components can cause Joule heating and

¹ While interfacial polarization may be present, it is usually most significant at lower frequencies.

² A conservative electric field is one that satisfies the relation $\oint \mathbf{E} \cdot d\mathbf{l} = 0$.

dielectric heating. The relative contributions of these mechanisms depend on the frequency and the properties of the material being heated.

If an insulating gap separates the coil and target material (or if the coil winding is electrically insulated), then the axial electric field must twice 'jump' the gap between the target material and the turns of the coil. At low frequencies the voltage across this capacitive gap is large, and the axial electric field is accordingly small. Eddy currents, induced by the non-conservative circumferential electric field, are thus the dominant source of heating at low frequencies. At higher frequencies the impedance of the gap can be made small, so that both electric field components produce significant heating.

1.3 The Semi-Cylindrical Solenoid

An important limitation of the solenoidal coil applicator is that the target material must be placed in its interior. In clinical hyperthermia applications this has limited the use of the device to the treatment of limbs. Other potential applications, such as thawing frozen soil, are not possible. The purpose of this thesis is to study the feasibility of radiofrequency heating of low conductivity materials with a semi-cylindrical solenoid, having a semicircular cross-section. The material to be heated would be placed outside the coil and adjacent to its flat side. This device would place no restrictions on the physical dimensions of

the target material.

The coil used for this investigation is 40 cm long, 10.5 cm in diameter, and consists of twenty turns of 6.35 mm (0.250 in) diameter annealed copper tubing wound on PVC pipe² (plate 1.1). No significant attempt has been made to optimize these dimensions. The coil was flush-mounted, flat side up, in the bottom of a wooden box having inside length, width, and depth of 60 cm, 40 cm, and 20 cm, respectively (figure 1.1). The box is filled with saline solution (the target material) whose conductivity is varied by adjusting the sodium chloride concentration. A thin dielectric was

²The coil was wound on a 40 cm long piece of 4 inch PVC schedule 40 pipe which had been split lengthwise after a helical groove with a 2 cm pitch was cut in its outer surface.

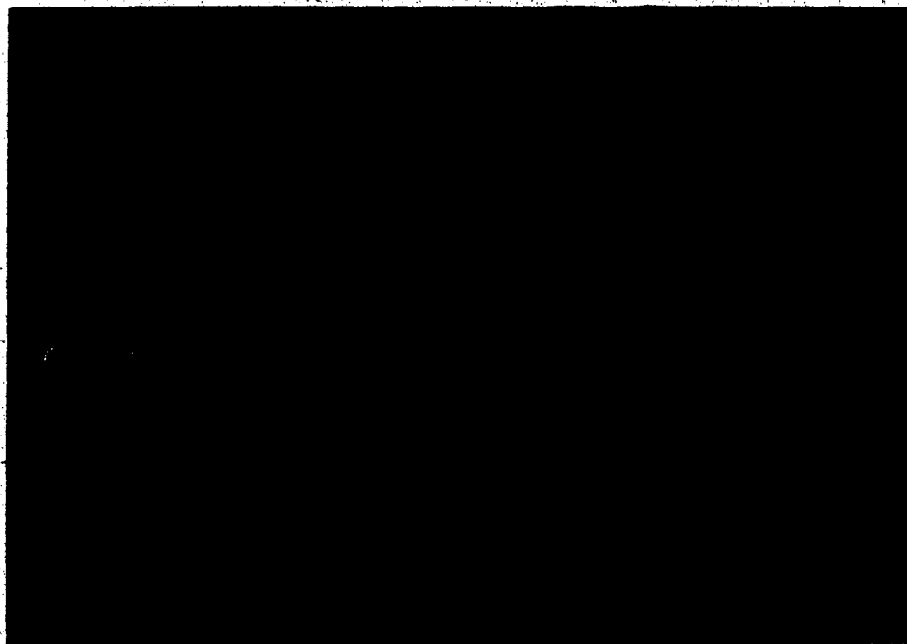


Plate 1.1 The Semi-Cylindrical Solenoidal Coil

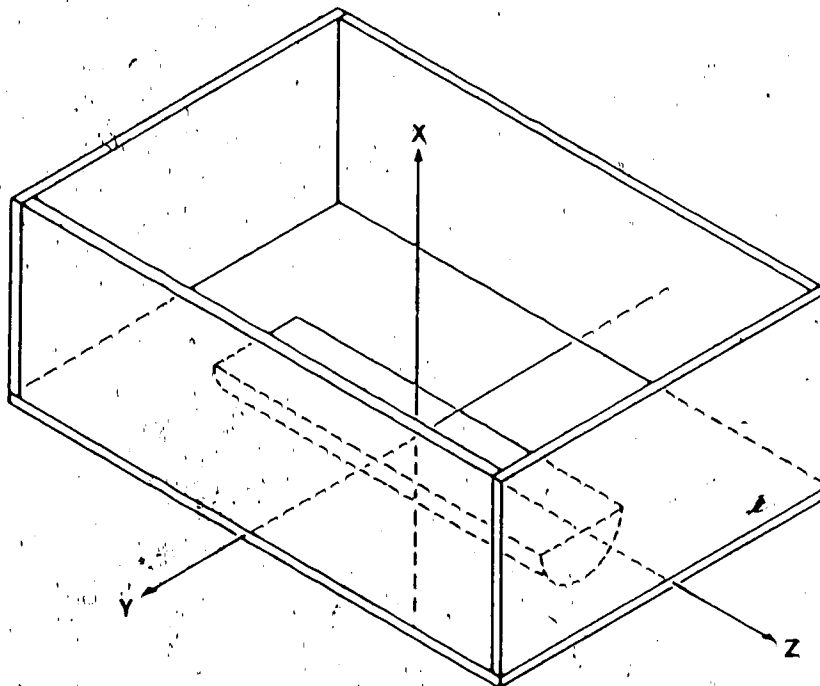


Figure 1.1 Positioning of the Coil and Definition of Coordinate System

used to insulate the coil from the solution.

It is expected that the insulating boundaries of the wooden box will have a minimal effect on the fields generated by the coil.

1.4 Related Research

The theoretical behavior of the single-layer solenoidal coil has been studied extensively by previous researchers. Much of this work, particularly the most recent, deals with the development of approximate solutions for the electric and magnetic fields generated. The complex geometry of the device has to date prevented the development of an exact solution. A thorough survey of early work was compiled by Sensiper (1955), and of later work by Gardiner (1982) and

Hagmann (1984). The interested reader is directed to the bibliographies contained in these theses.

Development of the solenoidal coil as an applicator for radiofrequency heating of low conductivity materials is more recent. Chute and Vermeulen (1981) used an approximate field solution based on the sheath helix model of an infinitely long solenoid with arbitrary materials in its interior and exterior regions to show that when the exterior region was air, this device could be used to uniformly heat materials of low conductivity in an efficient manner. They also showed that when the coil and interior core material are in direct contact, heating due to the axial electric field is at least several orders of magnitude greater than heating due to the circumferential electric field, regardless of the conductivity of the core material.

In a later paper Vermeulen and Chute (1983) presented a lumped R-L-C equivalent circuit representation of a finite-length coil having a length-to-diameter ratio much greater than one, for the case where the exterior region is air and an insulating gap separates the coil and interior core material. Using this equivalent circuit, they were able to accurately predict the coil's input resistance as a function of core conductivity for frequencies well below self-resonance.

A similar plot of input resistance versus core material conductivity for the insulated coil was obtained independently by Fugino *et al* (1981), when investigating the use of

a solenoidal coil to measure the high-frequency conductivity of electrolytic solutions. However, they attributed this resistance to dielectric and eddy current losses and overlooked the existence of an axial electric field. An equivalent circuit similar to that developed by Vermeulen and Chute was also presented, but was not discussed in detail.

The dominant nature of the capacitance between individual turns and the zero-potential midplane of an infinite solenoid excited with balanced excitation* was described by Mostafa and Gohar (1953). Chute and Vermeulen (1982) later showed that although the capacitance between a given turn and the zero-potential midplane is much less than the capacitance between adjacent turns, the potential between a given turn and the midplane is generally much greater than the potential between adjacent turns. Consequently, the current flowing between adjacent turns is small compared to that flowing between individual turns and the zero-potential midplane. Both groups concentrated their investigations on balanced excitation, but stated how the coil would behave if grounded at one end.

In the same paper Chute and Vermeulen (1982) went on to show that a second component of self-capacitance must exist in finite-length coils excited at frequencies below self-resonance to account for the storage of excess charge

*A balanced configuration exists when the device in question and its excitation are physically and electrically symmetric with respect to ground.

near the coil ends, and stated how this lumped component becomes increasingly dominant with decreasing length-to-diameter ratio.

Tyler (1974) used a magnetically coupled oscillator circuit to study the self-resonant modes of single-layer solenoidal coils excited without end connections. Both balanced and unbalanced configurations were investigated. Based on measurements made with coils of various geometries, an empirical formula was developed to predict the frequencies of self-resonant modes.

Ruggera and Kantor (1984) demonstrated experimentally that solenoidal coils could be used to produce transversely uniform heating in coaxially layered, simulated human fat-muscle tissue phantoms without excessive fat-layer heating. Their investigation concentrated on one-half wavelength and one wavelength self-resonant modes. They determined the heating pattern generated by splitting the phantom in half and viewing the exposed midplane with a thermographic camera. Transverse and longitudinal heating patterns were thus obtained. The validity of their results is questionable, however, because they attributed all the heating produced to dielectric losses and neglected Joule heating. Based on this assumption they allowed the two halves of the phantom to remain separated by polyethylene film during the heating phase. At the frequencies used, however, a significant portion of the observed heating should be Joule heating (see Stoy *et al* 1982, pp. 504, 508).

The flow of currents within the phantom would be perturbed by the polyethylene film, so that the resulting heating patterns are not necessarily the same as would be observed with the film removed.

Hagmann (1984) developed an approximate solution based on the infinite sheath helix model, and later used it to predict specific absorption rate (SAR) as a function of radial position in an infinitely long coaxially-layered human arm phantom enclosed by a solenoidal coil (Hagmann and Levin 1984). Self-resonance at one wavelength was examined in coils of various radii and pitch angle. Strohbehn (1982) had earlier performed similar calculations, but based his analysis on a mathematical model which included only the circumferential electric field.

Hagmann and Levin (1985) went on to make a calorimetric determination of the efficiency of solenoidal coils operating at one wavelength self-resonance. In a later paper, Hagmann *et al* (1985) compared the performance of helical coil applicators to that of microwave annular phased arrays for trunk and thigh heating. They observed very intense fields near the inside and outside surfaces of the coil. In one case the "aberrant" heating produced by these fields was found to be greater than that produced within the volume of the coil. They also found that when a BALUN^s was not used to excite the coil, both the shape of the heating pattern and the resonant frequency of the coil were

^sA BALUN is a balanced to unbalanced transformer.

dependent upon the length of the feed cable. Very intense fields were detected near the feed cable in this case.

The use of a coil with a semicircular cross-section has not, to the best of the author's knowledge, been investigated previously.

1.5 Discussion of Chapters and Appendices that Follow

Previous researchers have shown that the distributions of current and potential along the winding of a solenoidal coil are dependent not only upon the frequency of excitation, but also upon the manner in which the coil is excited. Since the heating distribution generated by the coil is determined by its electric field distribution, it is important to understand how this field is affected by the type of coil excitation. In Chapter Two the frequency of excitation and the excitation type (balanced or unbalanced) are studied to determine their effect on the heating pattern generated by the semi-cylindrical solenoid. Modes of excitation which may be useful for electromagnetic heating are identified.

In Chapter Three the input resistance of the modified solenoid is examined as a function of the conductivity of the adjacent saline solution. The efficiency of the device is thus evaluated. The equivalent circuit developed by Vermeulen and Chute (1983) to represent the cylindrical solenoid at frequencies well below self-resonance is shown also to accurately represent the semi-cylindrical solenoid under these conditions.

A more complete understanding of the heating pattern generated by the semi-cylindrical solenoid would be possible if the electric field generated by the device were known. Chapter Four describes the direct measurement of the electric field generated by the semi-cylindrical solenoid within an adjacent volume of saline solution. Two dipole measurement probes are developed. Four modes of operation are examined. The data collected are used to produce contour plots of relative field strength and power dissipation.

A summary of results with observations and conclusions is presented in Chapter Five.

Appendix A contains a theoretical explanation of the mechanisms of energy dissipation within a material exposed to an electromagnetic field. The discussion is restricted to nonmagnetic materials, and particular attention is given to aqueous electrolytes. The dielectric properties of aqueous sodium chloride are presented.

Appendix B contains a brief discussion of the theory of dipole probes in lossy media. This is followed by a description of the design, construction, and testing of two measurement probes and the associated instrumentation, as used to conduct the measurements described in Chapter Four.

Appendix C contains experimental data collected during measurements described in Chapters Three and Four.

Chapter 2

Coil Excitation

Previous researchers have shown that the distributions of current and potential on the winding of a solenoidal coil are dependent upon the frequency of excitation as well as the manner in which the coil is excited. The primary purpose of this chapter is to investigate what effect the type of excitation (balanced or unbalanced) has on the heating patterns generated by the semi-cylindrical solenoid. An attempt is also made to relate the heating patterns observed to the ideal distributions of current and potential on the coil winding. Due to end effects, however, exact agreement between the two is not expected.

2.1 Current Distribution on Solenoidal Coils

A qualitative explanation of the distributions of current and potential produced on solenoidal coils by balanced and unbalanced excitations is presented. It is felt that this will provide some insight into the behavior of the semi-cylindrical solenoid as well.

The finite-length solenoidal coil can be viewed as a section cut from an infinite solenoid. Although Tyler (1974) demonstrated that due to end effects the distributions of current and potential on a finite-length solenoidal coil are not strictly sinusoidal and thus may differ significantly from those on a corresponding segment excised from the infinite solenoid, it is helpful to assume for the time

being that they are sinusoidal.

The charge and potential on an infinite solenoid vary spatially as $\sin(\beta z)$, and the current in the winding varies spatially as $\cos(\beta z)$ (Vermeulen and Chute 1982). The current in the coil winding generates an axial magnetic field, which in turn generates a non-conservative circumferential electric field. Both the axial magnetic field and the circumferential electric field vary spatially as $\cos(\beta z)$. The distribution of charge on the coil winding generates a conservative electric field having components in the axial and radial directions. These axial and radial components vary spatially as $\cos(\beta z)$ and $\sin(\beta z)$, respectively.

The nature of the current distribution can be appreciated by examining the distributed self-capacitance models proposed by Mostafa and Gohar (1953) and by Chute and Vermeulen (1982) for a short section centered at a zero-potential plane. Capacitive coupling between this midplane and an incremental segment near one end of the section (a potential maximum), and between the midplane and a corresponding segment near the other end (a potential maximum in antiphase with the first) results in displacement current flowing out of the windings near one end of the section, through the zero-potential midplane, and into the windings near the other end of the section. These displacement currents are generated by the conservative electric field of the coil.

The distributions of conduction current, displacement current, and potential (I_c , I_d , and V) on a section of an infinite solenoid situated in free space are shown in figure 2.1. These distributions are exactly those that would exist on a lossless short-circuited transmission line, where the position of the short-circuit coincides with a zero-potential plane on the coil (Chute and Vermeulen 1982).

When a solenoidal coil is excited in a balanced manner, the terminal voltages oscillate with equal magnitude and opposite polarity. A coil excited in this way can be thought of as having been cut from the infinite solenoid so that the midplane of the coil corresponds to a zero-potential plane on the infinite solenoid. The resulting current distribution is symmetric about the midplane, and equal quantities of displacement current enter and leave the surface of the coil at any instant. At frequencies where the coil length is less than one-half wavelength it is reasonably clear that all displacement current paths begin and end on the surface of the coil. At higher frequencies this is not obvious. However, since there is no *net* flow of displacement current away from the coil, the device should not couple significantly to grounded objects located more than one coil-length from the coil surface, when excited in this manner.

When a solenoidal coil is excited with one end held at ground potential it is unbalanced. A coil excited in this manner can be thought of as having been cut from the infinite solenoid so that one end of the coil corresponds to

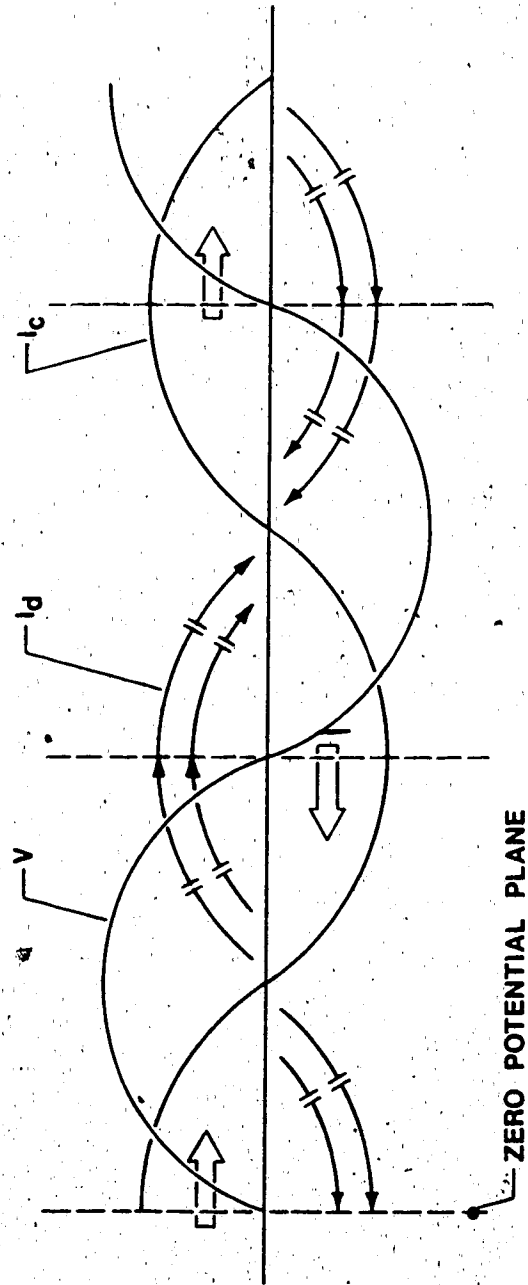


Figure 2.1 Distributions of Current and Potential on an Infinite Solenoid

a zero-potential plane on the infinite solenoid. At frequencies where the coil length is equal to an even number of half wavelengths, the current distribution is approximately the same as what would be produced by balanced excitation. Equal quantities of displacement current enter and leave the coil, and coupling to ground through external objects is negligible. At other frequencies the quantities of displacement current entering and leaving the coil are not equal, and some current must find an external return path to ground. The resulting coupling to nearby grounded objects can be very significant. The self-capacitance of the unbalanced coil is in fact partly determined by this external coupling (Tyler 1974, pp. 149).

2.2 Demonstration of Heating Patterns

A preliminary investigation was conducted to demonstrate the effects of frequency and the type of excitation on the shape of the heating pattern generated by the semi-cylindrical solenoid.

2.2.1 Procedure

The heating patterns generated by the semi-cylindrical solenoid were displayed using a method developed by Chute and Vermeulen (1981) to demonstrate two-dimensional electric fields. Temperature-sensitive cholesteric liquid crystal sheet is laminated to resistive Teledeltos paper. When placed in an electric field, currents are induced in the

resistive paper which generate heat and cause a change in the apparent color of the liquid crystal. Regions of uniform coloration thus correspond to regions of uniform field strength. The resulting patterns provide a general indication of the field geometry. A similar procedure, without the resistive paper, was used by Lerch and Kohn (1983) to display heating patterns produced in gelatin by coil-type hyperthermia applicators.

For this investigation a sheet of 3.18 mm (0.125 in) plexiglass was placed directly over the coil and sealed into the bottom of the previously described wooden box, as shown in figure 1.1. A sheet of Teledeltos paper was laminated to the upward-facing side of the plexiglass, covered by a layer of liquid crystal sheet, and by transparent PVC film. The apparent color of the liquid crystal shifted from black below 25°C to brown, yellow, green, blue, and back to black above 30°C.

Four operating conditions were investigated, corresponding to the coil length being much shorter than one wavelength, approximately equal to one-half wavelength, approximately equal to one wavelength, and approximately equal to two wavelengths.

In the balanced case self-resonances were located by monitoring the coil's input admittance versus frequency with a Wayne Kerr model B801B VHF admittance bridge and model SR268 source/detector. Frequencies where the equivalent shunt capacitance indicated by the bridge went to zero were

assumed to correspond to self-resonances, and were assumed to occur at one-half wavelength intervals. With 0.13 mm (0.005 in) polyethylene film covering the coil and the box filled with tap water ($\sigma \approx 0.02$ S/m), resonances were found to occur at 10.4 MHz, 20.8 MHz, 28.6 MHz, and 37.8 MHz. In the unbalanced case resonances were located by monitoring the coil's input impedance versus frequency with a Hewlett-Packard 4815A RF vector impedance meter. Frequencies where this impedance became purely real were assumed to correspond to self-resonances, and again were assumed to occur at one-half wavelength intervals. With 0.13 mm (0.005 in) polyethylene film covering the coil and the box filled with tap water ($\sigma \approx 0.02$ S/m), resonances were found to occur at 8.7 MHz, 21.7 MHz, 27.5 MHz, and 39.0 MHz. The fact that these self-resonant frequencies are not regularly spaced was noted by Tyler (1974), and is here attributed to end effects.

When the polyethylene film was replaced by the laminated plexiglass sheet these resonant frequencies were found to shift slightly. Frequencies of 10 MHz, 20 MHz, and 35.1 MHz were thus chosen to study the coil's behavior where its length is approximately equal to one-half, one, and two wavelengths, and 1 MHz was selected as an appropriate frequency at which to study the coil's low-frequency behavior.

The box was filled with tap water ($\sigma \approx 0.02$ S/m), and the coil was impedance-matched to the output of an

oscillator-driven amplifier*. The coil was energised at each of the above frequencies and the images generated in the liquid crystal were photographed. In each case the input power and water temperature were adjusted to give the clearest image. In some cases minor changes in frequency were necessary to obtain proper impedance matching.

To generate balanced excitation, a BALUN consisting of a half-wavelength section of RG-8/U coaxial cable was used, and the unbalanced input of the BALUN was impedance-matched to the amplifier output (figure 2.2). To generate unbalanced excitation, the matching network alone was used. One end of

*An Electronic Navigation Industries (ENI) model A-300 RF power amplifier and a Hewlett Packard model 8656A signal generator were used. A Philco-Sierra model 164B bi-directional power meter was used to monitor reflected power and optimize matching.

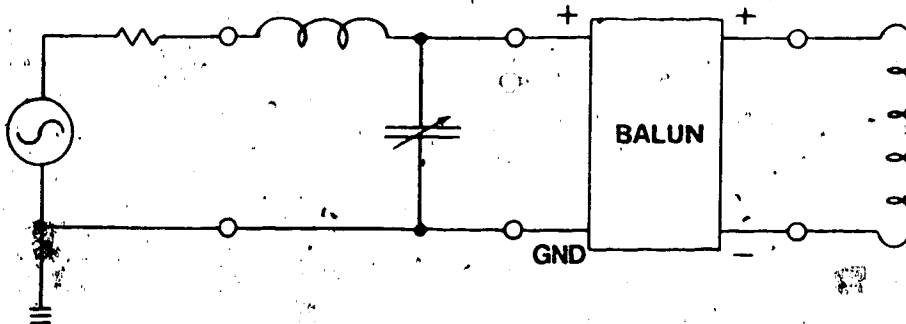


Figure 2.2

Balancing and Matching Network

the coil was thus held at ground potential.

2.2.2 Results

Heating patterns generated with balanced excitation are shown in plates 2.1, 2.2, and 2.3. Because of difficulties in constructing a suitable impedance-matching network, a heating pattern for the one wavelength self-resonant case could not be produced.

Heating patterns generated with unbalanced excitation are shown in plates 2.4, 2.5, and 2.6. Difficulties in constructing a suitable impedance-matching network again prevented the production of a heating pattern for the one wavelength self-resonant case.

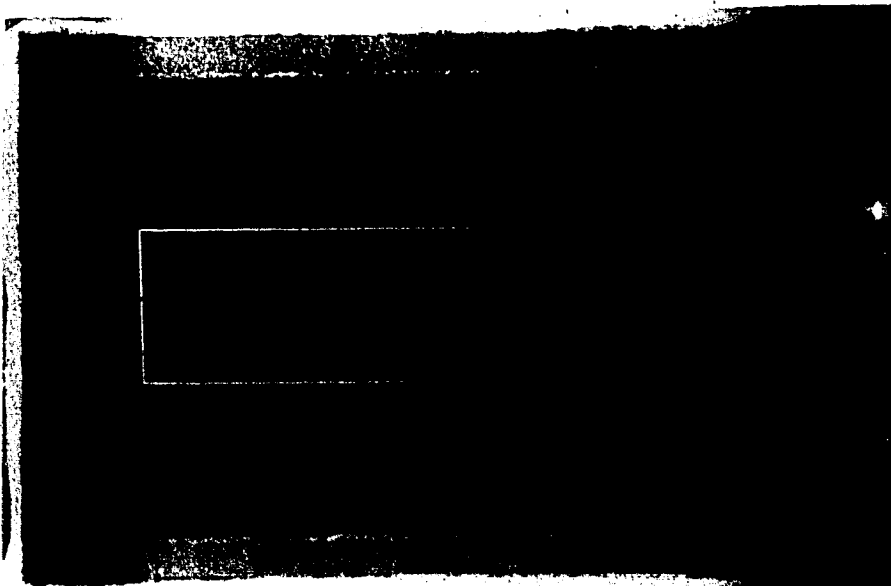


Plate 2.1 Heating Pattern Generated at 1 MHz by Balanced Excitation



Plate 2.2 Heating Pattern Generated at 10 MHz by Balanced Excitation



Plate 2.3 Heating Pattern Generated at 35.1 MHz by Balanced Excitation



Plate 2.4 Heating Pattern Generated at 1 MHz by Unbalanced Excitation



Plate 2.5 Heating Pattern Generated at 10 MHz by Unbalanced Excitation

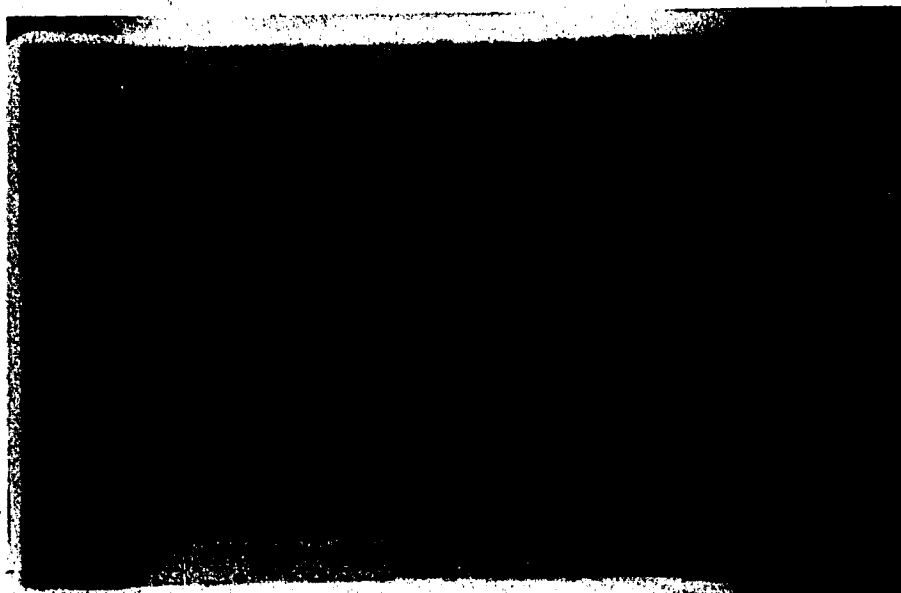


Plate 2.6 Heating Pattern Generated at 35.1 MHz by
Unbalanced Excitation

2.2.3 Discussion

In order to interpret the heating patterns presented in plates 2.1 to 2.6 it should be remembered that the axial and circumferential electric field components have (neglecting end effects) the same spatial distribution along the length of the coil as the conduction current in the coil winding, and that the radial electric field component has (neglecting end effects) the same spatial distribution along the length of the coil as the potential on the coil.

The heating pattern produced at 1 MHz by balanced excitation is shown in plate 2.1. No heating other than resistive losses in the coil winding can be discerned. The uniformity of the image generated suggests that the distribution of conduction current in the coil winding is

approximately uniform over the length of the coil. This agrees with the theoretical distributions of current and potential on a short balanced section excised from the infinite solenoid, shown in figure 2.3(a).

The heating pattern produced at 10 MHz by balanced excitation is shown in plate 2.2. At this frequency the length of the coil is approximately equal to one-half wavelength. Heating is produced near both ends of the coil, where the conservative electric field leaves the surface of the coil and extends outward into the target material. This agrees with the theoretical distributions of current and potential on a balanced one-half wavelength section excised from the infinite solenoid, shown in figure 2.3(c). Strictly speaking, only the axial component of the conservative electric field should produce heating in the resistive paper. The concentration of heating in regions where this field is primarily radial in direction is attributed to a distortion in the shape of the field due to the Teledeltos paper, causing the primarily radial electric field to become primarily axial in this plane. Heating by resistive losses in the coil winding is not apparent, due to the dominance of the losses in the target material.

The heating pattern produced at 35.1 MHz by balanced excitation is shown in plate 2.3. At this frequency the length of the coil is approximately equal to two wavelengths. The observed heating pattern is again produced by the conservative electric field of the coil. At this

frequency the conservative field is more tightly bound to the coil, and relatively little penetration into the target material occurs. As a result, both the radial and axial components of the conservative electric field produce heating in the plane of the resistive paper. The heating pattern observed agrees with the theoretical distributions of current and potential on a balanced two wavelength section excised from the infinite solenoid, shown in figure 2.3(e).

The heating pattern produced at 1 MHz by unbalanced excitation is shown in plate 2.4. As in the balanced case, no heating other than resistive losses in the coil winding can be discerned. The uniformity of the image generated again suggests that conduction current is uniformly distributed over the length of the coil. This agrees with the theoretical distributions of current and potential shown in figure 2.3(b) for a short unbalanced section excised from the infinite solenoid, and confirms that for frequencies well below self-resonance, the distribution of conduction current on the coil winding is approximately uniform regardless of how the coil is excited.

The heating pattern produced at 10 MHz by unbalanced excitation is shown in plate 2.5. At this frequency the length of the coil is approximately equal to one-half wavelength. The asymmetry in this heating pattern indicates that some of the displacement current leaving the surface of the coil returns to ground through paths which do not

include the coil winding. The theoretical distributions of current and potential on an unbalanced one-half wavelength section excised from the infinite solenoid are shown in figure 2.3(d).

The heating pattern produced at 35.1 MHz by unbalanced excitation is shown in plate 2.6. At this frequency the length of the coil is approximately equal to two wavelengths. This pattern is practically identical to the one shown in plate 2.3 for the balanced two wavelength case, confirming that at this frequency the distributions of current and potential produced by balanced and unbalanced excitations are alike. This likeness was noted by Ruggera and Kantor (1975). The theoretical distributions of current and potential on an unbalanced two wavelength section are shown in figure 2.3(e).

Further discussion of the heating patterns produced by the semi-cylindrical solenoid will be presented in Chapter Four.

It should be noted that the procedure used here only displays heating generated by the horizontal component of the electric field in the plane of the resistive paper. The contribution of the vertical field component is not displayed. The nature of the heating distribution generated in other planes is also not considered. In addition, the effects of the impedance mismatch between the resistive sheet and the water, and the effects of the nonconducting layers of plexiglass, liquid crystal and PVC film are not

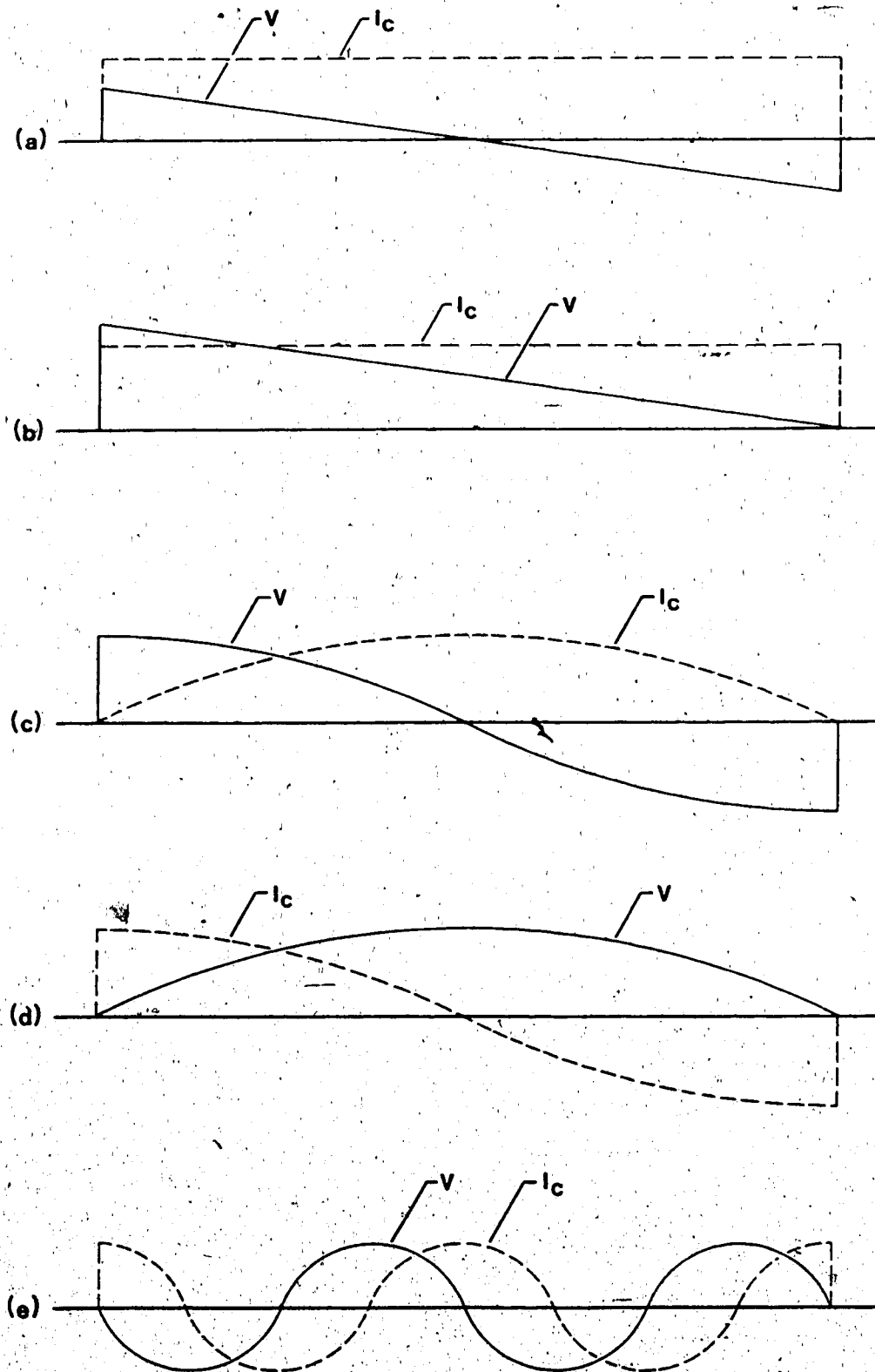


Figure 2.3 Ideal Distributions of Current and Potential on a Finite Solenoid

explored.

An unexpected phenomenon was observed when operating the coil with unbalanced excitation. Touching a grounded metal surface while standing in the vicinity of the energised coil resulted in a burn to the skin at the point of contact. This is due to the operator's body forming a low impedance path to ground for displacement current leaving the coil. This effect was most severe at 10 MHz and 20 MHz, and was only slightly noticeable at 1 MHz and 35.1 MHz. It was not observed at any frequency when using balanced excitation. Hagmann *et al* (1985) similarly observed dangerously intense fields near the feed cable when exciting a cylindrical solenoid at one wavelength self-resonance without use of a BALUN. Because of this it is clear that unbalanced excitation should only be used at frequencies where external coupling of displacement currents is not significant.

Based on this investigation, balanced coil excitation will be studied more thoroughly at 1 MHz, one-half wavelength self-resonance, one wavelength self-resonance, and two wavelength self-resonance. Since unbalanced excitation has been shown to produce the same heating patterns as balanced excitation would in the low-frequency and two wavelength cases, it is used in these cases. This will be discussed further in Chapter Three.

Chapter 3

Efficiency

The purpose of this chapter is to investigate the delivery of energy into the target material by the semi-cylindrical solenoid. The effect of the conductivity of the target material upon the efficiency of the device is of particular interest. The coil is examined at frequencies where its length is much less than a wavelength, equal to one-half wavelength, equal to one wavelength, and equal to two wavelengths.

3.1 Measurement of Input Resistance

The ability of the semi-cylindrical coil to deliver energy into the target material was evaluated by measuring the input resistance (or conductance) of the device as a function of the electrical conductivity of the target material. An estimate was then made of the resistive losses in the coil winding. All power delivered to the coil is assumed to be dissipated either in the target material or the coil winding, and radiation is neglected. Since unbalanced excitation is easier to implement in this measurement, it is used in the low-frequency and two wavelength cases. It is not used in the one wavelength case for reasons that will be explained later.

3.1.1. Procedure

—For this investigation a 0.13 mm (0.005 in) polyethylene film was placed over the coil and sealed to the bottom of the previously described wooden box. The box was then filled with distilled water, whose conductivity was gradually increased from approximately 2×10^{-4} S/m to approximately 20 S/m by adding small quantities of saturated NaCl solution. The temperature of the solution was maintained at approximately 25°C. At each increment the conductivity of the solution was measured and recorded, along with the input impedance (or admittance) of the coil and its resonant frequency.

The low-frequency conductivity of the saline solution (σ_{LF}) was determined by a four electrode measurement (Schwan and Ferris 1968) at 100 Hz using a submersible test cell (figure 3.1). The cell was submerged and allowed to fill with solution. A small, uniform current density was established inside it, and the resulting potential gradient was measured. The conductivity of the solution was then calculated according to

$$\sigma_{LF} = \frac{J}{E} = \frac{4l}{\pi d^2} \cdot \frac{I}{V} = 74 \cdot \frac{l}{V} \text{ S/m.} \quad [3.1]$$

This value was then adjusted, using the data presented in section A.2 of Appendix A, to include dielectric losses for the frequency at which the coil was being examined, and give the real effective conductivity, $\hat{\sigma}$, at that frequency. For the range of frequencies considered here, this adjustment was only significant for conductivities less than 0.01 S/m.

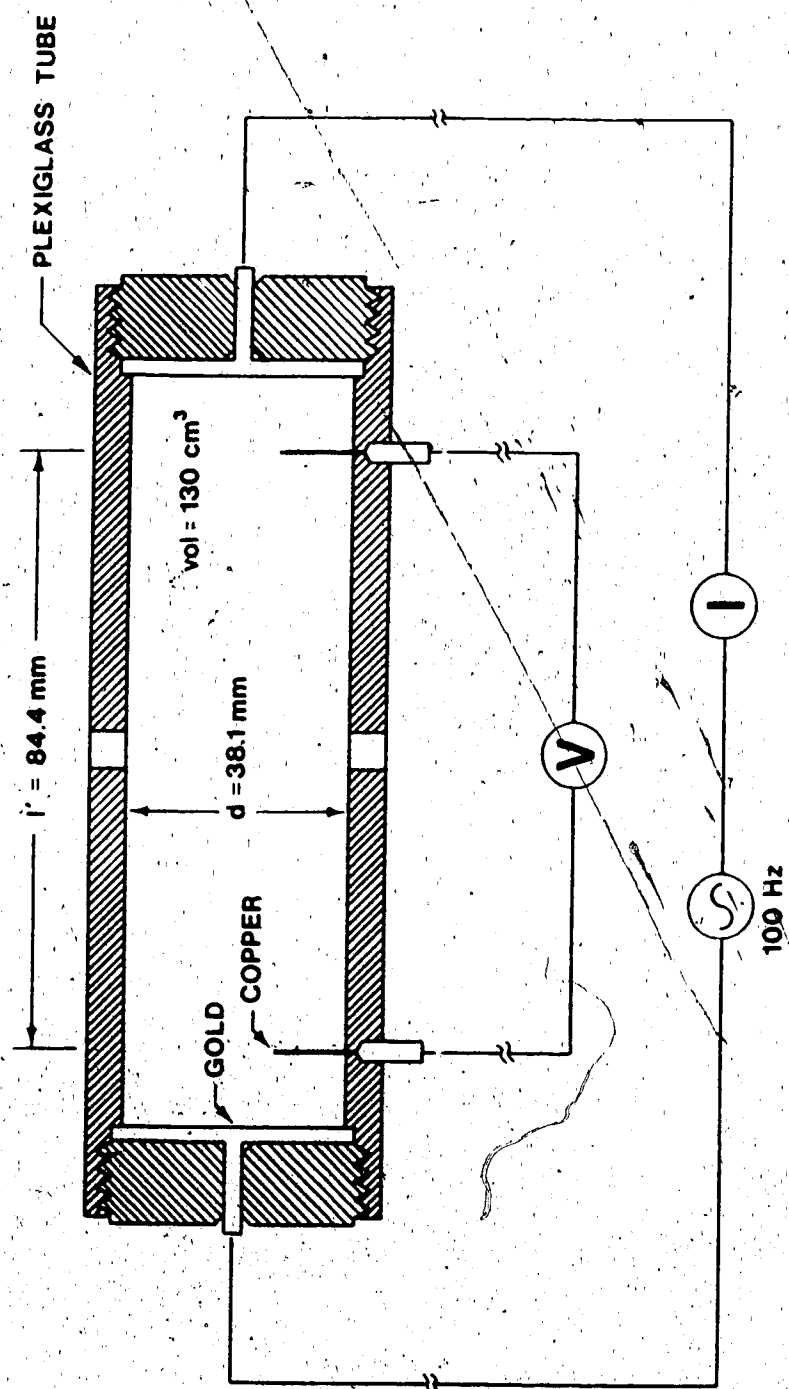


Figure 3.1

Conductivity Measurement Cell

In the low-frequency case (1 MHz), the coil was parallel resonated with a variable air-dielectric capacitor. The input resistance⁷ of this parallel combination was then measured with a Hewlett-Packard 4815A RF vector impedance meter. The coaxial measurement probe on this device is unbalanced (one terminal is tied to ground), and so will excite the coil in an unbalanced manner. However, the current distribution in the low-frequency case is approximately uniform regardless of the type of excitation, so that the impedance observed should be approximately the same under balanced and unbalanced excitations.

In the one-half wavelength self-resonant case, balanced impedance measurements cannot be made directly with the vector impedance meter probe, one terminal of which is grounded, since at this frequency balanced excitation implies potential maxima at both ends of the coil. A balanced admittance bridge⁸ was used to locate self-resonance and determine the resulting terminal admittance of the coil over the specified range of conductivities.

Use of the vector impedance meter for the balanced one wavelength measurement was not fruitful. Impedance values were observed to drift randomly with time, and the results were generally not reproducible. Use of a screened enclosure did not improve this. This problem was attributed to equipment malfunction and will not be discussed further. Use

⁷The value obtained is actually equal to the reciprocal of the input conductance.

⁸A Wayne Kerr model B801B VHF Admittance Bridge and model SR268 RF Source/Detector were used.

of the admittance bridge in this case was also difficult. The input susceptance of the coil blows up where $L=\lambda$, changing abruptly from a large shunt capacitance to a large shunt inductance. Indeed it has been shown that this susceptance varies as $\cotangent(\beta L/2)$, where L is the length of the coil in wavelengths (Chute and Vermeulen 1982). As a result, the admittance bridge cannot be balanced near resonance since the input susceptance of the coil becomes larger in magnitude than the instrument can measure. For this reason only the approximate frequency of self-resonance was recorded at low conductivities. As the conductivity of the solution was increased, however, susceptance values near resonance were observed to decrease, and the admittance bridge could be balanced. This decrease is thought to be due to the decrease in the "Q" of the coil as the saline solution becomes more lossy.

In the two wavelength self-resonant case, a balanced measurement of the coil's input impedance was made with the unbalanced probe of the vector impedance meter connected directly to the coil terminals. This generates approximately the same current distribution as balanced excitation would, because both the balanced case (midplane grounded) and the unbalanced case (endplane grounded) result in potential minima at the coil terminals when operating at two wavelength self-resonance. The two excitations do not produce exactly the same current distribution, however, since in the unbalanced case a finite voltage must exist at

one end to account for the nonzero input impedance of the coil. As a result, the current distribution generated is not completely symmetric. In the balanced case a finite (but smaller) voltage would exist at each end of the coil, and the current distribution would still be truly symmetric (but not strictly sinusoidal). The difference between the two current distributions is presumed to be small, so that the measurements made with the unbalanced instrument are accepted as being representative of a balanced measurement as well.

In all four cases resonance was maintained by adjusting the measurement frequency as required to keep the coil impedance purely real. The variable capacitor used in the low-frequency case was not adjusted after the original setting was made. The "resonant frequency" reported in this case is the frequency at which the variable capacitor and the shifting inductance of the semi-cylindrical solenoid continued to be resonant.

3.1.2 Results

The measured values of coil input resistance (or conductance) and resonant frequency are tabulated in tables C.1 to C.4 of Appendix C, and are plotted in figures 3.2 to 3.5. The resistance values shown in figures 3.3 and 3.4 for the one-half wavelength and one wavelength cases are equal to the reciprocal of the measured values of input conductance.

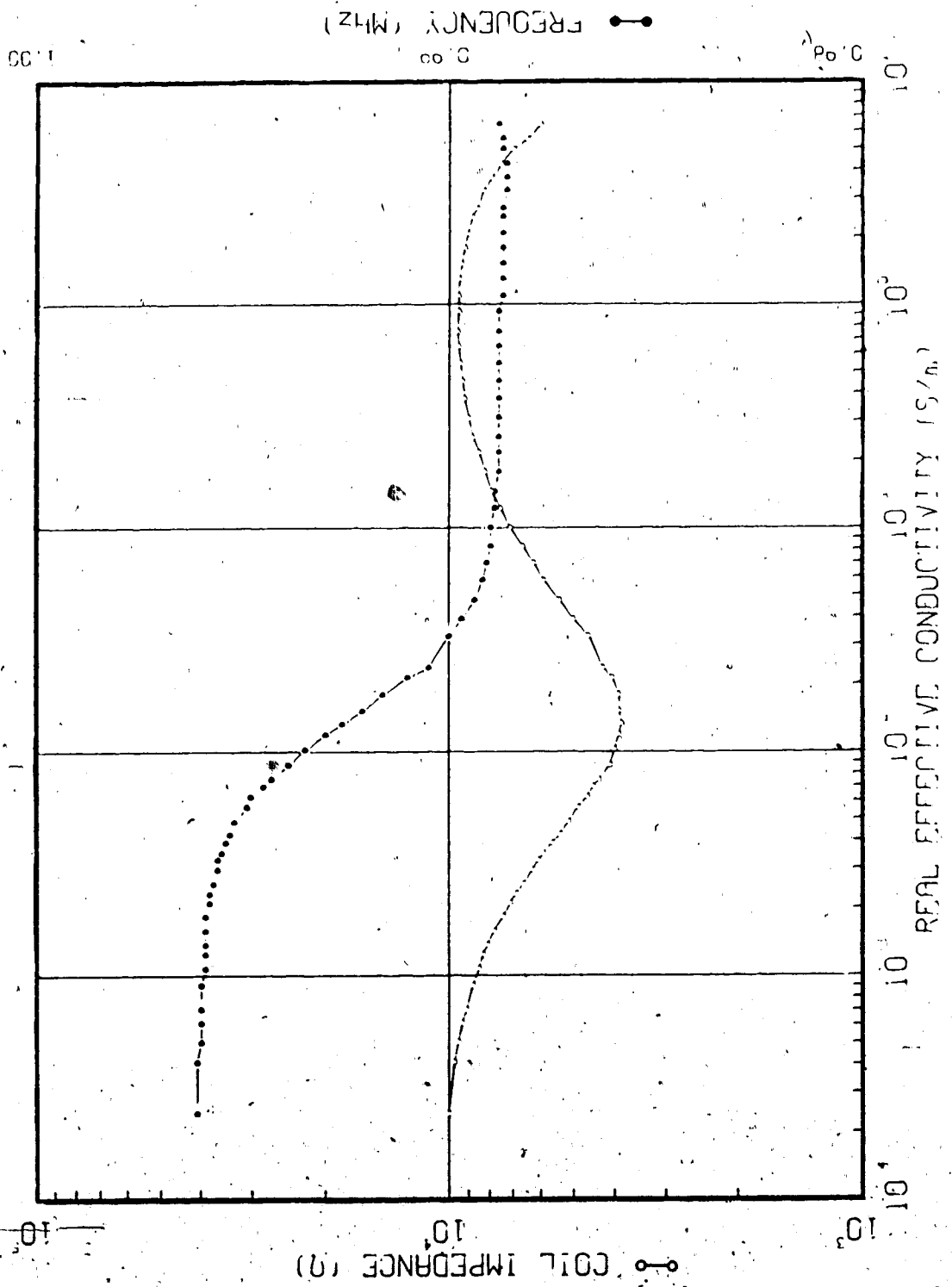


Figure 3.2 Input Resistance and Resonant Frequency of the Semi-Cylindrical Solenoid: Balanced Low-Frequency Case

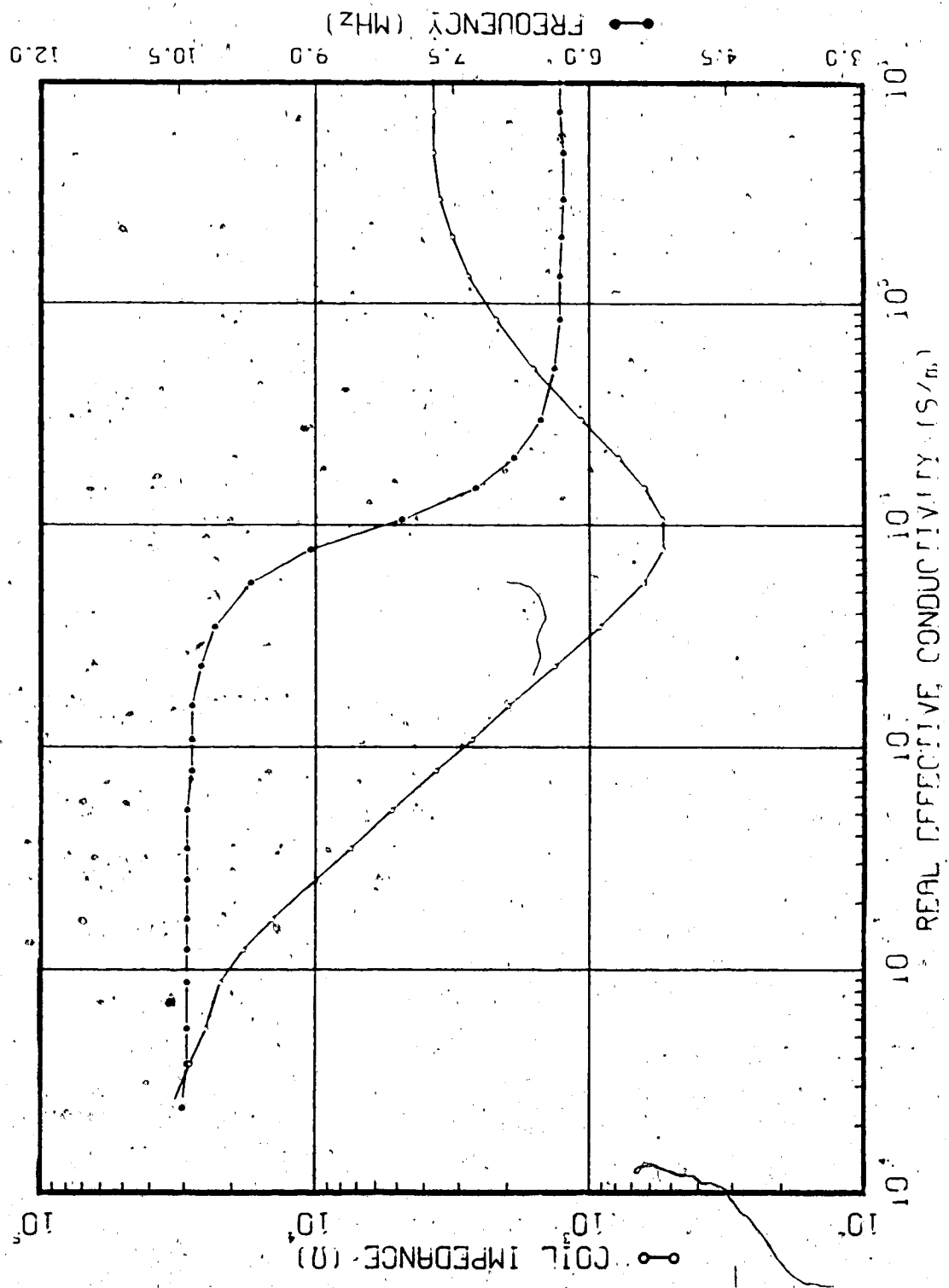


Figure 3.3 Input Resistance and Resonant Frequency of the Semi-Cylindrical Solenoid: One-Half Wavelength Balanced Self-Resonant Case

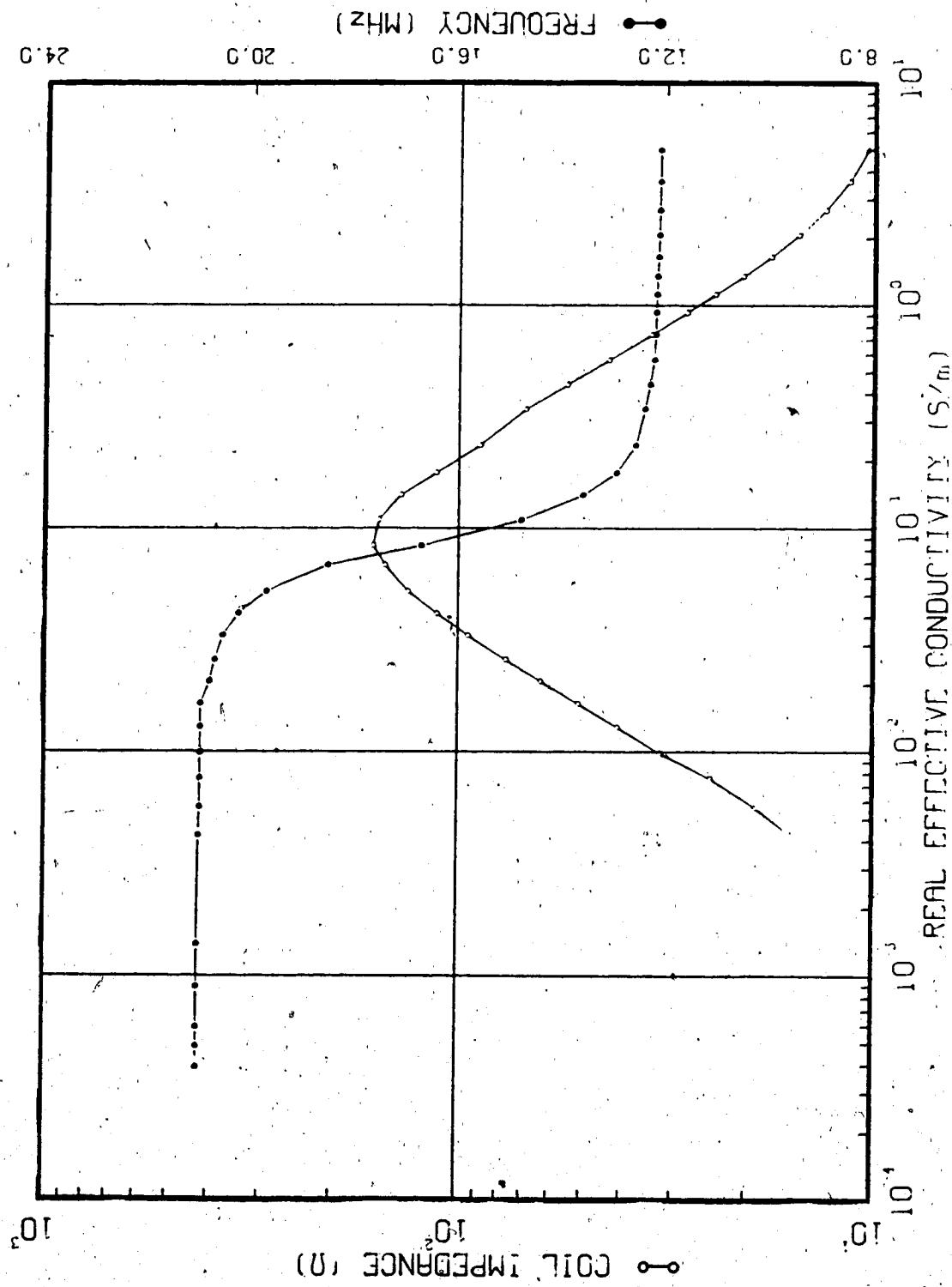


Figure 3.4 Input Resistance and Resonant Frequency of the Semi-Cylindrical Solenoid: One Wavelength Balanced Self-Resonant Case

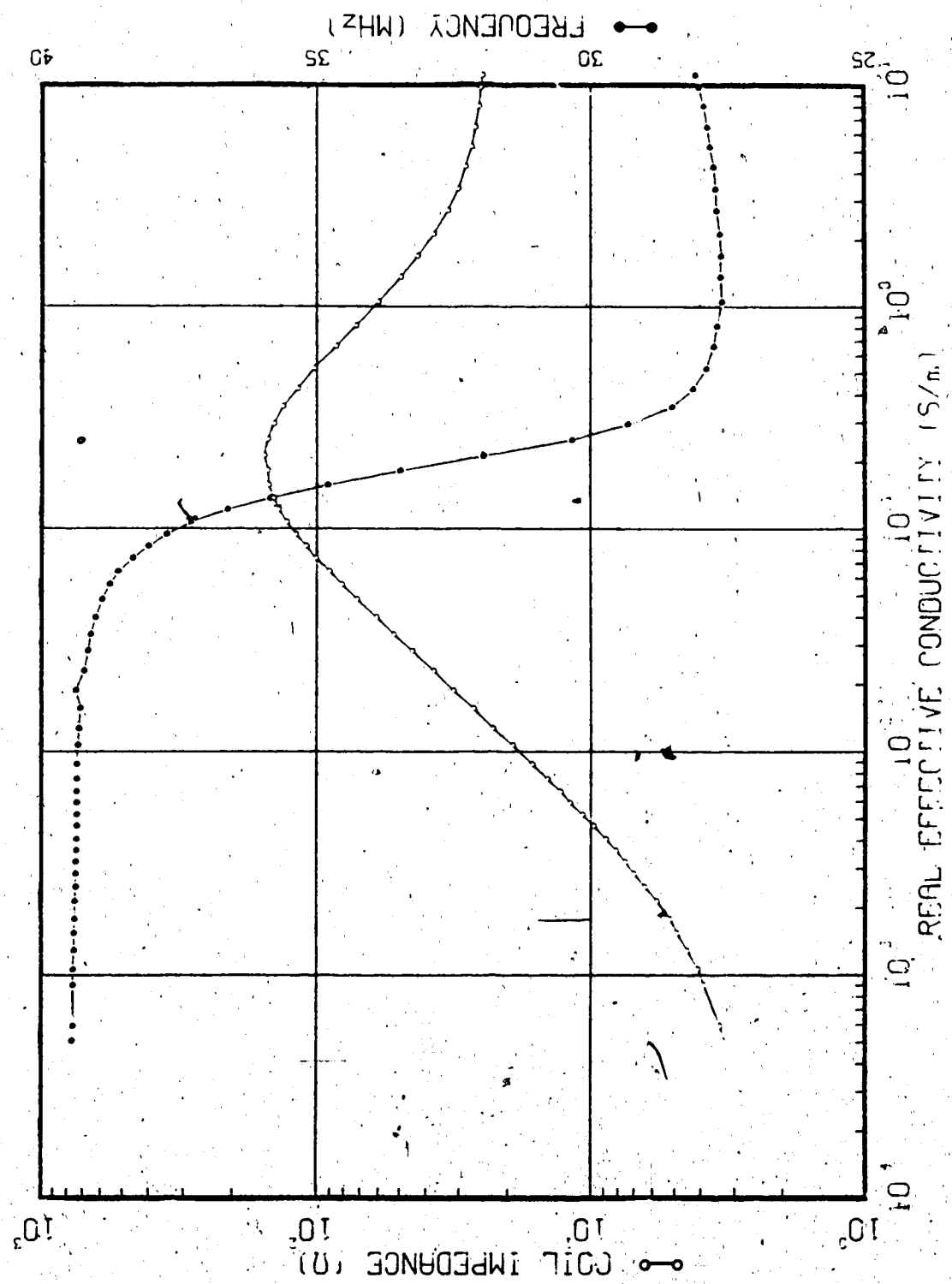


Figure 3.5 Input Resistance and Resonant Frequency of the Semi-Cylindrical Solenoid: Two Wavelength Balanced Self-Resonant Case

3.1.3 Discussion

It is interesting to note that in all four cases an abrupt decrease in the self-resonant frequency occurs as the loss tangent of the saline solution approaches unity. At this conductivity the currents generated by the coil's electric field shift from being primarily displacement currents, to being primarily conduction currents.

3.2 Estimation of Efficiency

In order to evaluate the efficiency of the semi-cylindrical solenoid it is necessary to estimate the resistive losses in the coil winding. These losses are assumed to vary with the current distribution on the coil and with frequency. At low frequencies the current distribution on the coil is always uniform, so that the losses in the coil winding are relatively independent of the constitutive parameters of the target material. The resistive losses in the coil winding can thus be determined by measuring the coil input resistance with the lossy target material removed. This procedure was used by Vermeulen and Chute (1983). At frequencies where the length of the coil is comparable to a wavelength, the current distribution on the coil is directly dependent upon the constitutive parameters of the target material, and such a measurement is not possible.

In the procedure used here, resistive losses in the coil are determined by estimating the asymptotic value of the input resistance as the real effective conductivity of

the target material goes to zero. These losses were in each case assumed to vary inversely with the skin depth of the copper as the resonant frequency shifted. Efficiency was then calculated as the ratio of power dissipated in the target material to total power delivered to the coil. While this method may be less exact than the calorimetric determination made by Hagmann and Levin (1985), it does provide an efficiency estimate for target material conductivities over five orders of magnitude.

In the low-frequency case the zero-conductivity asymptotic value of input resistance is 10.5 k Ω , and all subsequent values of input resistance at higher conductivities are smaller than this. For this reason the resistive losses are modelled by a fixed resistance R_w in parallel with a resistance representing the losses induced in the target material, and the measured input resistance R_{IN} is assumed to be the parallel combination of the two. In this case R_w is assumed to increase with increasing skin depth, and thus increase with decreasing frequency. The heating efficiency of the coil as a function of conductivity is then calculated as

$$\eta_{LF}(\hat{\sigma}) = 100\% \times [R_w(\hat{\sigma}) - R_{IN}(\hat{\sigma})]/R_w(\hat{\sigma}) . \quad [3.2]$$

The input impedance of a lossless coil excited at one-half wavelength balanced self-resonance is infinite. This is evident from the theoretical distributions of current and potential presented in figure 2.3(c). The zero-conductivity asymptotic value of input resistance (the

reciprocal of the measured input conductance) observed here for the semi-cylindrical coil is approximately $35.0 \text{ k}\Omega$, and subsequent input resistances at higher conductivities are smaller than this. For this reason the one-half wavelength self-resonant case is treated in the same way as the low-frequency case:

$$\eta_{\lambda/2}(\delta) = 100\% \times [(R_w(\delta) - R_l(\delta))/R_w(\delta)] \quad [3.3]$$

As previously discussed, an accurate measurement of the input admittance of the coil could not be made at low conductivities in the one wavelength balanced self-resonant case. Estimation of resistive losses in the coil and evaluation of heating efficiency were thus not possible. However, the data presented in figure 3.4 suggests that, based on the same model as used in the two wavelength case, the peak efficiency of the device exceeds 90 percent.

The input impedance of a lossless coil excited at two wavelength balanced self-resonance is zero Ohms. This is evident from the theoretical distributions of current and potential presented in figure 2.3(e). The zero-conductivity asymptotic value observed here for the semi-cylindrical coil is approximately 2.5Ω , and subsequent input resistances at higher conductivities are larger than this. For this reason the resistive losses in the coil are modelled by a fixed resistance R_v in series with a resistance representing the losses induced in the target material, and the measured input resistance R_{IN} is assumed to be the sum of the two. Here R_v is assumed to decrease with increasing skin depth, and

thus decrease with decreasing frequency. The heating efficiency of the coil as a function of conductivity is thus calculated as

$$\eta_{2\lambda}(\hat{\sigma}) = 100\% \times [R_{IN}(\hat{\sigma}) - R_w(\hat{\sigma})]/R_{IN}(\hat{\sigma}) \quad [3.4]$$

The efficiencies observed in the four cases are plotted together in figure 3.6. A curve for the one wavelength case is included for comparison only, and is based on an estimated low-conductivity asymptotic value of input resistance of 6Ω .

The efficiencies reported by Hagmann and Levin (1985) for the cylindrical solenoid operating at one wavelength self-resonance are much lower than those reported here. Possible explanations for this, apart from the fundamental differences between the two devices, include the larger conductor cross-section and lower frequency used here (both of which should result in lower resistive losses than experienced by Hagmann and Levin), and the much smaller gap between the coil and the target material used here.

3.3 Equivalent Circuit Models

It is possible to specify lumped values of inductance, capacitance, and resistance such that at a particular frequency these elements store and dissipate the same quantities of energy as the semi-cylindrical solenoid. These components can be used to construct an equivalent circuit representation of the coil. If the individual components of such a circuit can be related to specific mechanisms of

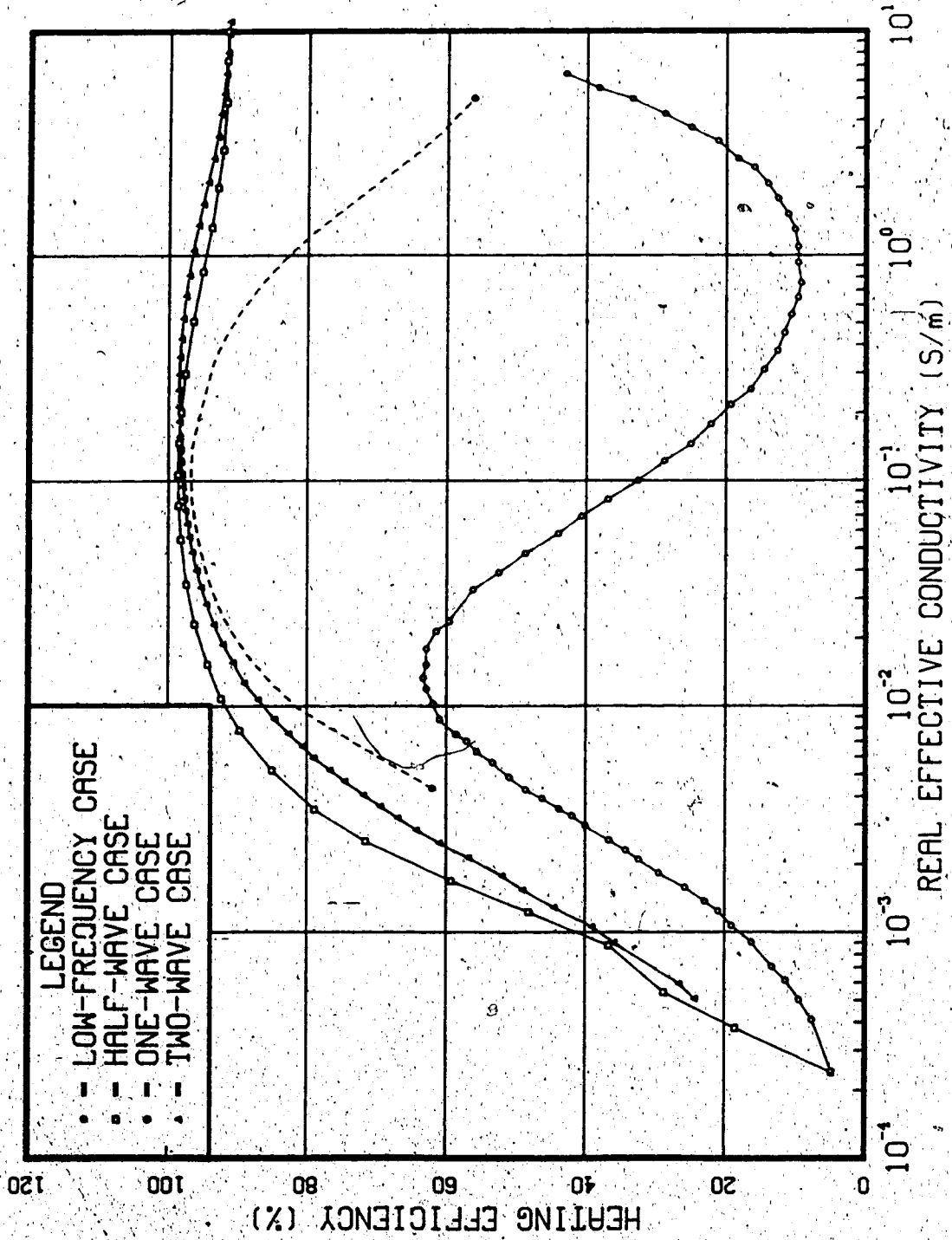


Figure 3.6 Heating Efficiency of the Semi-Cylindrical Solenoid: Four Cases

energy storage and dissipation, and to the physical parameters of the coil and target material, then the equivalent circuit becomes a useful tool for predicting the effect on the performance of the coil when these parameters are changed. If these components cannot be given some physical significance then the equivalent circuit is of little use in illuminating the phenomena involved.

3.3.1 Low Frequency Case

Vermeulen and Chute (1983) developed an equivalent circuit to represent cylindrical solenoidal coils having large length-to-diameter ratios at frequencies well below self-resonance. They calculated the energy stored and dissipated by the axial and circumferential electric fields of the coil, and equated this to the energy stored and dissipated in equivalent capacitors and resistors. Each element of the circuit thus represented a specific mechanism of energy storage or dissipation. They were also able to relate the size of each component to the physical parameters of the coil and the constitutive parameters of the lossy core.

Based on the similarity between the input impedance curve obtained for the semi-cylindrical solenoid and the curve presented by Vermeulen and Chute (1983) for the cylindrical solenoid, the same equivalent circuit (figure 3.7) is used here to represent the semi-cylindrical solenoid. Here C_2 , R_2 , C_e , and R_e represent (respectively) the energy stored and dissipated within the target material

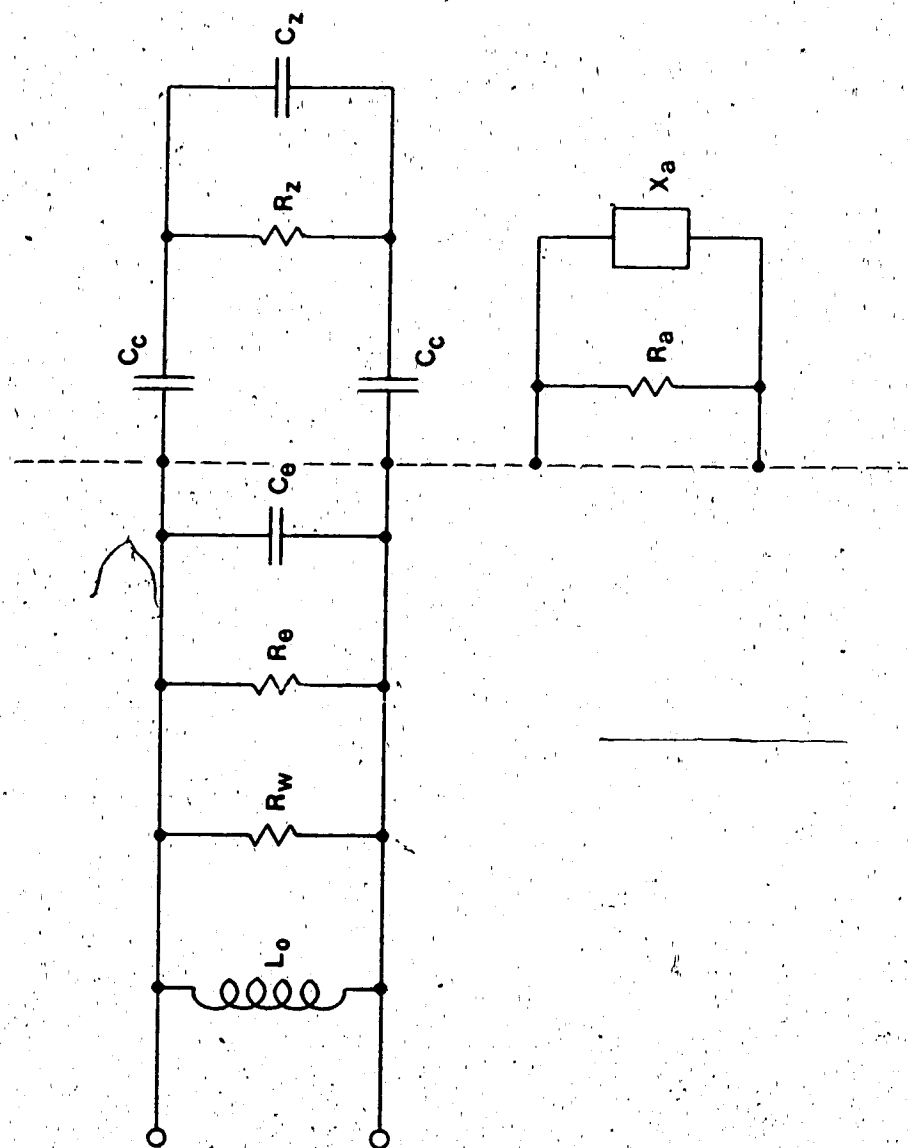


Figure 3.7

Low-Frequency Equivalent Circuit

by the conservative and non-conservative electric fields of the semi-cylindrical solenoid. L_0 represents the energy stored within the coil's magnetic field, R_v accounts for the resistive losses in the coil winding, and C_c represents the capacitance of the insulating gap between the coil and target material. A detailed development of this circuit was presented by Vermeulen and Chute (1983). Only the details relevant to the present discussion are reviewed here.

The input resistance of the proposed circuit (the reciprocal of the input conductance) is given by the parallel combination of R_v , R_e , and R_a , where

$$R_a = \frac{(2X_z X_c)^2 + R_z^2 (X_z + 2X_c)^2}{R_z X_z^2} \quad [3.5]$$

It has been shown that if R_e and R_z are assumed to vary inversely with $\hat{\sigma}$,

$$R_e = k_e / \hat{\sigma} \quad [3.6]$$

$$R_z = k_z / \hat{\sigma} \quad [3.7]$$

then R_a reaches a minimum value of R_a^m at $\hat{\sigma}^m$. By differentiating R_a with respect to $\hat{\sigma}$ and setting the result to zero, it can be shown that

$$R_a = \frac{1}{2} R_a^m \left[\frac{\hat{\sigma}}{\hat{\sigma}^m} + \frac{\hat{\sigma}^m}{\hat{\sigma}} \right] \quad [3.8]$$

The measured values of the coil input resistance (R_{IN}) and the resistive losses in the coil winding (R_v) are plotted against $\hat{\sigma}$ in figure 3.8. As in the equivalent circuit development, R_{IN} is assumed to be the parallel combination of R_v and another component, R_{a0} , which accounts for the losses induced in the target material. R_{a0} is itself

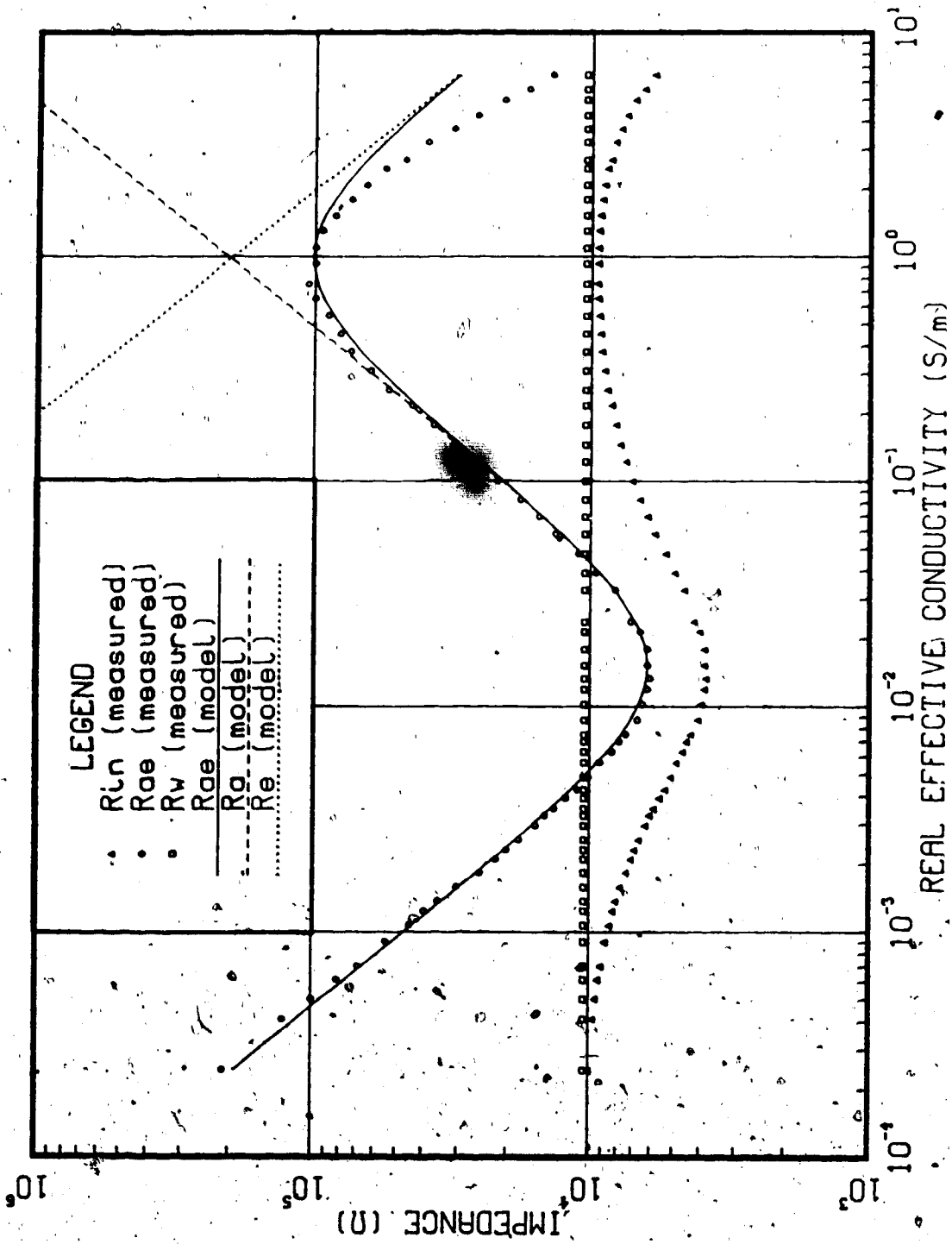


Figure 3.8 Low-Frequency Equivalent Circuit Component Values versus Target Material Conductivity

the parallel combination of R_a and R_e . Values of R_{ae} were calculated from the measured values of R_{IN} and R_v according to

$$R_{ae} = [R_{IN}^{-1} - R_v^{-1}]^{-1}, \quad [3.9]$$

and are plotted as " R_{ae} (measured)" in figure 3.8. From this curve values of R_a^m and $\hat{\sigma}^m$ can be determined, since at conductivities comparable to $\hat{\sigma}^m$, R_e is many orders of magnitude larger than R_a , so that R_{ae} is approximately equal to R_a . The values of R_a^m and $\hat{\sigma}^m$ so obtained were inserted into equation 3.8 to generate values of R_a . These values are plotted in figure 3.8 as " R_a (model)". A value of k_e was then selected to give the closest fit between R_{ae} (measured) and R_{ae} (model), which is the parallel combination of R_a (model) and R_e (model). Values of R_e (model) were generated by inserting this 'best-fit' value of k_e into equation 3.6. Curves corresponding to R_e (model) and R_{ae} (model) are also plotted in figure 3.8.

The assumption made that R_v should be constant is reasonably accurate since the shift in frequency as the target material conductivity is increased is very small in this case. The poor correlation between R_{ae} (model) and R_{ae} (measured) at conductivities greater than 1 S/m can be attributed to changes in the field distribution as the skin depth in the saline solution becomes comparable to the dimensions of the coil, as well as to the fundamental differences between the fields generated by this device and those generated by the cylindrical solenoid, on which the

model is based.

The impedance values generated by the proposed circuit are found to agree well with those measured. It is clear that for frequencies well below self-resonance, the equivalent circuit devised for the cylindrical solenoid accurately represents the semi-cylindrical solenoid as well. The elements of the circuit must thus represent the same mechanisms of energy storage and dissipation in both cases.

3.3.2 Self-Resonant Cases

At frequencies where the length of the coil is comparable to a wavelength, the coil is not well represented by a lumped equivalent circuit. Here the coil must be viewed as a distributed network, whose per unit length component values vary along the length of the coil to account for the nonuniform nature of the coupling between the coil and target material (Vermeulen and Chute 1983, pp. 95).

While circuits were devised which generated the same general variation of impedance with target material conductivity, the components of these circuits could not be linked to specific mechanisms of energy storage and dissipation. The use of such circuits is thus of limited value and was not pursued further.

Chapter 4

Distribution of Heating

The purpose of this chapter is to study in detail the geometry of the electric field generated within the target material by the semi-cylindrical solenoid. Of particular interest are the depth to which significant heating penetrates, and the axial distribution of that heating.

The author's primary interest is in possible biomedical applications of this device. The choice of target material conductivity for the following investigation was motivated by this interest.

4.1 Electric Field Distributions

The electric field distribution generated within the target material was measured using two nonperturbing dipole probes. Each of the four modes of coil excitation considered in Chapter Three was examined. These modes are low-frequency excitation, one-half wavelength self-resonance, one wavelength self-resonance, and two wavelength self-resonance. The conductivity of the target material was adjusted to a value characteristic of muscle tissue. Contour plots are presented which display the magnitudes of the field components produced. Conclusions are drawn regarding the relative contributions of the conservative and non-conservative electric fields. The direction of the conservative electric field vector is determined at each measurement point. The distributions of relative electric

energy density are computed from the measured electric field distributions and plotted.

4.1.1 Procedure

For this investigation a sheet of 0.13 mm (0.005 in) polyethylene was placed over the coil. The wooden box was then filled with saline solution whose conductivity was adjusted to 0.5 S/m. Within the range of frequencies considered here, this value is typical of muscle tissue at normal physiological temperature (Stoy *et al* 1982, pp. 508; Pethig 1979, pp. 228). Hagmann *et al* (1985) reported a value for muscle tissue which is 50 percent larger than this, but accepted 0.5 S/m as being representative of the volume-average of tissues within a torso or limb. The temperature of the solution was maintained at approximately 25°C. In each case the coil was energised using enough power to produce suitable field strengths. Input power levels were not recorded.

Two dipole probes were used to measure the Cartesian components of the electric field generated within the saline solution. The presence of the probes was observed to have a negligible effect on the input impedance of the coil. The design and construction of the probes and associated instrumentation is described in Appendix B. Measurements were made in the x-z plane of the coil' at 2 cm intervals

*The rectangular coordinate system associated with the coil is defined by equating the longitudinal axis of the coil with the z-axis and centering the coil about the origin. The flat side of the coil lies in the y-z plane with the

from $x=2$ cm to $x=14$ cm, and from $z=+24$ cm to $z=-24$ cm, using each of three mutually orthogonal dipole orientations. The flat side of the coil occupies the $y-z$ plane from $y=+5.25$ cm to $y=-5.25$ cm, and from $z=+20$ cm to $z=-20$ cm.

4.1.2 Results

The electric field measurement data are tabulated in tables C.5(a) to C.8(c) of Appendix C. These data are also used to generate contour plots of relative field strength, shown in figures 4.1 to 4.12. In each case the field strength is plotted in decibels relative to the maximum value of the radial (E_x) component measured at that frequency.

4.1.3 Discussion

The plots of electric field strength clearly show that at this conductivity the contribution of the conservative electric field to the total observed heating is in all cases much larger than the contribution of the non-conservative circumferential electric field. The plot of the axial electric field (E_z) obtained for the one wavelength self-resonant case (12.8 MHz) compares well with the plots obtained by Ruggera and Kantor (1984) for the electric field just outside of a cylindrical solenoid excited at one wavelength.

'(cont'd) positive x-axis extending into the target material. This is also shown in figure 1.1.

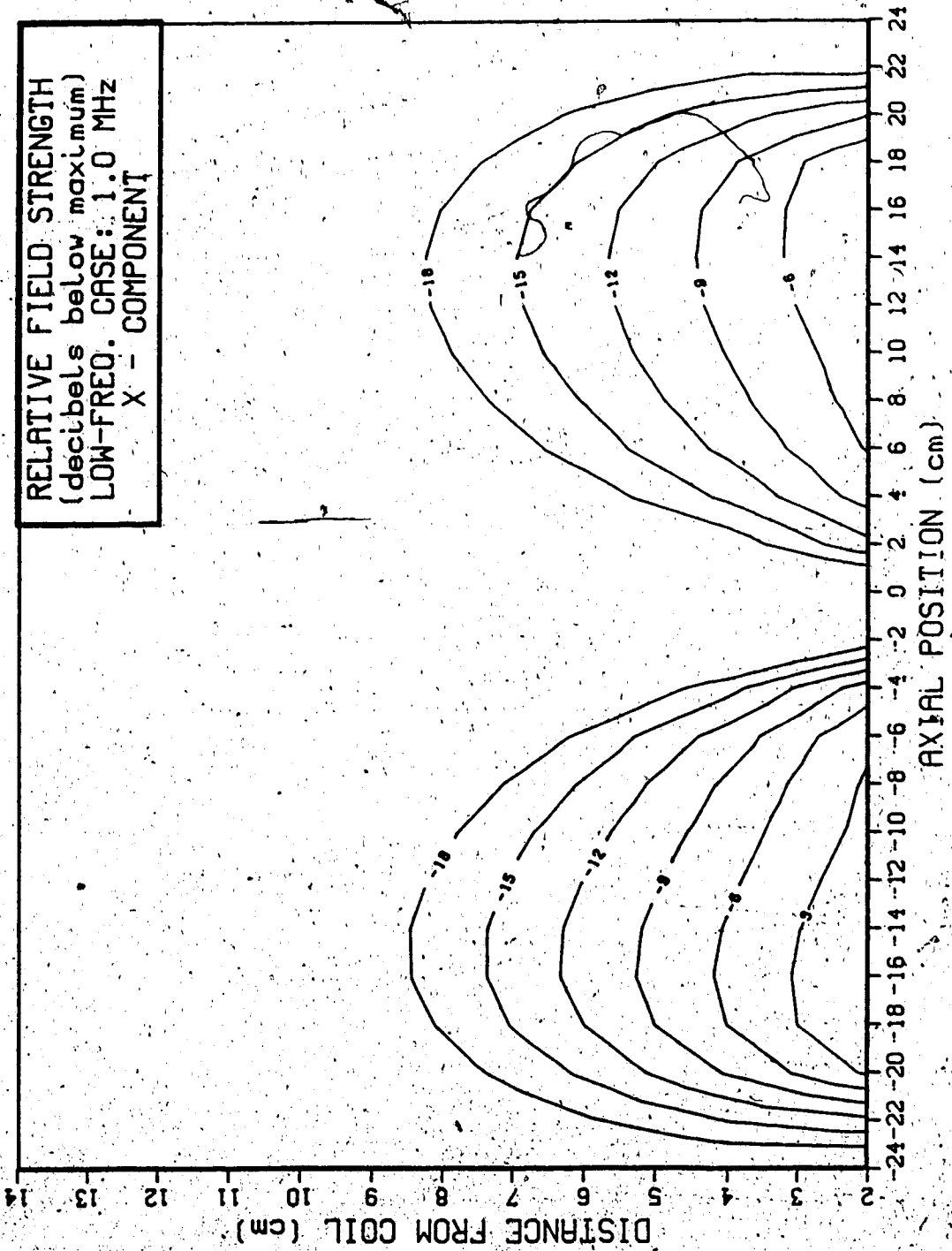


Figure 4.1

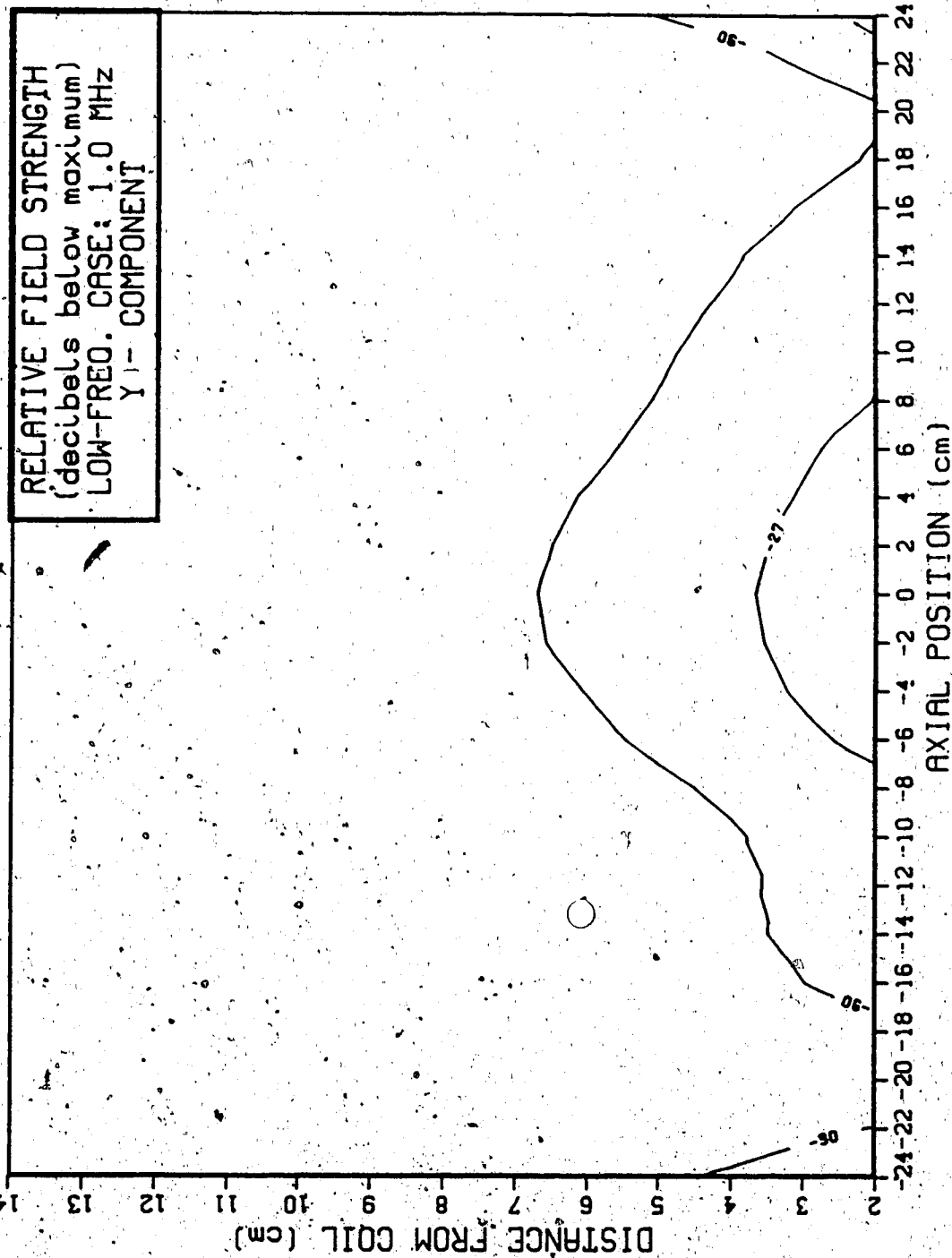


Figure 4.2

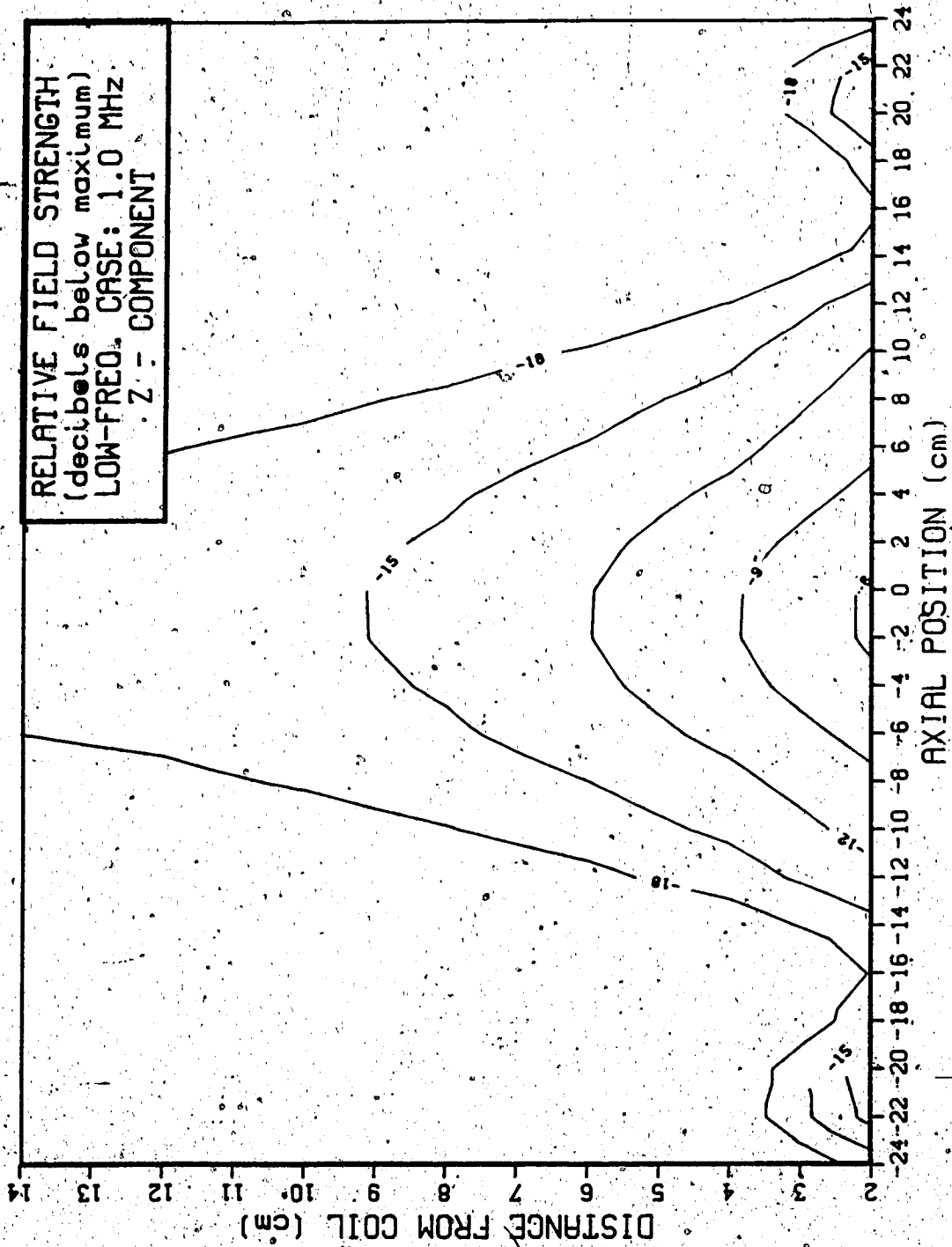


Figure 4.3

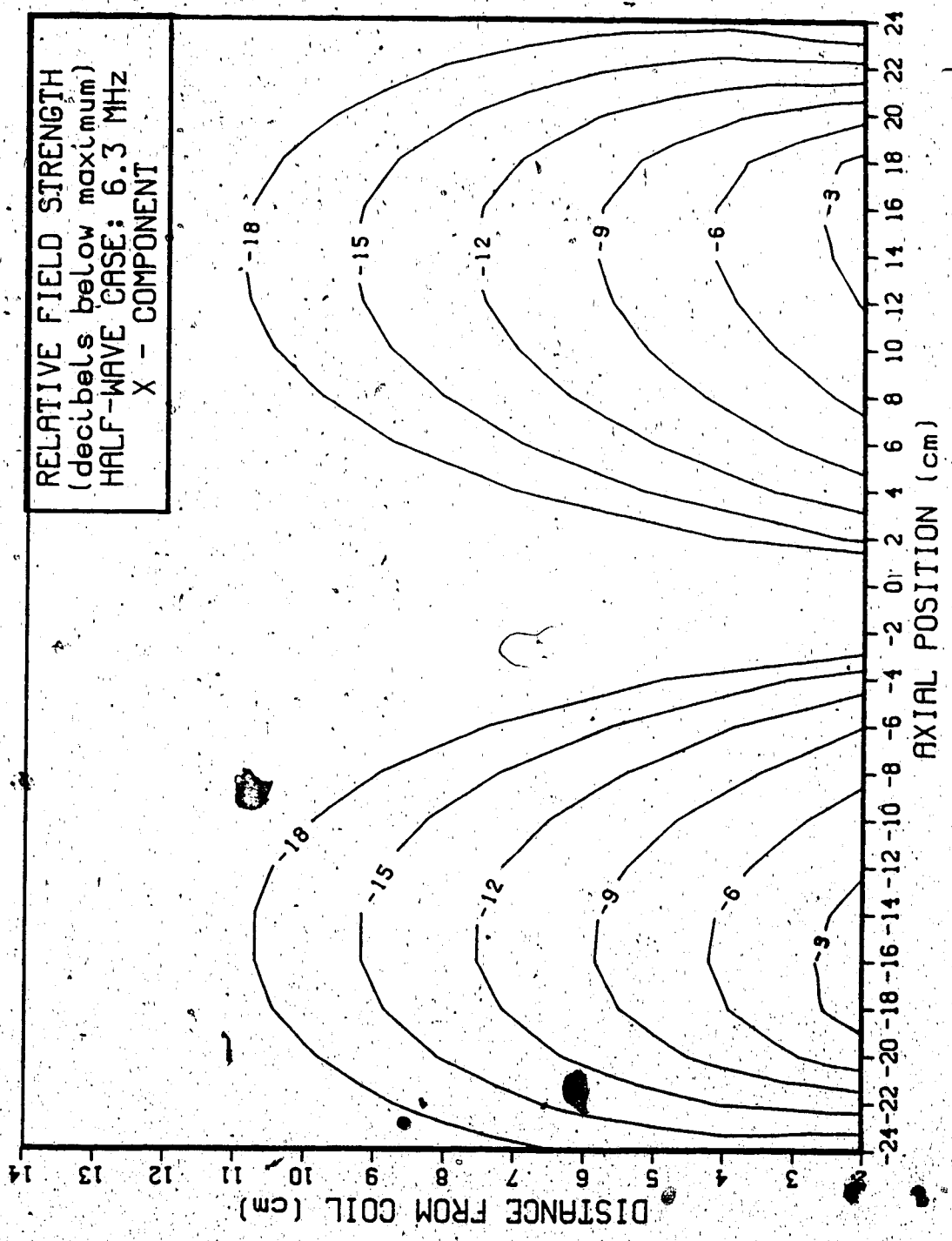


Figure 4.4

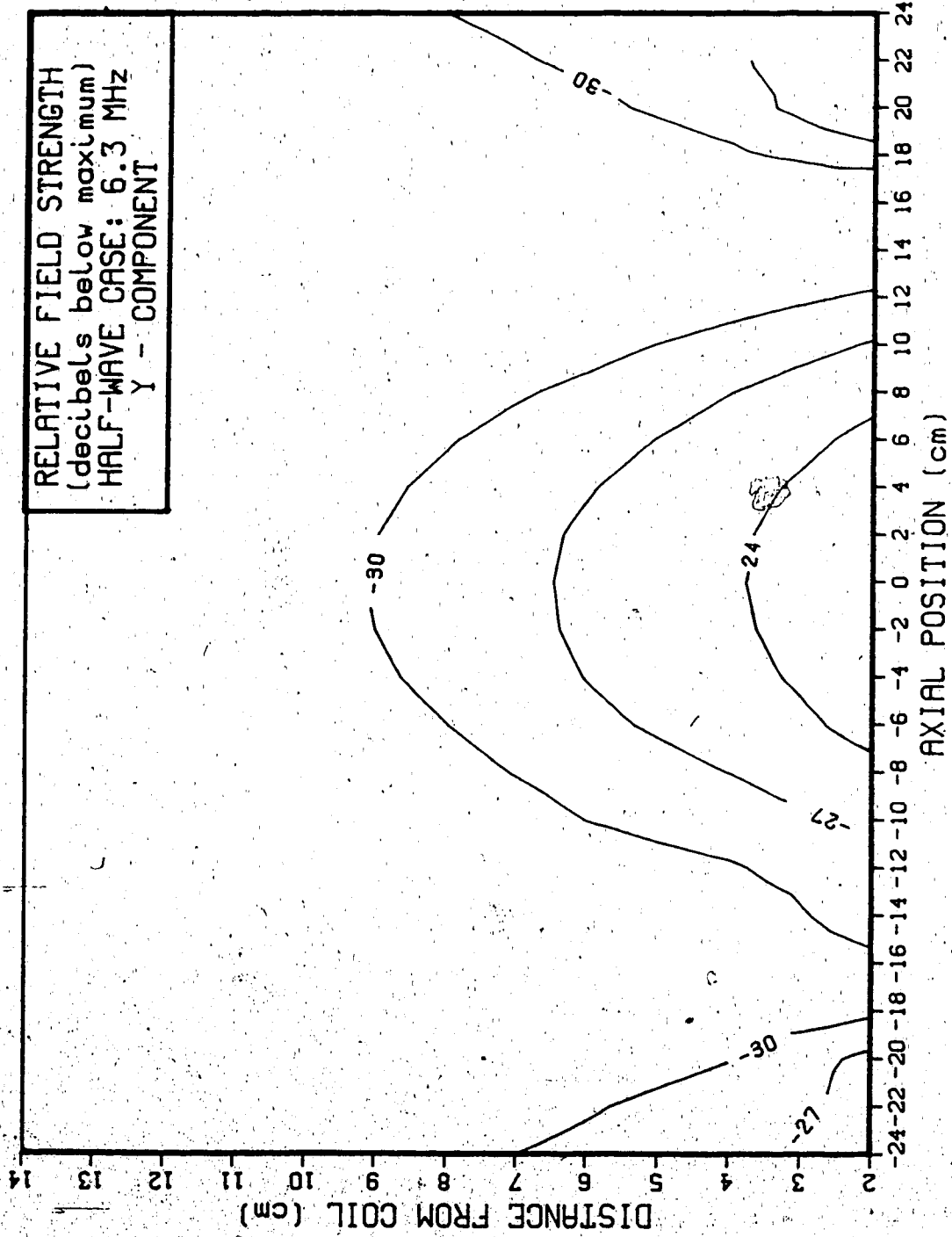


Figure 4.5

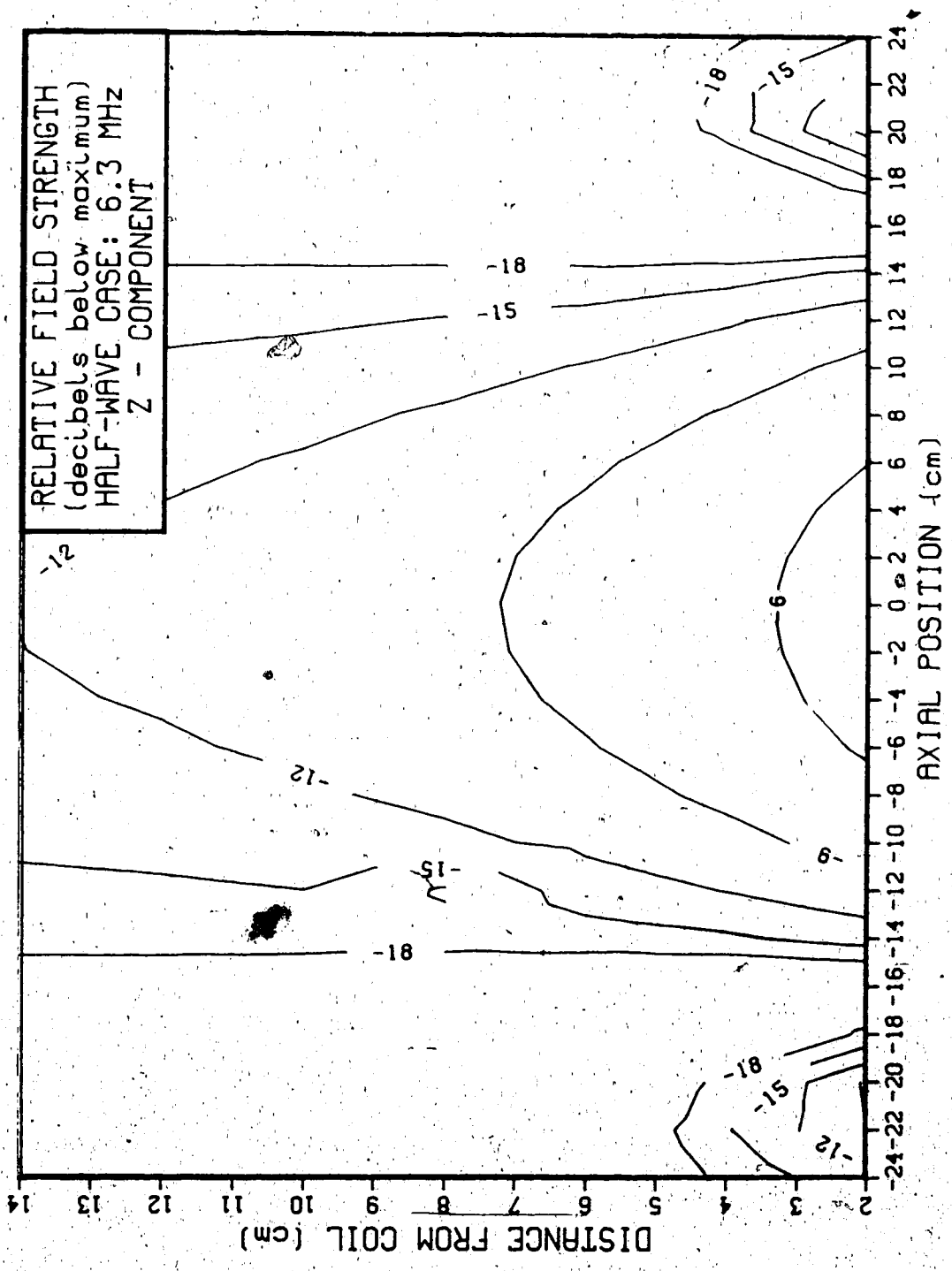


Figure 4.6

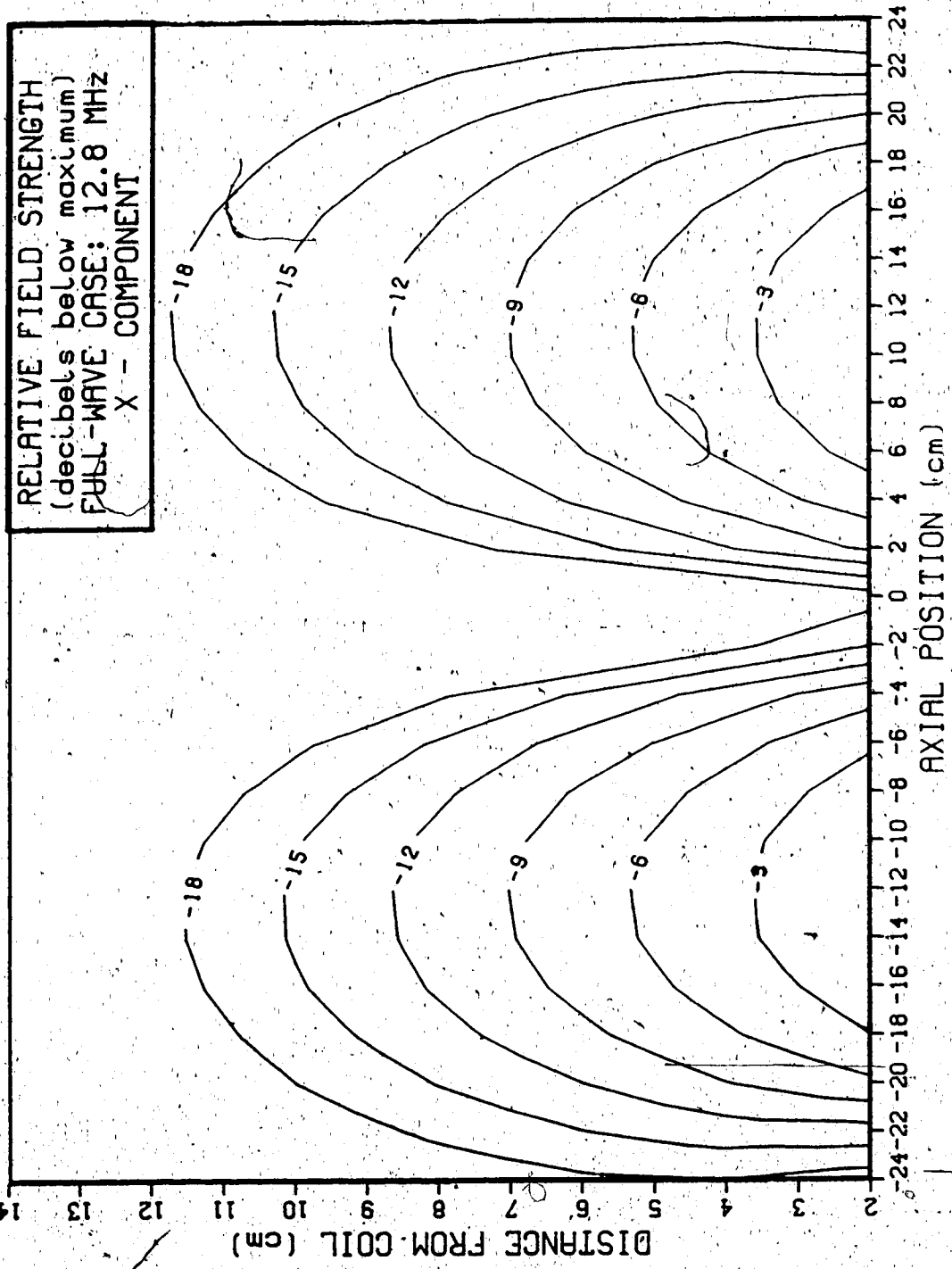


Figure 4.7

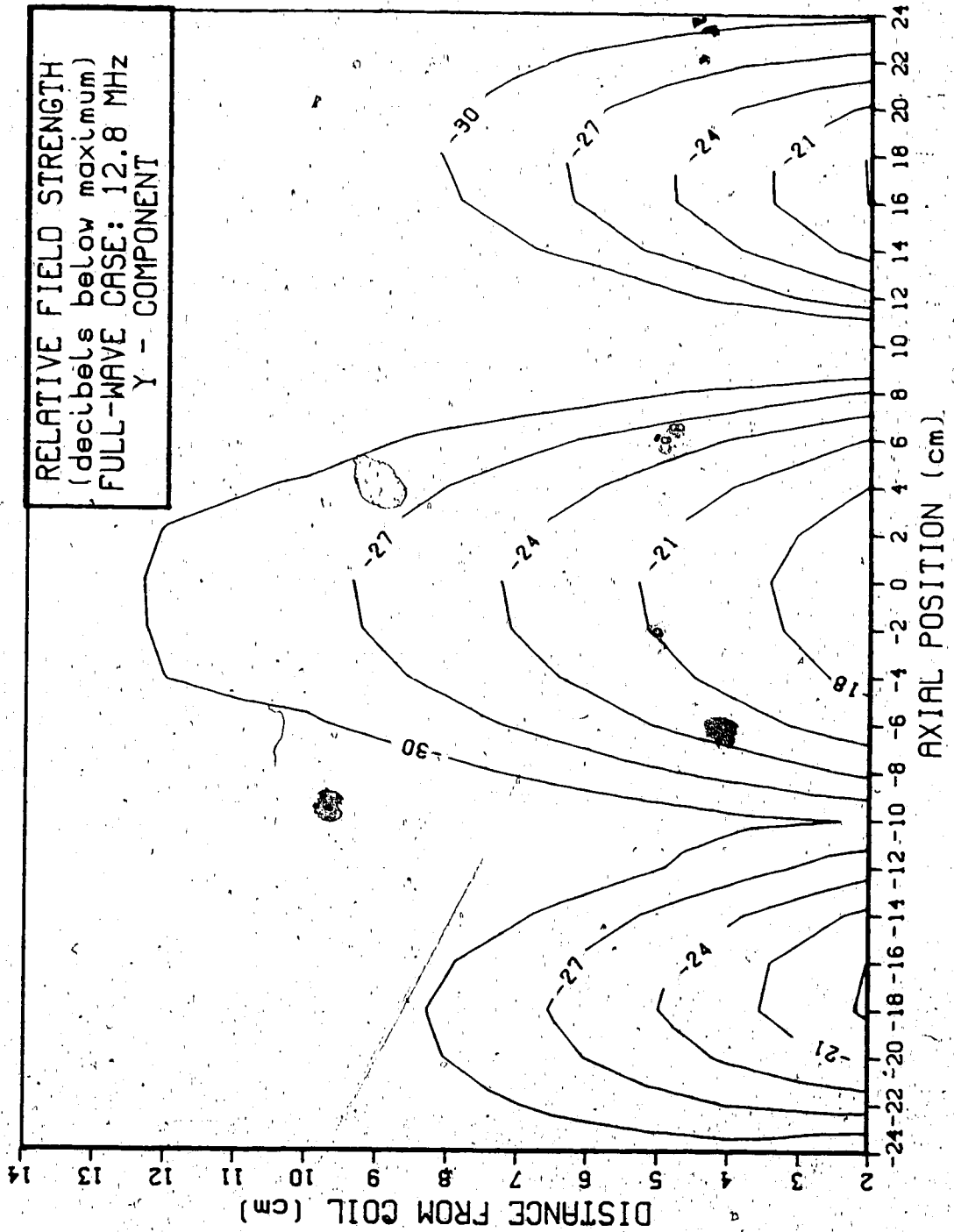
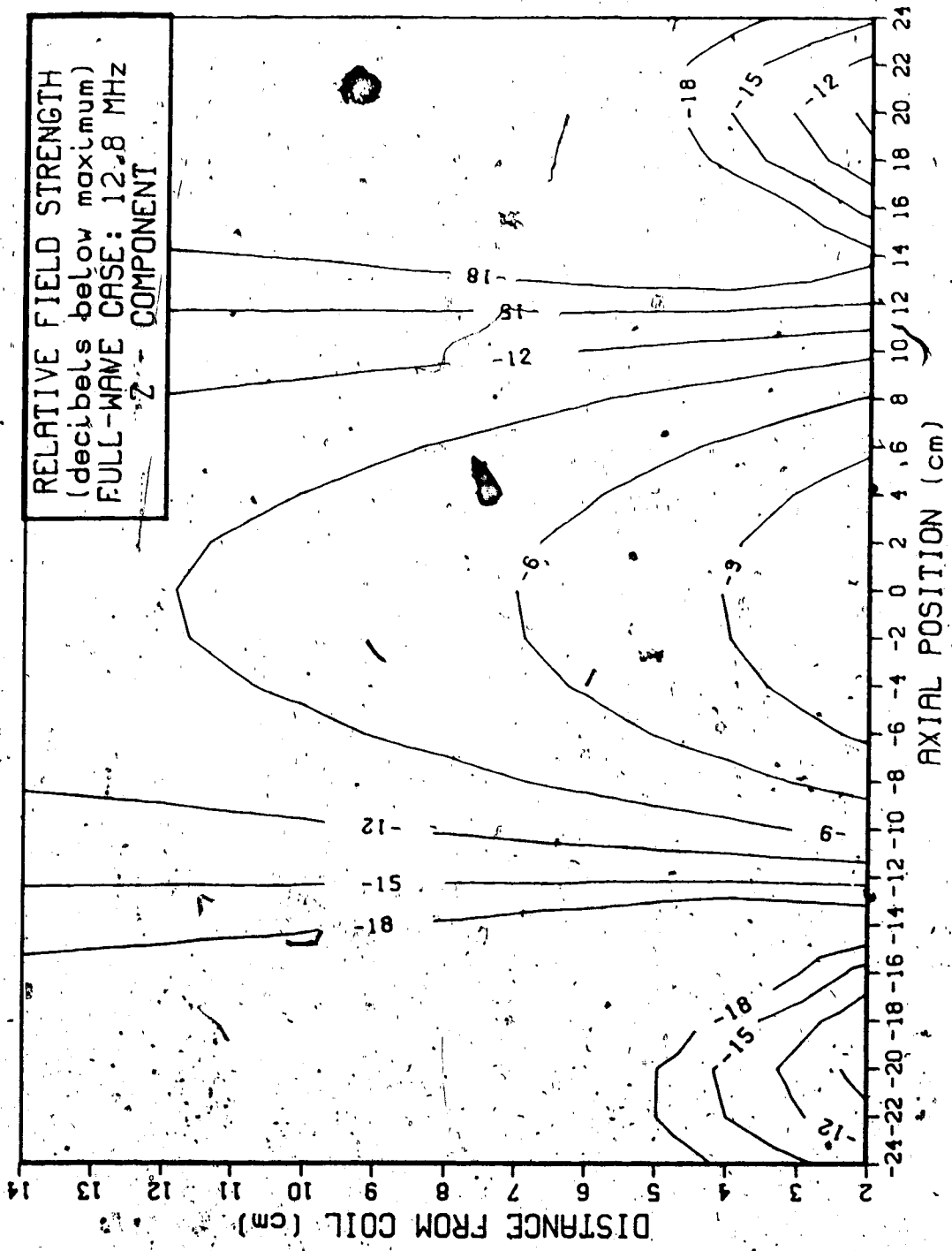


Figure 4.8



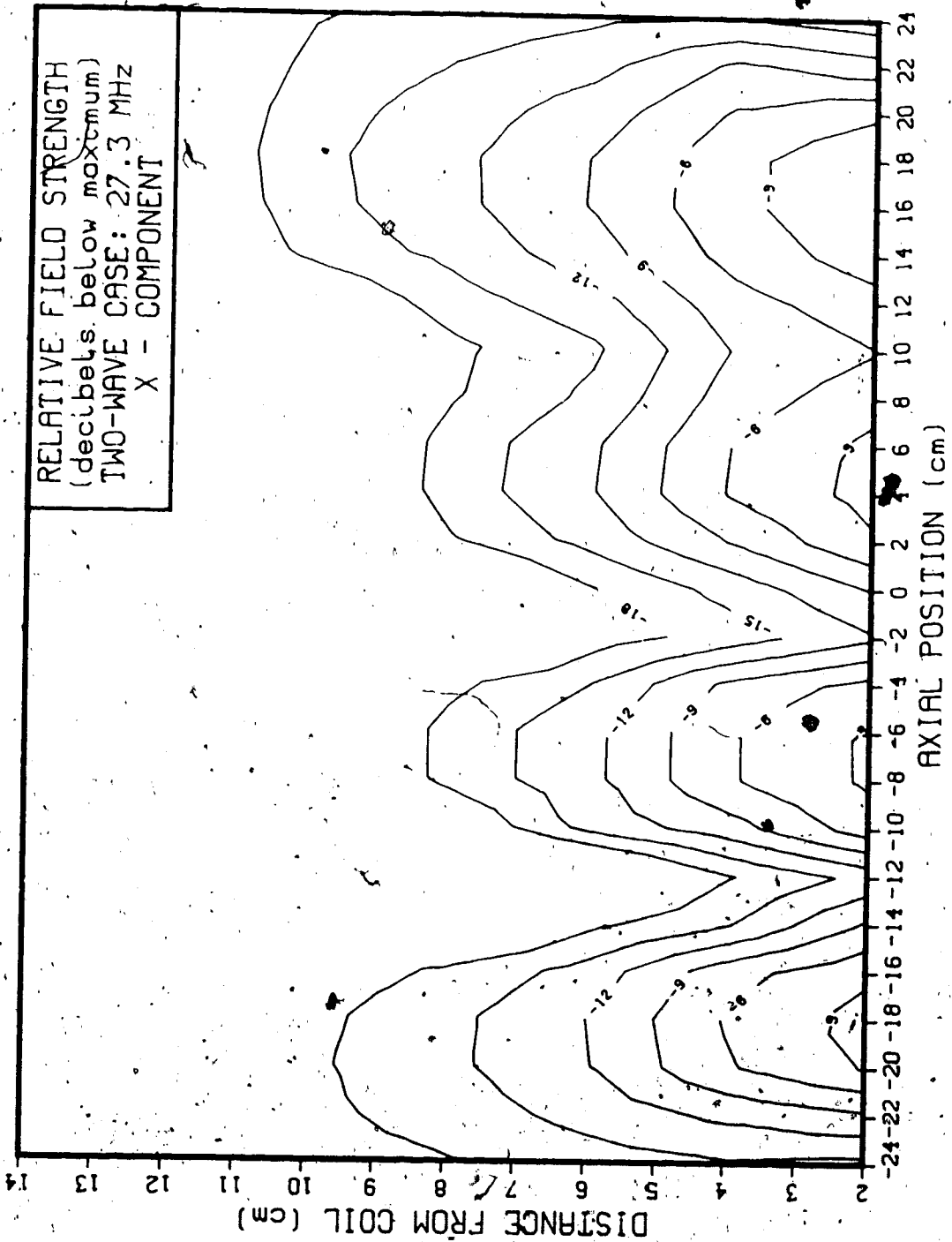


Figure 4.10

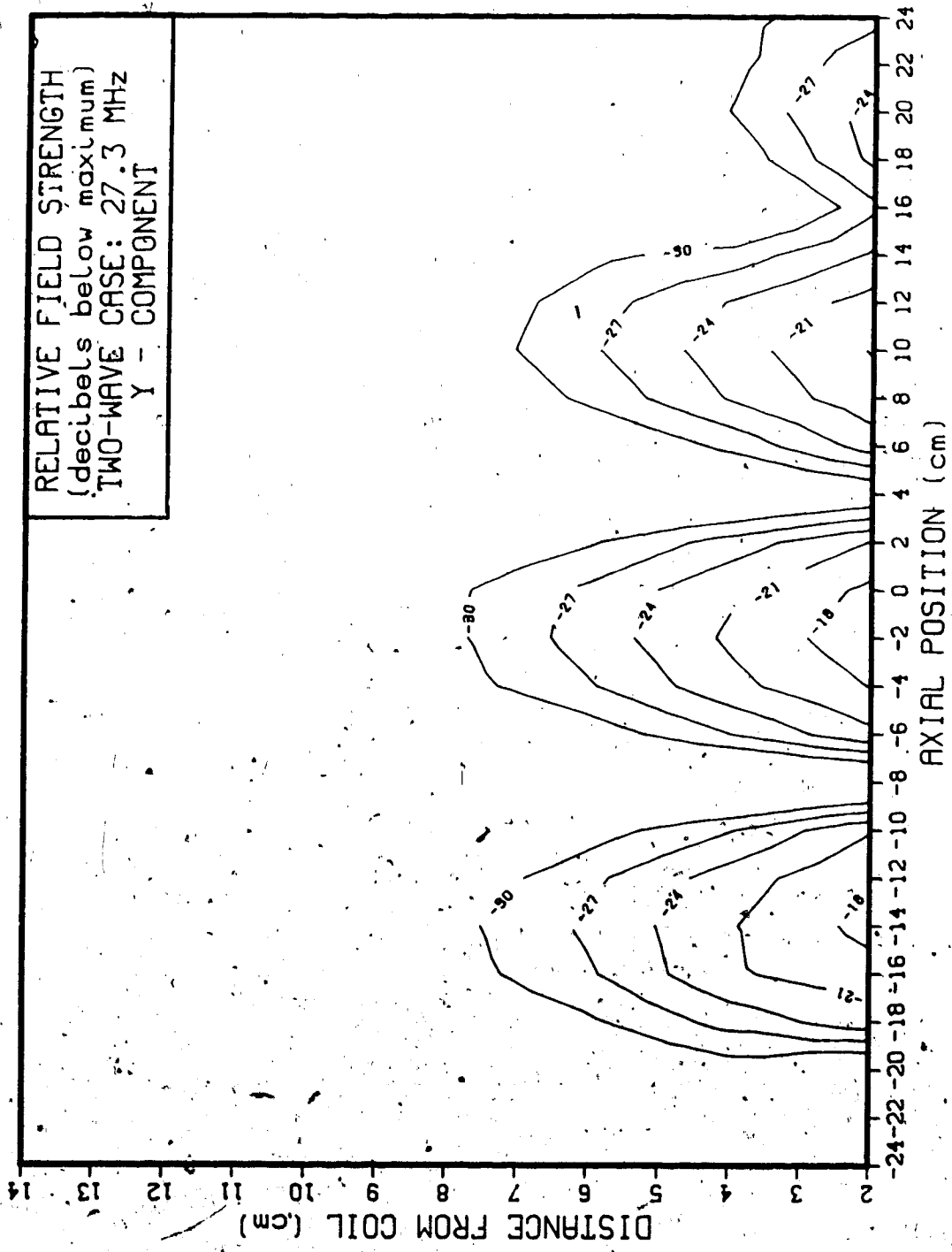


Figure 4.11

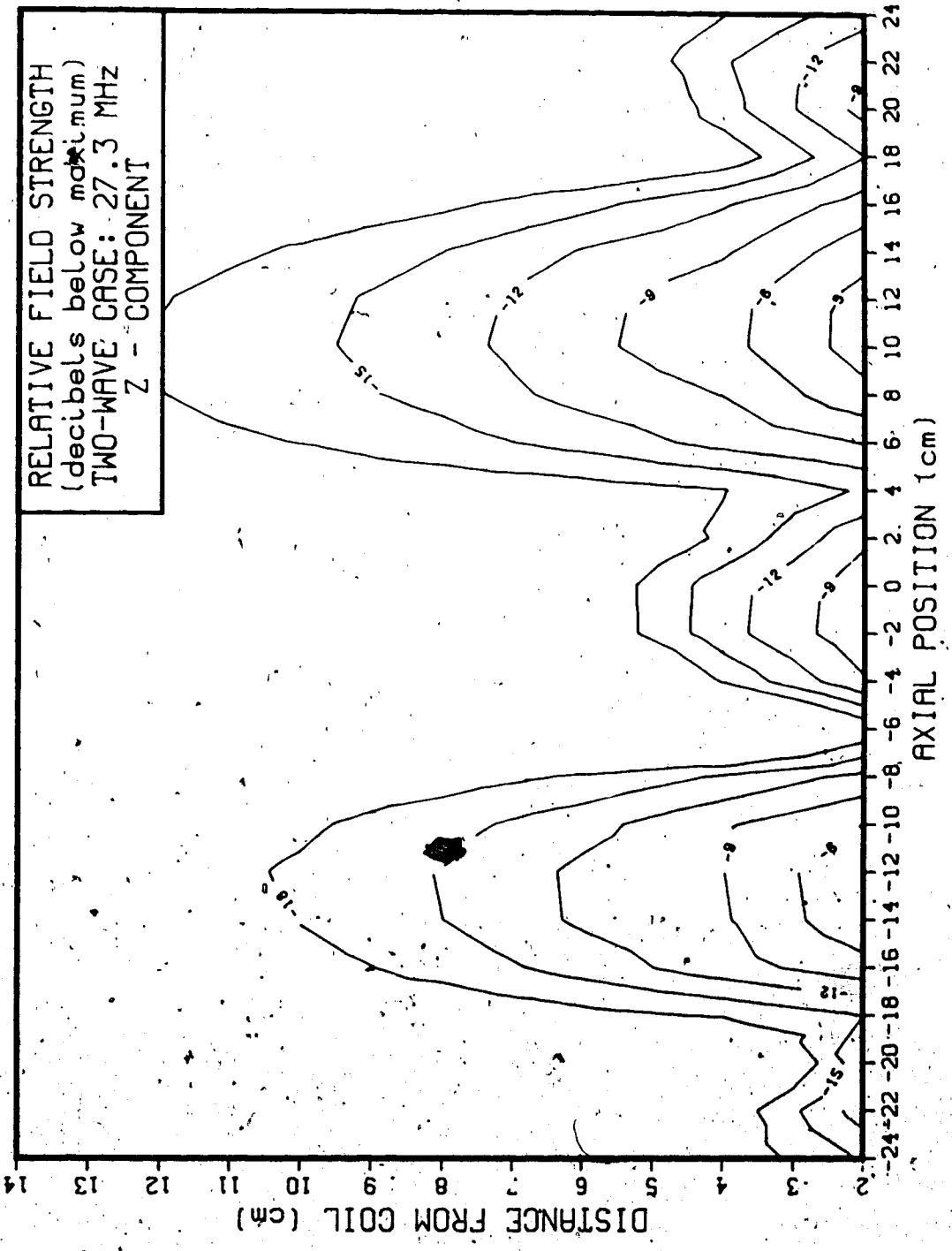


Figure 4.12

4.2 Conservative Electric Field Vector

The axial (E_z) and radial (E_x) electric fields are, in the x-z plane, components of the conservative electric field generated by the semi-cylindrical solenoid. This field is produced by the distribution of charge on the coil winding, and (in free space) generates the displacement currents discussed earlier. The conservative electric field is responsible for most of the power dissipation observed in the target material.

In figures 4.13 to 4.16 the conservative electric field vector is reconstructed at each measurement point and represented by a line segment. The length of each line segment is proportional to the magnitude of the conservative field, and its orientation is parallel to the field.

These plots show that the basic shape of the conservative electric field remains relatively unchanged until the length of the coil exceeds one wavelength. Closer inspection also suggests that as the frequency is increased, the lines of force of this field stay closer to the coil surface, and their penetration into the target material becomes more shallow. This agrees with what might be expected considering the decreasing skin depth of the saline solution as the frequency is increased. The existence of a strong conservative electric field in the 1 MHz case is not predicted by the idealized distributions of current and potential discussed in Chapter Two. This field is generated by the accumulation of charge near the coil extremities, as

discussed by Chyte and Vermeulen (1982).

4.3 Power Dissipation

In figures 4.17 to 4.20, plots of relative electric energy density, calculated as

$$\frac{|E_x|^2 + |E_y|^2 + |E_z|^2}{(|E_x|^2 + |E_y|^2 + |E_z|^2)_{\max}} \quad [4.1]$$

are presented. Here E_x , E_y , and E_z are the measured values of the three orthogonal electric field components at each measurement point. Contour values are in decibels relative to the maximum electric energy density measured at that frequency. Since the saline solution is homogeneous, the resulting plot is exactly identical to the relative distribution of power dissipation within the target material.

The plots generated display the same features as the heating patterns generated in Chapter Two, with the exception of the 1 MHz case. They also agree with the results obtained by Ruggera and Kantor (1984) and by Hagmann *et al* (1985) for the cylindrical solenoid. In all cases heat is generated almost entirely by the conservative electric field. The localization of this heating toward the ends of the coil in the 1 MHz and 6.3 MHz cases reflects the primarily radial direction of the field near the coil ends, as in these cases the electric lines of force penetrate deep into the target material. The more uniform heating distributions over the length of the coil at 12.8 MHz and over each half of the coil at 27.3 MHz reflect the more shallow penetration of the electric lines of force

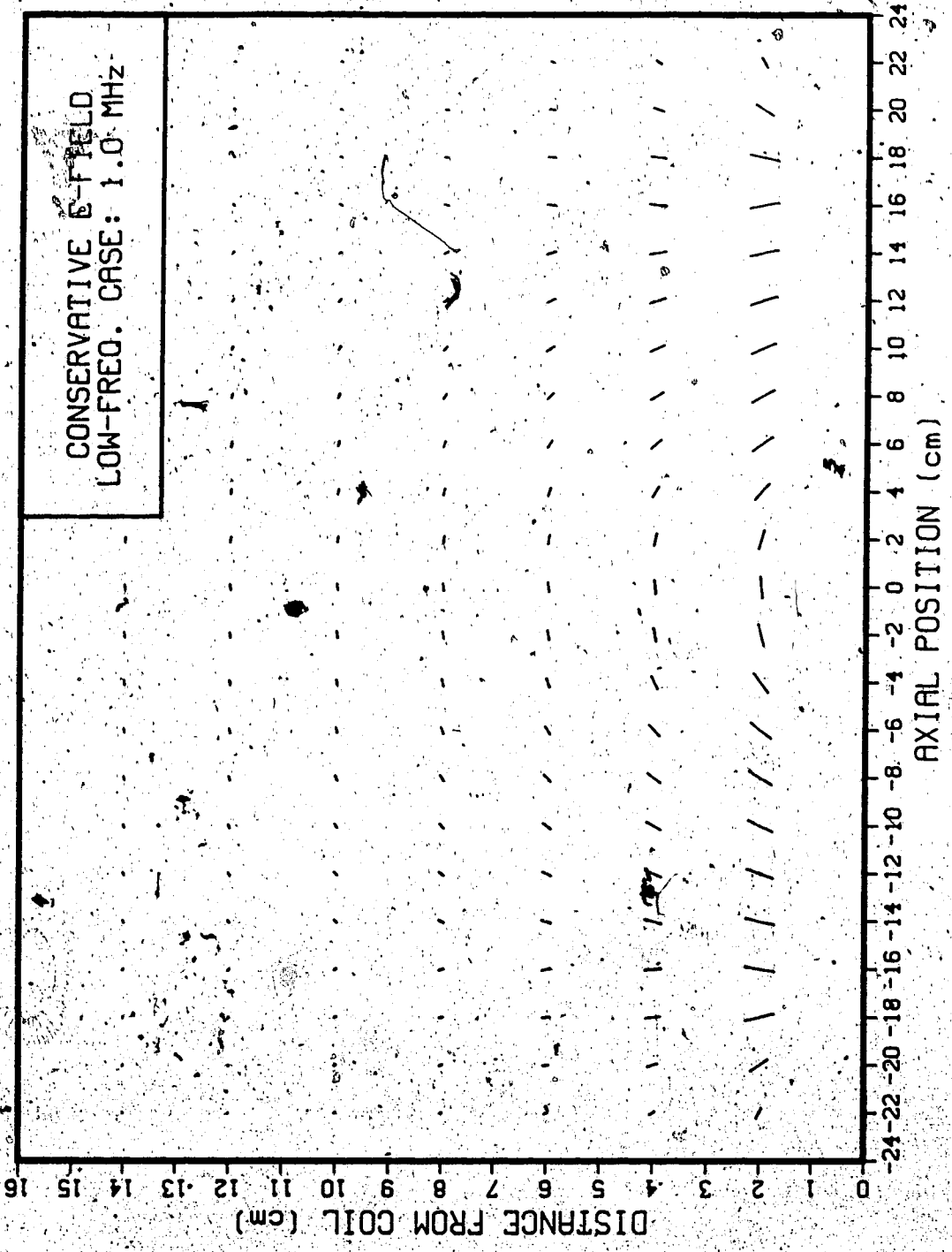


Figure 4.13

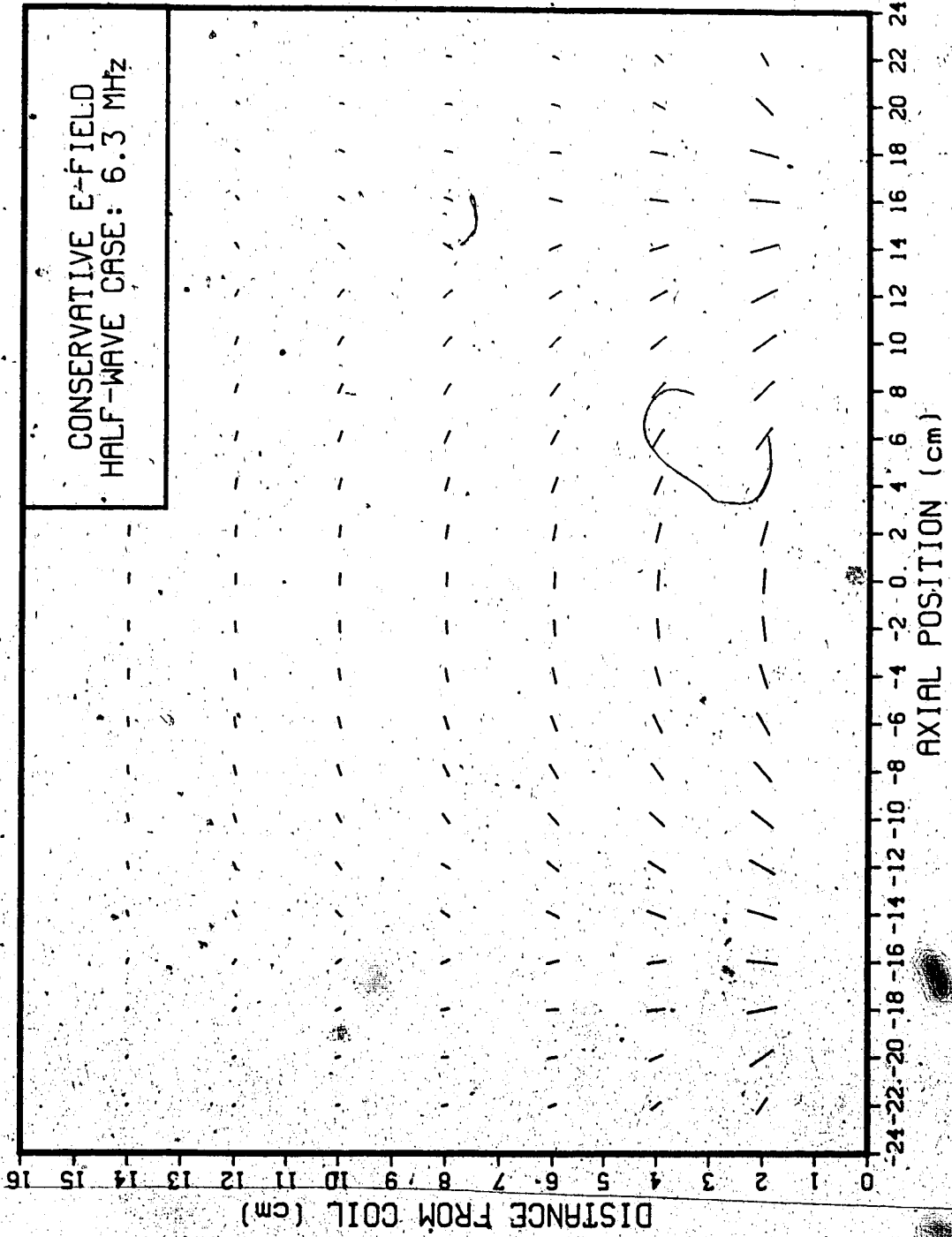


Figure 4.14

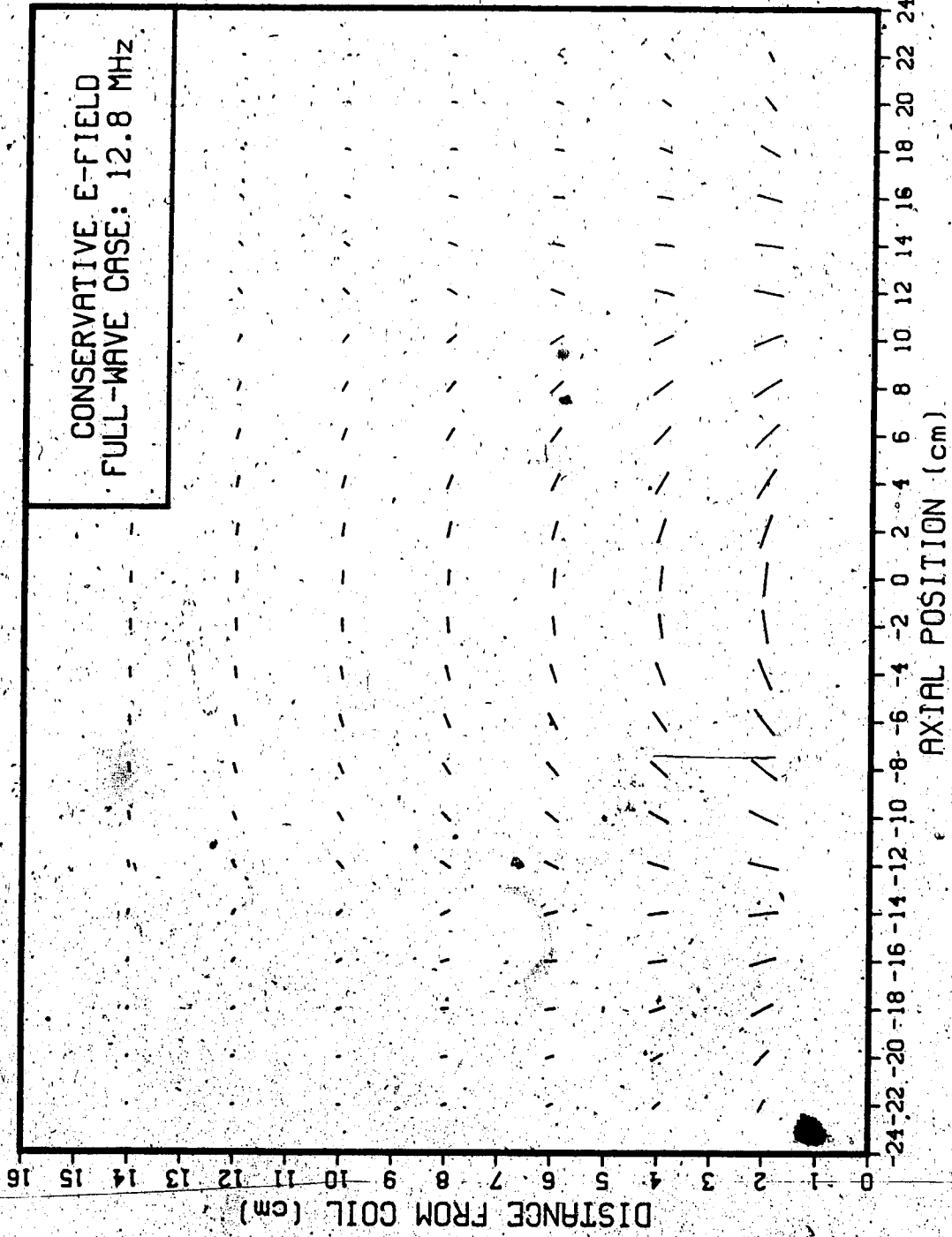


Figure 4.15

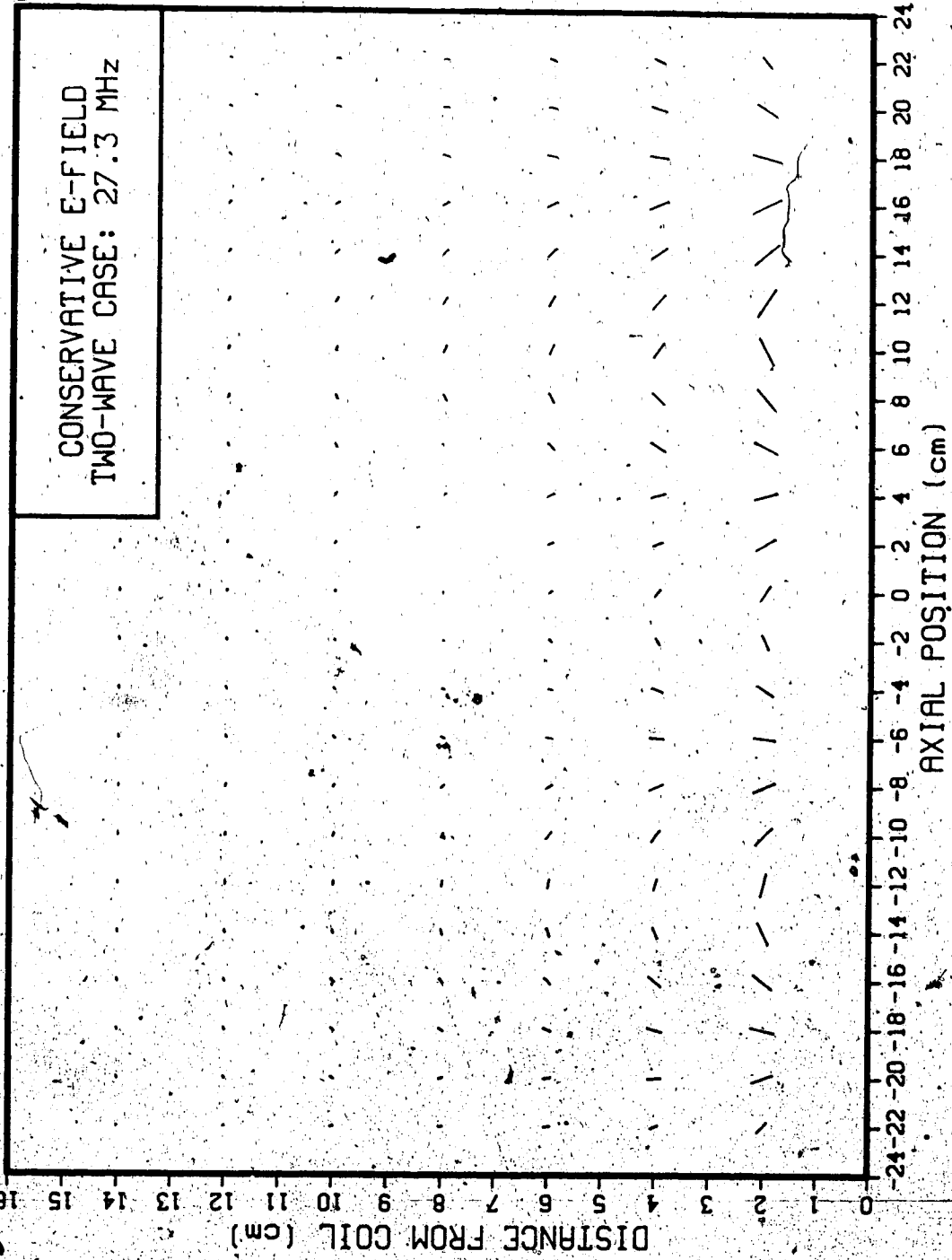


Figure 4.16

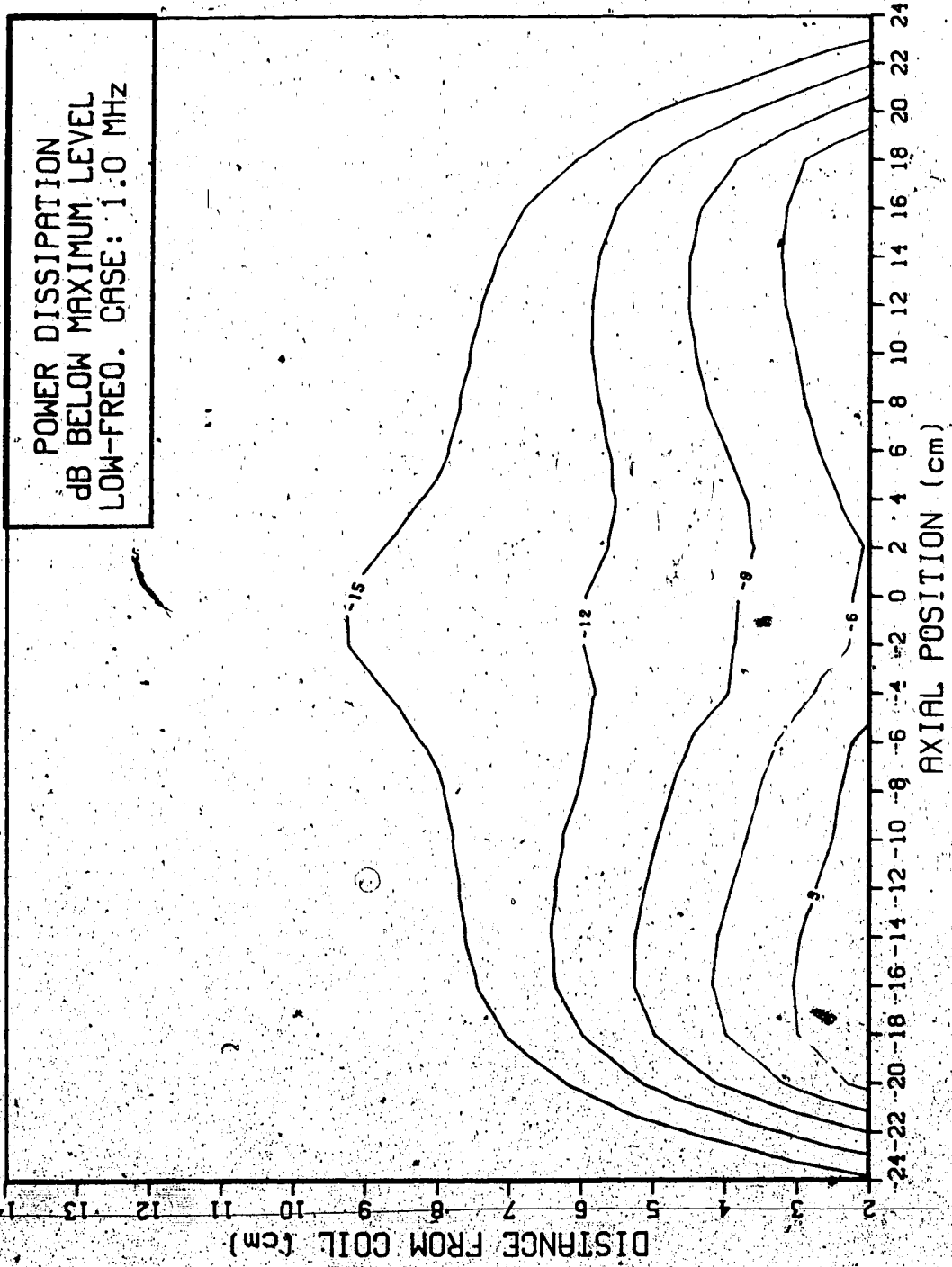


Figure 4.17

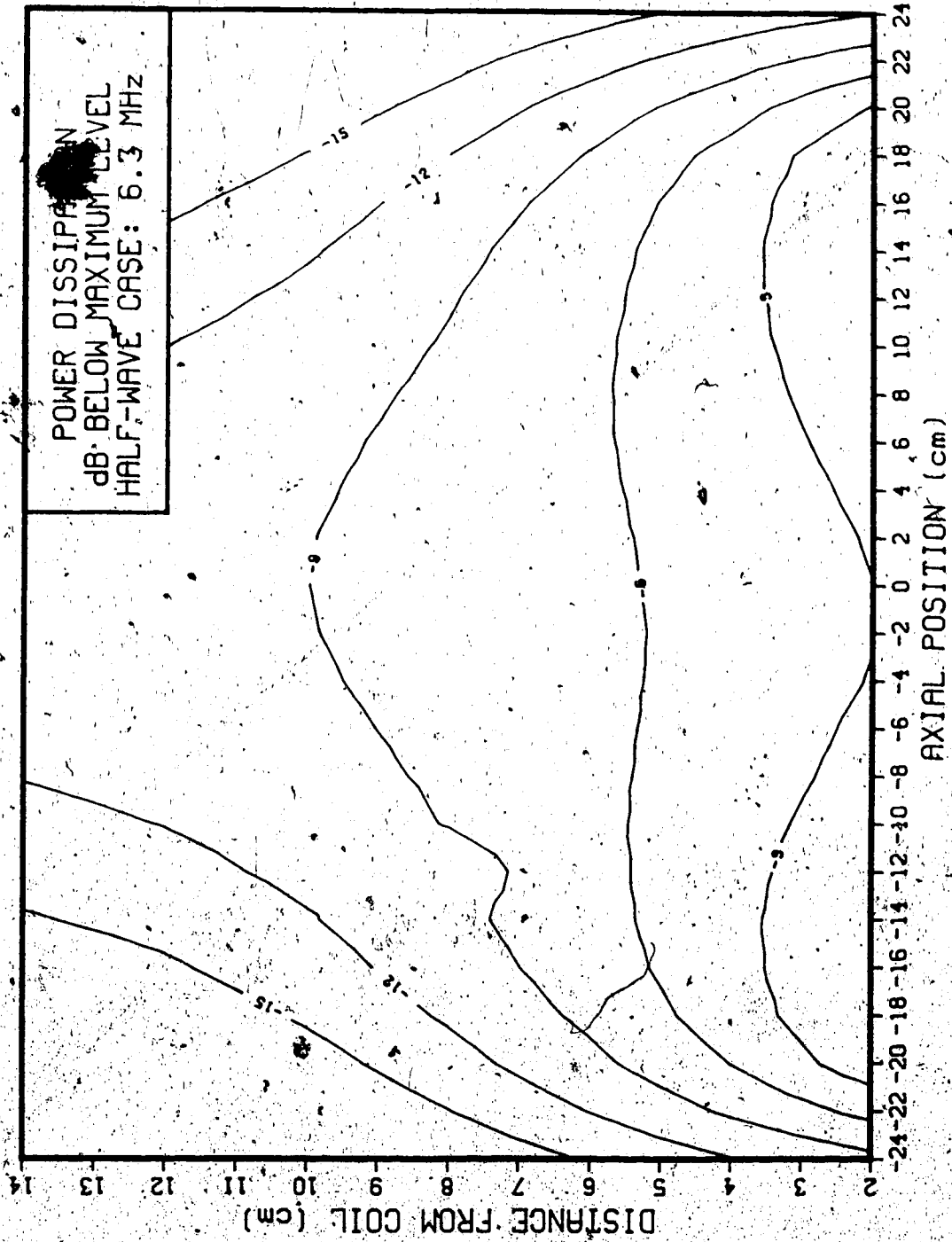


Figure 4.18

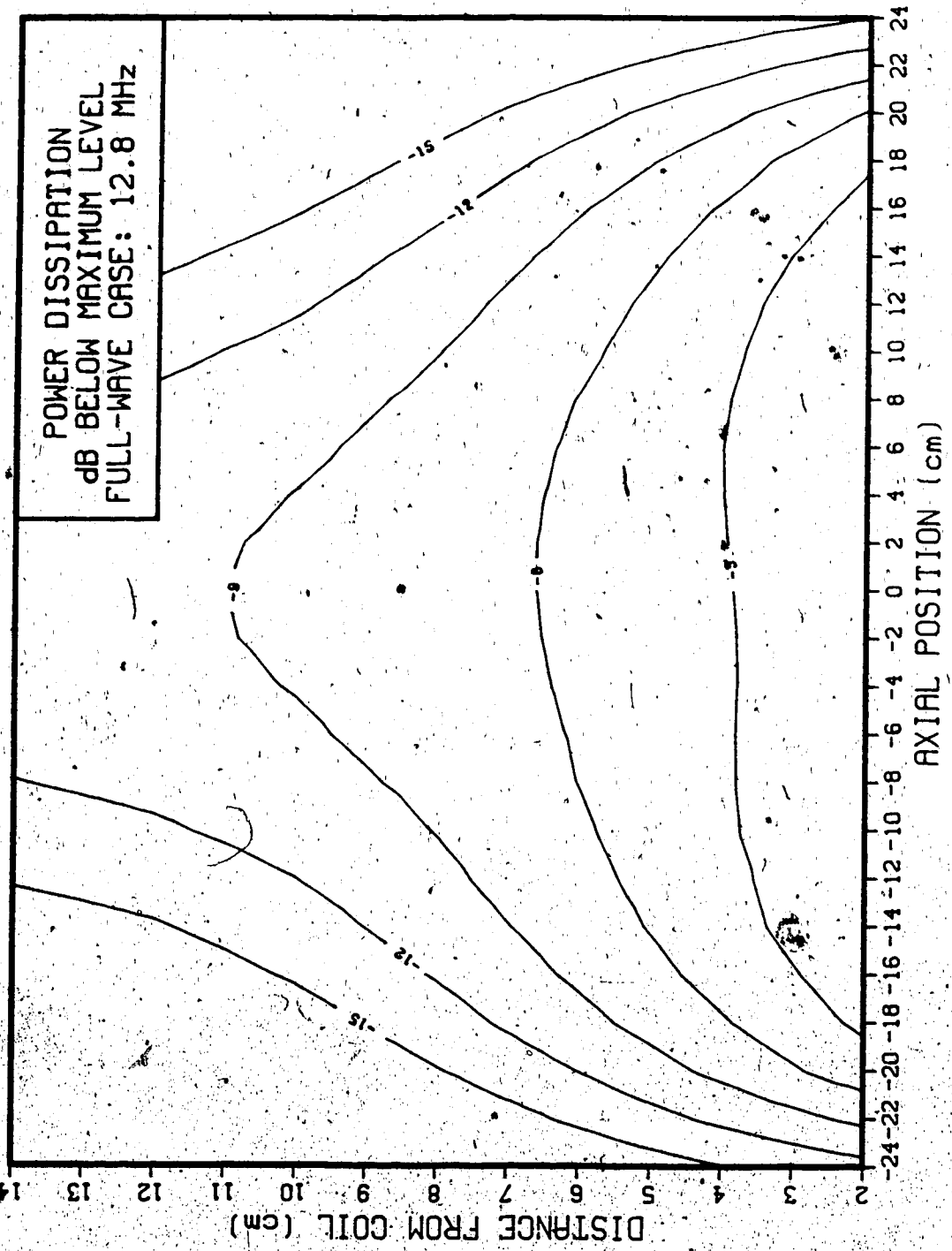


Figure 4.19

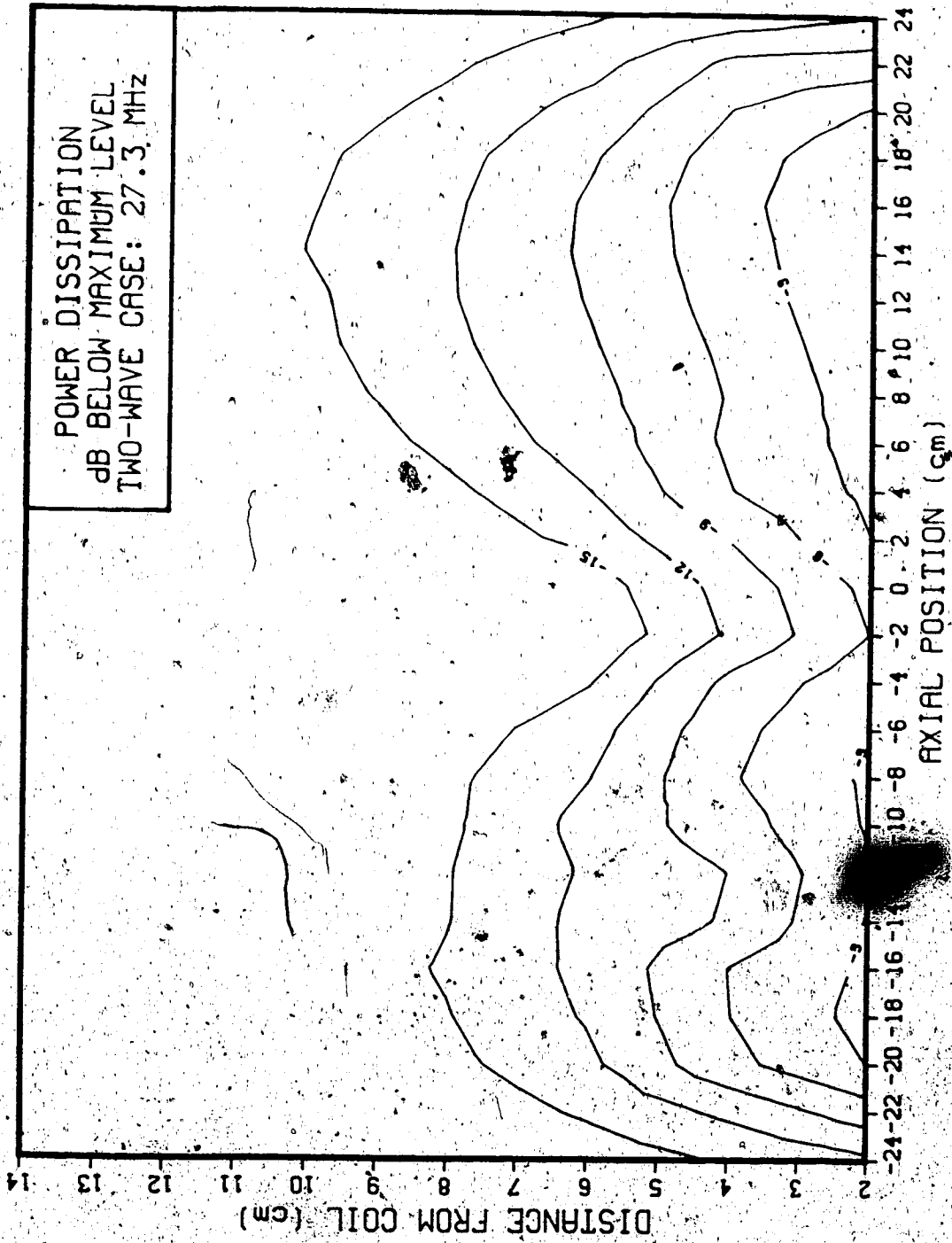


Figure 4.20

of the conservative field in these cases.

The heating patterns generated for the low-frequency case (figure 4.17) and the two wavelength self-resonant case (figure 4.20) were produced using unbalanced excitation, since balanced and unbalanced excitation were shown earlier to produce nearly identical current distributions in these cases. This was also the method used by Ruggera and Kantor (1984). The asymmetry in these heating patterns demonstrates that in these cases, balanced and unbalanced excitations will not produce exactly the same current distribution unless the power entering the coil is zero. In the two wavelength case the potential at both ends of the coil is ideally zero, so that the input impedance also goes to zero at self-resonance. If power is being delivered to the coil then a finite voltage must exist at one end to account for the nonzero input impedance. The current distribution is no longer symmetric, and the excitation can no longer be considered balanced. The asymmetry in the distribution of power dissipation at 1 MHz demonstrates that at this frequency the current distribution on the coil has started to become slightly nonuniform.

The results of this investigation show that even under optimal conditions, the semi-cylindrical solenoid deposits most of its energy near the surface of the target material.

Chapter 5

Summary

In this chapter the experimental work is summarized, and the main conclusions are presented. The possibility for further research is outlined.

5.1 Review

The purpose of this investigation has been to study the semi-cylindrical solenoidal coil as a possible applicator for radiofrequency heating of low conductivity materials.

Four modes of coil excitation have been examined, corresponding to the length of the coil being much shorter than a wavelength, approximately equal to one-half wavelength, approximately equal to one wavelength, and approximately equal to two wavelengths. The effects of balanced versus unbalanced excitation on the heating patterns generated by the device in each of these four modes have been studied. The observed behavior has been explained in terms of the ideal distributions of current and potential on an infinite, lossless solenoidal coil.

The input impedance of the semi-cylindrical solenoid has been measured as a function of the conductivity of an adjacent volume of saline solution, for each of the four modes of excitation described. An estimate of the efficiency of the device has thus been obtained for each of these four modes, and for target material conductivities extending over five orders of magnitude. An equivalent circuit devised to.

represent the cylindrical solenoid at frequencies well below self-resonance is examined, and is found to accurately represent the semi-cylindrical solenoid under these conditions.

Two non-perturbing dipole electric field probes and associated instrumentation are designed and built. These are used to measure the electric field generated within the target material by the semi-cylindrical solenoid for each of the four modes of excitation previously described. The nature of the fields generated by the device is elucidated, and comparison is again made to the ideal distributions of current and potential on an infinite, lossless solenoidal coil. Plots of relative power dissipation are also produced, which clearly show where in the target material heating is generated.

5.2 Conclusions

The solenoidal coil is an inherently balanced device: it is physically symmetric with respect to the feed point. If this symmetry is to be preserved in its electrical behavior, then the coil must be excited in a balanced manner. Physical symmetry with respect to ground should also be sought when positioning the device. While unbalanced excitation may produce satisfactory performance in cases where approximately the same current distribution is produced by both balanced and unbalanced excitations (frequencies where the coil length is equal to a multiple of whole wavelengths), it is apparent that even at these frequencies

a small degree of asymmetry must exist in the current distribution produced on the coil. In addition to perturbing the heating pattern this asymmetry in the current distribution implies that a finite amount of displacement current must flow from the coil surface to ground through a path external to the coil. Such a flow of displacement current has been shown to be hazardous.

Some investigators have suggested operating solenoidal coils in self-resonant modes. Ruggera and Kantor (1984) suggest that this would simplify the task of impedance matching. Indeed, it was shown in Chapter Three that the device can operate very efficiently when its length becomes comparable to a wavelength. However, where the operating frequency is required to coincide with a designated ISM (Industrial, Scientific, and Medical) frequency, this is clearly not practical. The electric and magnetic field distributions, and thus the self-resonant frequencies of the coil, are affected by the constitutive parameters of the target material. The only way to "tune" such a device to resonance for a given target material would be to adjust the coil dimensions or the length of the coil winding. This was done by Ruggera and Kantor (1984). The alternative is to operate the coil between resonant modes, and externally "resonate" the coil with a variable reactance. This is most easily done where the input reactance of the coil is inductive, so that a variable capacitor can be used. An appropriate matching and balancing network is shown in figure

5.1.

While operation at frequencies well below self-resonance has the advantage of a well-developed equivalent circuit, it has been shown that the semi-cylindrical solenoid is not particularly efficient in this case.

The results obtained in this investigation indicate that while the traditional solenoidal coil is capable of producing uniform, deep heating in cylindrical objects, the semi-cylindrical solenoid is more applicable to the heating of surface layers.

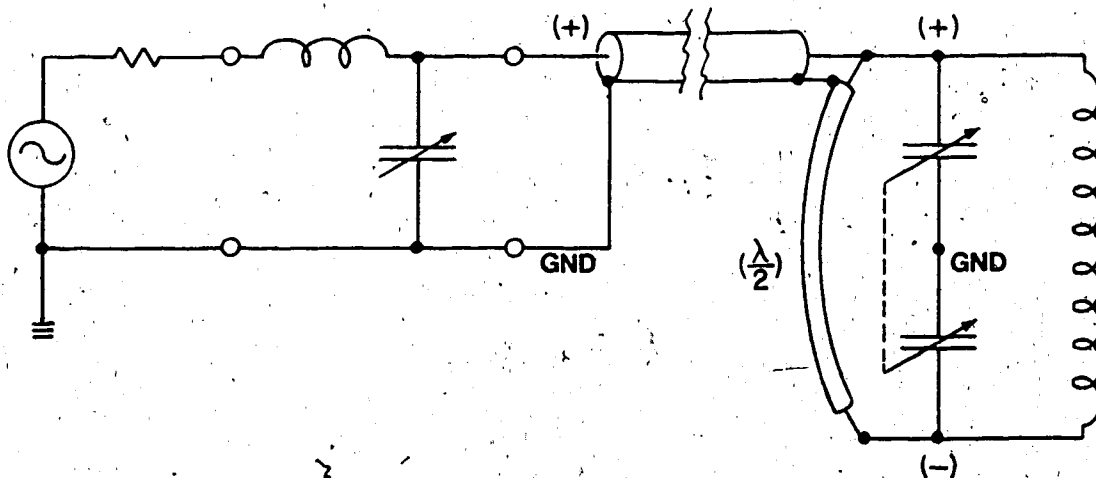


Figure 5.1

Balancing and Matching Network

5.3 Further Research

The results of this investigation indicate that the semi-cylindrical solenoid could be a useful tool both for the therapeutic heating of biological tissues, and the heating or thawing of earth-type materials. In both of these cases the effects of a layered, anisotropic target material must be evaluated. For further investigation of potential biomedical applications, a target material whose permittivity more closely models that of biological tissues must also be found.

Further work to optimize the coil dimensions may be fruitful. Other modifications, such as varying the pitch distance, or the coil radius, or both, over the length of the coil might help to optimize the device for specific applications. The use of metal foil rather than a round conductor to produce a tape helix of the same shape has been reported to improve the performance of the cylindrical solenoid (Hagmann *et al* 1985). This too should be evaluated.

Bibliography

- Bassen, H.I., and Smith, G.S., 1983. "Electric Field Probes - A Review". *IEEE Trans. Antennas and Propagation*, 31(5), pp. 710-718.
- Bleaney, B.I., and Bleaney, B., 1976. *Electricity and Magnetism, 3rd Ed.* London: Oxford University Press.
- Cheremisinoff, P.N. (Ed.), Farah, O.G. (Ed.), and Ouellette, R.P. (Ed.), 1985. *Radio Frequency/Radiation and Plasma Processing*. Lancaster, Pennsylvania: Technomic Publishing Company Ltd.
- Chute, F.S., Vermeulen, F.E., and Cervenak, M.R., 1981. "On the electromagnetic heating of low-loss materials using induction coils". *Can. Elec. Eng. J.*, 6(1), pp. 20-28.
- Chute, F.S., and Vermeulen, F.E., 1981. "A Visual Demonstration of the Electric Field of a Coil carrying a Time-Varying Current". *IEEE Trans. Education*, 24(4), pp. 278-283.
- Chute, F.S. and Vermeulen, F.E., 1982. "On the Self-capacitance of Solenoidal Coils". *Can. Elec. Eng. J.*, 7(2), pp. 31-37.
- Coelho, R., 1979. *Physics of Dielectrics for the Engineer*. Amsterdam: Elsevier Scientific.
- Cole, K.S., and Cole, R.H., 1941. "Dispersion and Absorption in Dielectrics". *J. Chemical Phys.*, 9, pp. 341-351.
- Elliott, R.S., 1966. *Electromagnetics*. New York: McGraw-Hill Inc.
- Franks, F., ed., 1973. *Water: A Comprehensive Treatise. Volume 3 - Aqueous Solutions of Simple Electrolytes*. New York: Plenum Press. Chapter 8.
- Fujino, M., Masuda, Y., Gozu, T., and Ichijo, B., 1981. "No contact system for measuring liquid conductance at high frequencies". *IEEE EEMTC Digest*, pp. 225-228.

- Gardiner, D., 1982. "Field Solution for a Lossy Sheath Helix". M.Sc. Thesis, Department of Electrical Engineering, University of Alberta, 432 pages.
- Hagmann, M.J., 1984. "Propagation on a Sheath Helix in a Coaxially Layered Lossy Dielectric Medium". *IEEE Trans. Microwave Theory and Techniques*, 32(1), pp. 122-126.
- Hagmann, M.J., and Levin, R.L., 1984. "Analysis of the Helix as an Applicator for Hyperthermia". *Electronics Letters*, 20(8), pp. 337-338.
- Hagmann, M.J., and Levin, R.L., 1985. "Coupling Efficiency of Helical Coil Hyperthermia Applications". *IEEE Trans. Biomedical Eng.*, 32(7), pp. 539-540.
- Hagmann, M.J., Levin, R.L., and Turner, P.F., 1985. "A Comparison of the Annular Phased Array to Helical Coil Applicators for Limb and Torso Hyperthermia". *IEEE Trans. Biomedical Eng.*, 32(11), pp. 916-927.
- Hasted, J.B., 1973. *Aqueous Dielectrics*. London: Chapman and Hall Ltd. Chapter 6.
- Hulls, P.J., 1982. "Development of the Industrial Use of Microwave Heating in the United Kingdom". *J. Microwave Power*, 17(1), pp. 29-35.
- Johnk, C.T.A., 1975. *Engineering Electromagnetic Fields and Waves*. New York: John Wiley and Sons, Ltd.
- King, R.W.P., and Smith, G.S., 1981. *Antennas in Matter*. Cambridge, Massachusetts: The MIT Press.
- Lerch, I.A., and Kohn, S., 1983. "Radiofrequency Hyperthermia: The Design of Coil Transducers for Local Heating". *Int. J. Radiation Oncology Biol. Phys.*, 9, pp. 939-948.
- Metaxas, A.C., and Meredith, R.J., 1983. *Industrial Microwave Heating*. London: Peter Peregrinus Ltd.

- Mostafa, A.E., and Gohar, M.K., 1953. "Determination of Voltage, Current, and Magnetic Field Distributions together with the Self-capacitance, Inductance, and HF Resistance of Single-Layer Coils". *Proc. IRE*, 41(4), pp. 537-547.
- Pethig, R., 1979. *Dielectric and Electronic Properties of Biological Materials*. New York: John Wiley and Sons, Ltd. Chapter 7.
- Ruggera, P.S., and Kantor, G., 1984. "Development of a Family of RF Helical Coil Applicators Which Produce Transversely Uniform Axially Distributed Heating in Cylindrical Fat-Muscle Phantoms". *IEEE Trans. Biomedical Eng.*, 31(1), pp. 98-106.
- Schwan, H.P., and Ferris, C.D., 1968. "Four-Electrode Null Techniques for Impedance Measurement with High Resolution". *Rev. Sci. Instr.*, 39(4), pp. 481-485.
- Siegal, B., and Pendleton, E., 1975. "Zero-Bias Schottky Diodes as Microwave Detectors". *Microwave J.*, 18(9), pp. 40-43.
- Sensiper, S., 1955. "Electromagnetic Wave Propagation on Helical Structures (A Review and Survey of Recent Progress)". *Proc. IRE*, 43, pp. 149-161.
- Shurmer, H.V., 1971. *Microwave Semiconductor Devices*. London: Pitman Press.
- Smith, G.S., 1975. "A Comparison of Electrically Short Bare and Insulated Probes for Measuring the Local Radio-Frequency Electric Field in Biological Systems". *IEEE Trans. Biomedical Eng.*, 22(6), pp. 477-483.
- Smith, G.S., 1979. "The Electric-Field Probe Near a Material Interface with Application to the Probing of Fields in Biological Bodies". *IEEE Trans. Microwave Theory and Techniques*, 27(3), pp. 270-278.
- Smith, G.S., 1984. "Limitations on the Size of Miniature Electric Field Probes". *IEEE Trans. Microwave Theory and Techniques*, 32(6), pp. 594-600.

- Sterzer, F., Paglione, R.W., Mendecki, J., Freidenthal, E., and Botstein, C., 1980. "RF Therapy for Malignancy". *IEEE Spectrum*, December 1980, pp. 32-37.
- Stogryn, A., 1971. "Equations for Calculating the Dielectric Constant of Saline Water". *IEEE Trans. Microwave Theory and Techniques*, 19(8), pp. 733-736.
- Stoy, R.D., Foster, K.R., and Schwan, H.P., 1982. "Dielectric properties of mammalian tissues from 0.1 to 100 MHz: a summary of recent data". *Phys. Med. Biol.*, 27(4), pp.504-513.
- Strohbehn, J.W., 1982. "Theoretical temperature distributions for solenoidal-type hyperthermia systems". *Med. Phys.* 9(5), pp. 673-682.
- Tyler, V.J., 1974. "Self-Resonance in Single-Layer Solenoids". *Amalgamated Wireless Australasia (AWA) Technical Review*, 15(4), pp. 149-165.
- Vermeulen, F.E., and Chute, F.S., 1983. "On the axial and eddy currents induced in a cylindrical core of lossy material heated by an induction coil". *Can. Elec. Eng. J.*, 8(3), pp. 93-99.
- Weast, R.C., ed., 1974. *CRC Handbook of Chemistry and Physics*, 55th edition. Cleveland, Ohio: The CRC Press.
- Weissberger, A., and Rossiter, B.W., ed., 1971. *Techniques of Chemistry. Volume I, Part II(a): Electrochemical Methods*. New York: John Wiley and Sons, Inc. Chapter 3.

Appendix A: Loss Mechanisms

This appendix contains a description of the mechanisms of energy dissipation within a material exposed to an electromagnetic field. The constitutive parameters of aqueous sodium chloride are described and the significant loss mechanisms are summarized.

Energy Dissipation in an Electromagnetic Field

The energy dissipated within an isotropic material when exposed to an electromagnetic field can be determined from Maxwell's curl equations,

$$\begin{aligned}\nabla \times \mathbf{H} &= \mathbf{J} + \partial \mathbf{D} / \partial t, \\ \nabla \times \mathbf{E} &= -\partial \mathbf{B} / \partial t,\end{aligned}\quad [\text{A.1}]$$

and the scalar constitutive parameters of the material:

$$\begin{aligned}\epsilon &= \epsilon' - j\epsilon'' \\ \mu &= \mu' - j\mu'' \\ \sigma &= \sigma' - j\sigma''\end{aligned}\quad [\text{A.2}]$$

Assuming a sinusoidal oscillation of the field and inserting Ohm's law, the first curl equation becomes

$$\nabla \times \mathbf{H} = [(\sigma' - j\sigma'') + j\omega(\epsilon' - j\epsilon'')] \mathbf{E} = [\hat{\sigma} + j\omega\hat{\epsilon}] \mathbf{E}, \quad [\text{A.3}]$$

where $\hat{\sigma}$ and $\hat{\epsilon}$ are, respectively, the real effective conductivity and the real effective permittivity, defined as

$$\begin{aligned}\hat{\sigma} &= \sigma' + \omega\epsilon'' \\ \hat{\epsilon} &= \epsilon' - \sigma''/\omega.\end{aligned}\quad [\text{A.4}]$$

Taking the complex conjugate of all terms in equation A.3 and forming a scalar product with \mathbf{E} ,

$$\mathbf{E} \cdot (\nabla \times \mathbf{H}^*) = (\hat{\sigma} - j\omega\hat{\epsilon}) \mathbf{E} \cdot \mathbf{E}^* . \quad [\text{A.5}]$$

In a similar way, the second curl equation becomes

$$\mathbf{H}^* \cdot (\nabla \times \mathbf{E}) = -\omega(\mu'' + j\mu') \mathbf{H} \cdot \mathbf{H}^* . \quad [\text{A.6}]$$

Combining the two results by applying a vector identity,

$$-\nabla \cdot (\mathbf{E} \times \mathbf{H}^*) = \omega(\mu'' + j\mu') \mathbf{H} \cdot \mathbf{H}^* + (\sigma - j\omega\epsilon) \mathbf{E} \cdot \mathbf{E}^* . \quad [\text{A.7}]$$

Integrating over the volume of the material and applying the divergence theorem gives

$$-\oint (\mathbf{E} \times \mathbf{H}^*) \cdot d\mathbf{s} = \int [\omega(\mu'' + j\mu') \mathbf{H} \cdot \mathbf{H}^* + (\sigma - j\omega\epsilon) \mathbf{E} \cdot \mathbf{E}^*] dv . \quad [\text{A.8}]$$

The time-average power entering the material is given by the integral over the surface enclosing the material:

$$\bar{P} = -\frac{1}{2} \oint \text{Re}(\mathbf{E} \times \mathbf{H}^*) \cdot d\mathbf{s} \quad [\text{A.9}]$$

so that in the general case the average power entering the volume and dissipated within the medium is (Johnk 1975, pp. 421)

$$\bar{P} = \frac{1}{2} \int (\sigma \mathbf{E} \cdot \mathbf{E}^* + \omega \mu'' \mathbf{H} \cdot \mathbf{H}^*) dv . \quad [\text{A.10}]$$

In isotropic materials which are homogeneous and nonmagnetic, this becomes

$$\bar{P} = \frac{1}{2} \int \sigma |\mathbf{E}|^2 dv . \quad [\text{A.11}]$$

A.2 Loss Mechanisms in Aqueous Sodium Chloride

Two sources of energy dissipation are significant in aqueous sodium chloride exposed to an electromagnetic field. These are Joule heating due to electrolytic conduction, and dielectric losses due to relaxation phenomena in polar molecules.

A.2.1 Joule Heating

Joule heating is generated by conduction currents, which characterize the motion of unbound charge carriers in an

electric field. This motion can be modelled by the d.c. conductivity (Bleaney and Bleaney 1976, pp. 64):

$$\sigma = \eta \xi v . \quad [A.12]$$

Here v is the charge carrier mobility, ξ is the charge on each charge carrier, and η is the number of charge carriers per unit volume. Since several charge carrier species with different mobilities, densities, and charges will be present, the correct expression is

$$\sigma = \sum (\eta_i \xi_i v_i) . \quad [A.13]$$

The resulting current density is given explicitly by Ohm's law:

$$J = \sigma E . \quad [A.14]$$

For aqueous electrolytes ξ and η are fixed, and v increases slightly with temperature. At sufficiently high frequencies ionic conductivity is found to increase above the low-frequency value due to relaxation of the ion atmosphere (Hasted 1973, pp. 165; Weissberger and Rossiter 1971, pp. 166). However, this effect is not observed in aqueous sodium chloride at the frequencies of interest here.

A.2.2 Dielectric Losses

Dielectric losses can be attributed to "polarization currents", generated by a time varying electrical polarization, $\partial P / \partial t$. If the polarization vector P is not totally in phase with the applied field, then the polarization current density, $j\omega P$, will have a component in phase with the field, and energy will be dissipated as heat.

The polarization observed in water can be separated into two components: induced (electronic and ionic) polarization and orientation polarization.

Induced polarization is due to small changes in the relative positions of bound charges within atoms and molecules such that a dipole moment is induced parallel to the applied electric field. The effects of electronic and ionic polarization only become significant at optical wavelengths, causing resonant absorption in the ultraviolet and infrared ranges, respectively (Elliott 1966, pp. 383).

Orientation polarization is due to the tendency for permanent electric dipoles within the material to align themselves with an external electric field. This alignment process is opposed by the effects of thermal agitation and molecular interaction, so that the resulting polarization approaches its maximum value exponentially:

$$P(t) \approx P_{IND} + P_0[1 - \exp(-t/\tau)] \quad [A.15]$$

The relaxation time τ characterizes the time required for the orientation of the permanent dipoles to respond to the applied field. It varies with temperature as described by the Boltzmann condition

$$\tau = \tau_0 e^{E/kT} \quad [A.16]$$

where E is the activation energy, k is Boltzmann's constant, and T is the absolute temperature (King and Smith 1981, pp. 400). The Debye equations relate this to the real and imaginary parts of the complex permittivity:

$$\epsilon'(\omega) = \epsilon_{\infty} + (\epsilon_s - \epsilon_{\infty}) / (1 + \omega^2 \tau^2) , \quad [\text{A.17}]$$

$$\epsilon''(\omega) = \omega \tau (\epsilon_s - \epsilon_{\infty}) / (1 + \omega^2 \tau^2) , \quad [\text{A.18}]$$

where ϵ_s is the static permittivity, including the effects of both induced and orientation polarization, and ϵ_{∞} is the high-frequency permittivity, including the effects of only induced polarization. At radio frequencies the Debye equations describing water become

$$\epsilon'(\omega) \cong \epsilon_s , \quad [\text{A.19}]$$

$$\epsilon''(\omega) \cong \omega \tau (\epsilon_s - \epsilon_{\infty}) .$$

If ϵ_s , ϵ_{∞} , and τ are known, then it should be possible to accurately predict dielectric losses at any frequency. However, Debye pointed out that very few substances exhibit a single relaxation time. Most substances exhibit a distribution of relaxation times. As a result, observed behavior generally consists of a broader frequency range of dispersion and absorption and a smaller maximum value for $\epsilon''(\omega)$ than is predicted by the Debye equations (Cole and Cole 1941, pp. 342). In addition, since the Debye equations are based on an idealized model of a dilute gas, there is some question as to their validity in describing dense materials containing polar molecules (Coelho 1979, pp. 77).

For many substances the single-resonance model does offer a satisfactory approximation of the observed behavior. The relaxation of water is well described by the Debye equations with a single relaxation time (King and Smith 1981, pp. 408, Stogryn 1971, pp. 736). The dielectric properties of water are listed in table A.1.

$\epsilon_{\infty} = 5.5\epsilon_0$		
T(°C)	ϵ_s/ϵ_0	τ (psec)
0	88.2	17.8
5	86.2	15.1
10	84.2	12.7
15	82.3	10.9
20	80.4	9.50
25	78.2	8.31
30	76.7	7.36
35	75.0	6.58
40	73.1	5.95
45	71.4	5.37
50	69.8	4.87
55	68.2	4.44
60	66.6	4.03
65	65.0	3.72
70	63.6	3.45
75	62.1	3.23

Table A.1 Dielectric Properties of Water
(from King and Smith 1981, pp. 409)

The presence of dissolved electrolytes has a significant effect on the dielectric properties of water. The static permittivity ϵ_s of aqueous electrolytes is found to be less than that of pure water (Hasted 1973, pp. 139). This is due to the replacement of polar water molecules with nonpolar atoms, together with the orienting effect of the strong local electric fields around solvated ions, which makes this shell of oriented water molecules less able to respond to external fields. No variation in ϵ_{∞} with ionic concentration has been observed, and its variation with temperature is unclear (Stogryn 1971, pp. 734). For this investigation ϵ_{∞} is assumed to be independent of both temperature and electrolyte concentration. The dipole relaxation time τ is also found to be decreased in aqueous

electrolytes, due to the disruption of the structure of water by solvated ions (Hasted 1973, pp. 154).

The variation in the static permittivity, relaxation time, and low-frequency conductivity of aqueous sodium chloride at 25°C is shown in figure A.1 (from Weast 1974, pp. D-194; Franks 1973, Chapter 8; Hasted 1973, pp. 156).

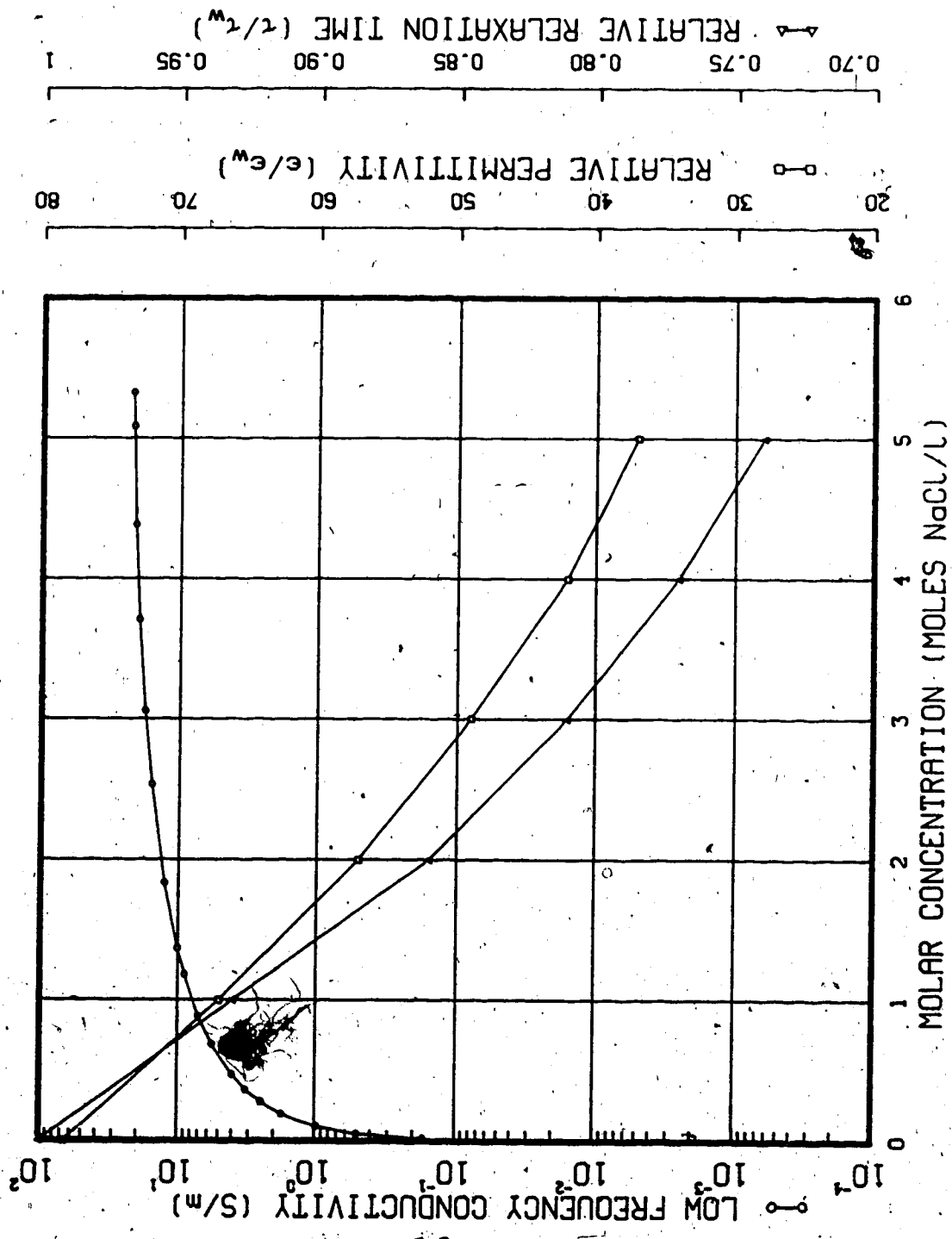


Figure A.1 Dielectric Properties of Aqueous NaCl at 25°C

Appendix B: Theory and Design of an Electric Field Probe

B.1 Theory of the Dipole Probe

Dipole probes have been studied extensively by many investigators, and their theory is well developed. This analysis follows that of Smith, and only the pertinent details are included.

A typical measuring probe consists of an electrically short dipole antenna, a nonlinear detector, a resistive parallel-wire transmission line, and a measuring instrument. The component of the incident electric field parallel to the dipole induces a current in the dipole and through the nonlinear detector. A potential is developed across the detector with components proportional to the square of the current amplitude. The low-frequency components of this potential travel down the resistive transmission line to the measuring instrument.

B.1.1 The Cylindrical Dipole

The geometry of the cylindrical dipole is illustrated in figure B.1. If the dipole is thin ($a \ll h$) and electrically short in the surrounding lossy medium ($\alpha h, \beta h \ll 1$), then the current distribution along the antenna is approximately triangular and the charge distribution is approximately uniform. In this case the input admittance of the bare dipole is approximately (Smith 1975, pp. 478)

$$Y_{\text{bare}} = G + j\omega C \approx \frac{\pi h(\hat{\sigma} + j\omega\hat{\epsilon})}{\ln(h/a) - 1} \quad [\text{B.1}]$$

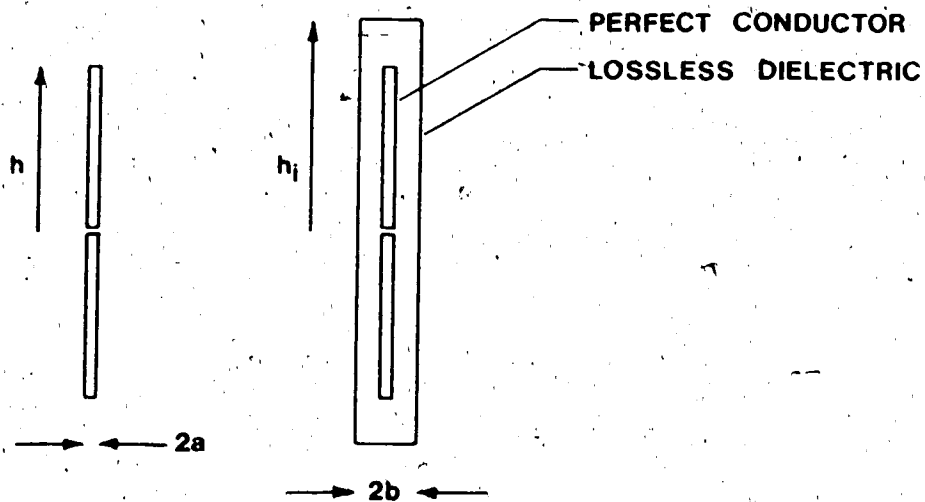


Figure B.1 Bare and Insulated Dipoles

The insulated cylindrical dipole is constructed by adding a concentric sheath of lossless dielectric material ϵ_1 to the bare cylindrical dipole. The input admittance of the insulated dipole is obtained by adding a capacitive admittance $j\omega C_s$ in series with the admittance of an equivalent bare dipole of length $2h$ and radius b , so that

$$Y_{ins} = [(G + j\omega C)^{-1} + (j\omega C_s)^{-1}]^{-1} \quad [B.2]$$

The capacitance C_s is just $2h$ times the coaxial capacitance per unit length of the insulating sheath:

$$C_s = \frac{4\pi h \epsilon_1}{\ln(b/a)} \quad [B.3]$$

If the insulation is thick ($b \gg a$), and is chosen so that the ratio of the permittivity of the external medium to that of the insulation is large ($\hat{\epsilon}/\epsilon_1 \gg 1$), then the input admittance

of the insulated probe is approximately that of the sheath (Smith 1975, pp. 479):

$$Y_{ins} \approx j\omega C_s \approx \frac{j\omega 4\pi h \epsilon_1}{\ln(b/a)} \quad [B.4]$$

Thus while the input admittance of the bare probe is directly related to the electrical properties of the surrounding medium, the admittance of the insulated probe can be made to be approximately independent of those properties.

When placed in an electric field, the receiving dipole (bare or insulated) will produce an open circuit voltage at its terminals which is proportional to the incident field strength:

$$V_{oc} = -2h_e E_z \quad [B.5]$$

E_z is the electric field component parallel to the dipole and $2h_e$ is the effective height of the dipole. For electrically short dipoles this is equal to the actual height, h . The electrically short receiving dipole can thus be represented by a Norton equivalent circuit consisting of a terminal admittance Y_d and a current source,

$$I_{sc} = Y_d V_{oc} = -Y_d h E_z \quad [B.6]$$

B.1.2 Detection

The primary function of the detector is to produce a low-frequency output signal whose amplitude is related to the amplitude of the high-frequency input signal. This is done by passing the high-frequency signal through a nonlinear device. If the V-I characteristic of the detector is described by the relation $I=f(V)$, then the small-signal

response of such a device operating without d.c. bias can be expressed as

$$\delta i = f(V=0) + \frac{f'(V=0)\delta v}{1!} + \frac{f''(V=0)\delta v^2}{2!} + \dots \quad [B.7]$$

where δi and δv are incremental values of current and voltage. For signals of sufficiently small amplitude, the *nonlinear* response will be due primarily to the second-order term. Terms containing higher powers in δv will be very small in comparison.

The desired output signal, then, is approximately proportional to the square of the amplitude of the input signal, and the constant of proportionality is related to the curvature of the detector's V-I characteristic around the origin. The devices most suitable for use as unbiased detectors are those whose V-I characteristic bend most sharply through the origin. For this reason point-contact, tunnel, backward, and zero-bias Schottky diodes are commonly used (Siegal and Pendleton 1975, pp. 41). Conventional Schottky barrier diodes can also be used as unbiased detectors, but require larger input signals to drive them into the square-law region, and thus yield probes which are less sensitive to small field amplitudes.

In figure B.2 an equivalent circuit for the detector diode is shown. Parasitic terms due to packaging have been omitted. The two sections of the circuit represent the diode as a passive load at high frequencies and as a Thevenin voltage source at low frequencies. The high-frequency section consists of the junction resistance R_j and capacitance

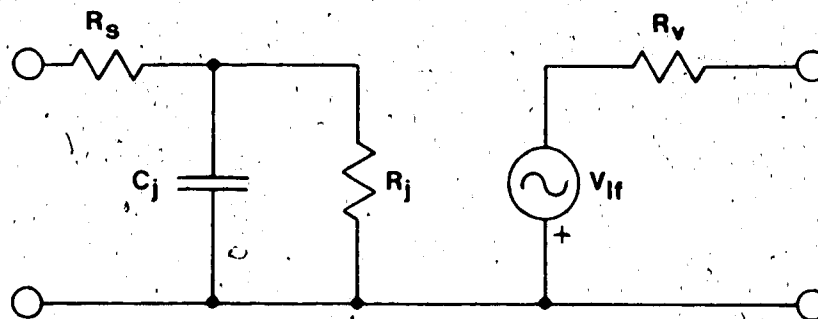


Figure B.2 Equivalent Circuit of a Detector Diode

C_j , and the series resistance R_s of the semiconductor material. Since R_s is typically much less than the junction impedance, it is also neglected. The resistance R_j is approximately equal to the reciprocal of the slope of the diode characteristic at the origin.

The low-frequency section consists of a voltage source V_{if} and the diode video resistance, $R_v \approx R_s + R_j$. For square-law operation V_{if} is proportional to the time-average power absorbed by the diode:

$$V_{if} = \gamma_d \bar{P}_d = \gamma_d \left[\frac{Y_d}{Y_d + \omega C_j + 1/R_j} \right]^2 \frac{h^2 E_z^2}{2R_j} \quad [B.8]$$

where γ_d is the voltage sensitivity of the diode (Bassen and Smith 1983, pp. 711). The voltage sensitivity is equal to the product of the current sensitivity and the diode video

resistance (Shurmer 1971, pp. 9):

$$\gamma_d = \beta_d R_v .$$

[B.9]

B.1.3 Transmission

The dipole and detector are usually connected to the measuring instrument by a resistive parallel-wire transmission line. Resistive line is used so that the electric field under study is not perturbed by the introduction of a conductive current path. The transmission line has series resistance r^i per unit length per conductor, and shunt capacitance c per unit length. Since r^i and c are large, the series inductance and shunt conductance of the line are neglected. The wave number and characteristic impedance associated with the line are in this case given by

$$k_0(\omega) \cong (1-j)[r^i \omega c]^{1/2} , \quad [B.10]$$

$$Z_0(\omega) \cong (1-j)[r^i / \omega c]^{1/2} . \quad [B.11]$$

The high resistance per unit length of the line produces three effects. First, it reduces the direct reception of the incident field by the line. This direct reception produces a signal at the detector due to field components adjacent to the transmission line, and possibly quite different from those in the vicinity of the dipole. Second, the high resistance per unit length reduces the scattering cross-section of the line (Bassen and Smith 1983, pp. 712). Currents induced in the dipole and transmission line by the electromagnetic field under study are the source of a

'scattered' field. This scattered field can induce currents in nearby objects, which in turn are the source of a second scattered field. This second scattered field is received by the probe and interpreted as being part of the original field, and an error may result. Third, the distributed series resistance and shunt capacitance of the line form a lowpass filter, with a 3dB cutoff frequency occurring where $|k_0(\omega)s|=1$ (Smith 1984, pp. 595). If c , r , and the line length s are chosen so that

$$|k_0(\omega_0)s|^2 \approx \omega_0 c \cdot 2r^2 s^2 \ll 1 \quad [\text{B.12}]$$

at the carrier frequency, and so that

$$|k_0(\omega_m)s|^2 \approx \omega_m c \cdot 2r^2 s^2 \gg 1 \quad [\text{B.13}]$$

at the frequency of the probe output signal, then the transmission line will attenuate the carrier-frequency signal and pass the desired low-frequency signal.

B.1.4 Modulation

If the electric field under study is amplitude-modulated, then (assuming that the quasi-static approximation is valid so that spatial and temporal field variations are separable) it varies as

$$E(r,t) = E(r) \cdot (1 + \kappa \cos \omega_m t) \cdot \cos \omega_0 t, \quad [\text{B.14}]$$

where ω_0 is the carrier frequency, ω_m is the modulating frequency, and κ is the modulation level ($0 \leq \kappa \leq 1$). The detector generates an output proportional to the square of the incident field strength. This produces low-frequency output components proportional to

$$f''(V=0)[(2+\kappa^2) + 2\kappa\cos\omega_m t + \kappa^2\cos 2\omega_m t], \quad [\text{B.15}]$$

as well as components with frequencies $2\omega_0$, $2\omega_0 \pm \omega_m$, and $2\omega_0 \pm 2\omega_m$. Usually the monitoring instrumentation includes a narrow bandwidth amplifier so that only one of the low-frequency components is actually measured.

If the electric field under study is not amplitude-modulated ($\kappa=0$), then the only output components are at d.c. and at twice the carrier frequency. The d.c. component is monitored by the instrumentation.

B.2 Design and Construction of the Dipole Probe

The probe was designed to measure the Cartesian components of a nonuniform, amplitude-modulated electric field at carrier frequencies from 1 MHz to 50 MHz, with a modulation frequency of 1 kHz. Measurements were made within 0.04 M saline solution ($\sigma=0.5 \text{ S/m}$, $\epsilon \approx 77.6\epsilon_0$). The insulated dipole probe was chosen primarily to prevent physical damage to the dipole.

Two working probes were actually built (plate B.1). The first probe consisted of a 30 cm 'vertical' shaft with a 'horizontal' dipole on the end. This probe was designed to measure components of the electric field parallel to the flat side of the coil. The second probe consisted of a 30 cm 'vertical' shaft, a 90° bend, and a 5 cm 'horizontal' shaft with a 'vertical' dipole on the end. This probe was used to measure the component of the electric field normal to the flat side of the coil.

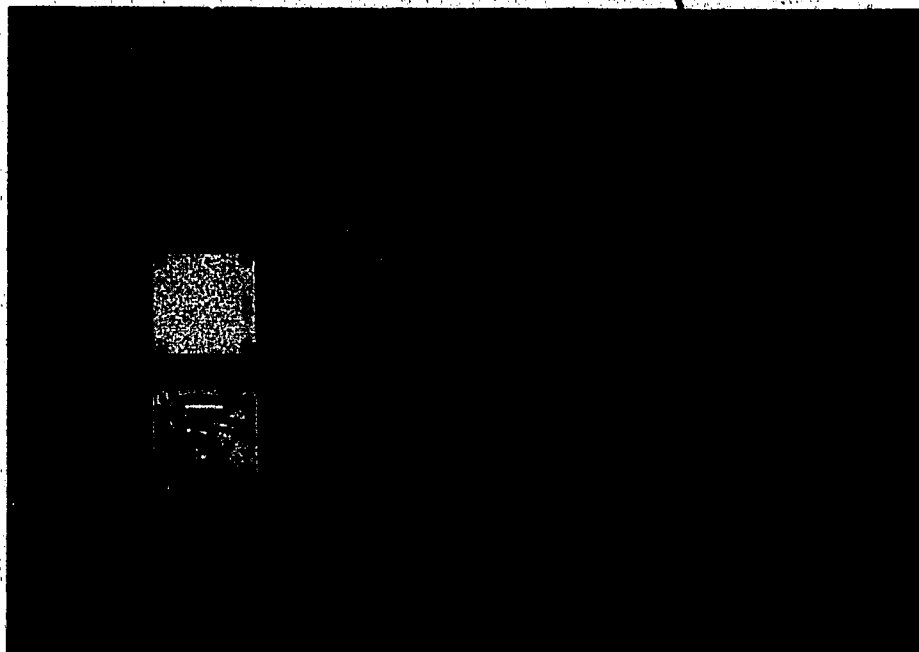


Plate B.1

Completed Probes

Factors concerning the design of the probe were:

- (1) The probe should be nonmetallic and its overall size as small as possible to minimize the perturbation of the field.
- (2) The dipole should be sufficiently small to allow adequate spatial resolution of the field, and to allow measurements to be made reasonably close to metallic interfaces without altering the response of the probe.
- (3) The dipole should be sufficiently large to permit adequate "discrimination" against field components perpendicular to it.

B.2.1 Transmission Line

The probe was connected to the instrumentation by a parallel-wire transmission line consisting of two carbon-impregnated teflon conductors covered by an insulating nylon sheath, which is commercially available from the Polymer Corporation (Reading, Pennsylvania, USA) as "Fluorosint 819 Dual Line". The resistance of the conductors is quoted as $1.0 \pm 20\%$ $M\Omega/m$, which was found to be accurate. An imbalance of up to 20 percent between the resistances of the two conductors was also observed. Based on its geometry (figure B.3), the capacitance per unit length of the line is approximately 79 pF/m.

Electrical contact was made with the transmission line by wrapping a short section of 30 AWG "wire-wrap wire" onto

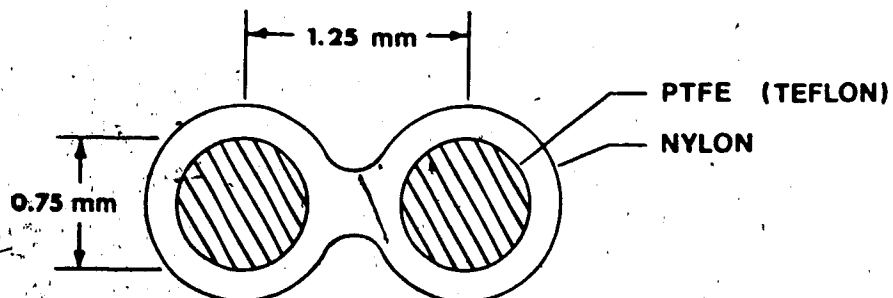


Figure B.3

Resistive Transmission Line

each of the exposed teflon conductors, then encapsulating the wrapped segments in epoxy.

B.2.2 Dipole and Detector

The dipole was constructed from a glass-encapsulated axial-lead diode, with the diode leads forming the arms of the dipole ($2a=0.38$ mm). Because of extremely long delivery times quoted for zero-bias Schottky diodes and other conventional unbiased detectors, locally available Schottky barrier diodes (Hewlett-Packard 5082-2835) were used. Typical junction parameters for this diode are $R_j=50$ k Ω , $C_j=1$ pF. Since adequate probe performance was obtained using these diodes, more exotic detectors were not pursued.

The dipole arms were covered with an insulating polyethylene sheath ($\epsilon_i=2.26\epsilon_0$, $2b=1.52$ mm, $h_i=11.0$ mm, $C_g=1.8$ pF), and the first 30 cm of transmission line and connections were encased in 5 mm O.D. glass tubing. Clear epoxy was used to cement on the polyethylene sheath, encapsulate the diode connections, and seal the glass tubing at both ends.

It was necessary to include a discrete RC lowpass filter (figure B.4) between the diode and the transmission line to prevent signals induced in the line from reaching the diode. The component values ($R_{1p}=1$ M Ω , $C_{1p}=3.9$ pF) were chosen to maximize the attenuation of high-frequency signals travelling from the transmission line to the diode, and to minimize the attenuation of low-frequency signals travelling

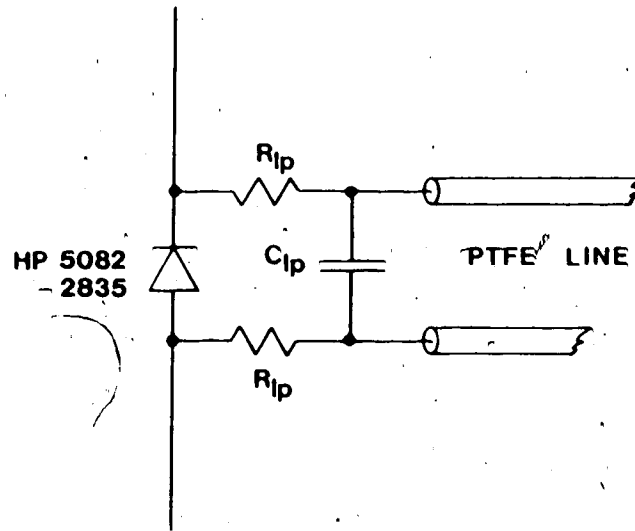


Figure B.4

Lowpass Filter

from the diode to the transmission line. This network was soldered directly adjacent to the diode, and was made small enough to slide inside the glass tubing.

An equivalent circuit for the complete probe is shown in figure B.5, divided into high-frequency and low-frequency sections. The transmission line is represented in the low-frequency circuit by an equivalent PI network. Since the impedance of the lowpass filter (R_{1p}, C_{1p}) is large compared to the diode impedance, and the frequency of the output signal is well below the lowpass cutoff frequencies of the filter and the transmission line, the low-frequency output signal across Z_m (the input impedance of the measuring instrument) is given approximately by

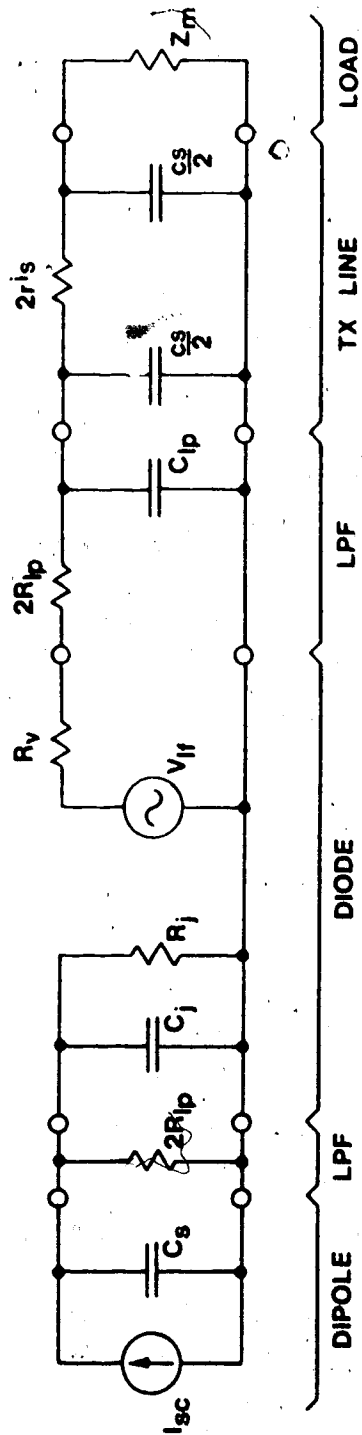


Figure B.5

Equivalent Circuit of a Probe

$$|V_m| \approx \beta_d \left[\frac{C_s / (C_s + C_j)}{1 + (\omega_c / \omega)} \right]^2 \cdot \frac{h^2 E_z^2}{2} \cdot \left[\frac{Z_m}{Z_m + R_v + 2R^1 s + 2R_{1p}} \right] \quad [B.16]$$

$$\text{where } \omega_c = 2\pi f_c = 1/R_j (C_s + C_j) \quad [B.17]$$

At frequencies well below f_c (1.2 MHz) the admittances of the antenna and junction capacitance are less than the admittance of the junction resistance, and most of the current flows through R_j . The output signal V_{1f} increases as the square of the frequency in this region. At frequencies well above f_c the admittances of the antenna and junction capacitance are larger than the admittance of the junction resistance. The majority of the current I_{sc} now flows through these admittances, and V_{1f} becomes approximately independent of frequency.

B.2.3 Instrumentation

The measuring instrument consists of an isolated buffer circuit coupled to a Hewlett-Packard HP415E standing-wave ratio (SWR) meter.

The SWR meter is a high gain audio-frequency amplifier with a square-law calibrated meter readout. As used it has an input impedance of 5 k Ω and a bandwidth of 15 Hz centered at 1 kHz. The electric field under study was amplitude-modulated ($\kappa=0.90$) with a 1 kHz sinusoid.

The buffer circuit (figure B.6) consists mainly of an audio-frequency transformer and two voltage-follower amplifiers. It performs two functions. First, it provides total d.c. isolation between the probe and the ground potential associated with the surrounding equipment. Second,

it presents a low output impedance to drive the magnetically coupled SWR meter, and a high input impedance to terminate the resistive transmission line.

The amplifiers used were type TL072 JFET-input, low-noise operational amplifiers. The high input impedance of these devices ensures that at 1 kHz the terminating impedance seen by the transmission line is entirely due to the two 10 M Ω shunt resistors.

The buffer circuit was placed in a diecast aluminum box (5 \times 5 \times 3 cm), which was mounted directly on the end of the glass shaft of the probe. RG-174 coaxial cable was run from the box to the SWR meter and from the box to a floating d.c. power supply.

B.2.4 Testing

Measurements of probe response versus dipole height h were initially made in a water-filled parallel plate capacitor. It was thus found that a probe with a 2 cm dipole would produce over 35 dB more output signal when parallel to the field than when perpendicular to it. This level of discrimination was accepted as a suitable compromise between spatial resolution and measurement accuracy. The response of the probe was also found to be slightly nonlinear. In addition, the probe's ability to discriminate against field components perpendicular to the dipole was observed to decrease slightly with increasing field amplitude.

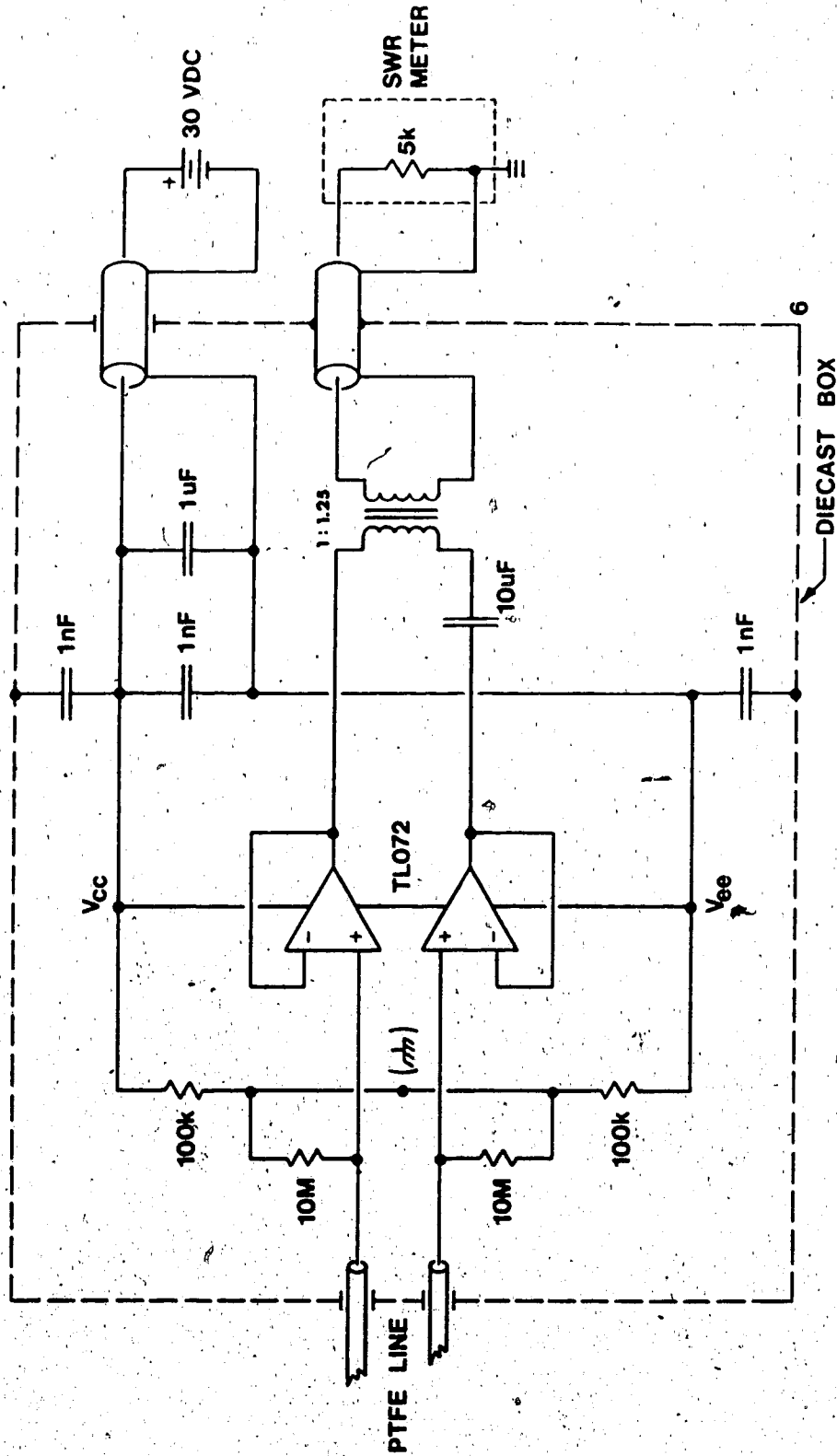


Figure B.6

Buffer Circuit Schematic

A water-filled, open-ended coaxial capacitor, having an inner radius of 1.7 cm and an outer radius of 12.1 cm, was also constructed. The probes were used to measure the electric field within this region, and the results compared to an analytic solution. From this, conclusions were drawn regarding the performance limitations of the probe.

In order to obtain an accurate mapping of the field under study, the dipole should be small enough that the field does not vary significantly over its length. Conversely, the resulting map shouldn't be expected to show detail on a scale smaller than the dipole length. Measurements of the electric field within the coaxial capacitor were made at 0.5 cm intervals with a 2 cm dipole. The result at each measurement point (taken as the position of the center of the dipole) was within ± 2 percent of the theoretical value, despite the severe nonuniformity of the field. Subsequent measurements were made at 2.0 cm intervals.

The interaction between the probe and an interface is due to the scattering of electromagnetic energy by the probe and the interface. A worst-case estimate of the effect of the interface on the probe performance was made by Smith (1979), who considered a dipole antenna parallel to a perfectly conducting plane. His results indicate that in free space it is possible to bring the probe to within one dipole-length of the interface with less than one percent error caused by changes in the dipole admittance. In a lossy

medium, it should be possible to bring the dipole much closer without significant perturbation. Measurements made with the lossy coaxial capacitor confirmed this.

Appendix C: Tabulated Data

Table C.1 Input Resistance and Resonant Frequency of the Semi-Cylindrical Solenoid versus Target Material Conductivity: Low-Frequency Case

σ_{LF} (S/m)	$\hat{\sigma}$ (S/m)	R_{IN} (Ω)	Frequency (MHz)
2.43×10^{-4}	2.43×10^{-4}	10000	0.9961
4.10	4.10	9700	0.9961
5.03	5.03	9500	0.9960
6.13	6.13	9300	0.9960
7.05	7.05	9100	0.9960
9.03	9.03	8800	0.9960
1.07×10^{-3}	1.07×10^{-3}	8500	0.9959
1.24	1.24	8300	0.9959
1.37	1.37	8100	0.9959
1.58	1.58	7800	0.9959
1.83	1.83	7400	0.9959
2.10	2.10	7100	0.9958
2.31	2.31	6900	0.9958
2.56	2.56	6650	0.9957
2.96	2.96	6300	0.9956
3.28	3.28	6100	0.9956
3.52	3.52	5900	0.9955
3.92	3.92	5650	0.9954
4.27	4.27	5400	0.9953
4.86	4.86	5150	0.9952
5.64	5.64	4900	0.9949
6.29	6.29	4650	0.9948
6.98	6.98	4500	0.9945
7.50	7.50	4350	0.9943
8.70	8.70	4100	0.9939
1.02×10^{-2}	1.02×10^{-2}	4000	0.9935
1.19	1.19	3900	0.9930
1.33	1.33	3850	0.9926
1.52	1.52	3900	0.9921
1.79	1.79	3900	0.9916
2.14	2.14	4050	0.9910
2.37	2.37	4250	0.9905
3.28	3.28	4600	0.9900
3.90	3.90	5000	0.9897
4.74	4.74	5400	0.9894
5.81	5.81	5900	0.9892
6.94	6.94	6250	0.9891
8.26	8.26	6650	0.9890
1.00×10^{-1}	1.00×10^{-1}	7100	0.9890
1.22	1.22	7500	0.9889
1.45	1.45	7900	0.9889

1.78	1.78	8200	0.9888
2.17	2.17	8500	0.9888
2.54	2.54	8800	0.9888
3.10	3.10	9000	0.9888
3.77	3.77	9200	0.9888
4.52	4.52	9300	0.9888
5.44	5.44	9400	0.9888
6.49	6.49	9500	0.9888
7.54	7.54	9550	0.9888
9.27	9.27	9500	0.9888
1.09×10 ⁰	1.09×10 ⁰	9500	0.9887
1.30	1.30	9450	0.9887
1.52	1.52	9350	0.9887
1.79	1.79	9200	0.9887
2.08	2.08	9050	0.9887
2.46	2.46	8850	0.9887
2.69	2.69	8600	0.9887
3.23	3.23	8300	0.9886
3.70	3.70	7900	0.9886
4.25	4.25	7500	0.9886
4.98	4.98	7000	0.9887
5.55	5.55	6500	0.9887
6.44	6.44	6000	0.9888

Table C.2 Input Conductance and Resonant Frequency of the Semi-Cylindrical Solenoid versus Target Material Conductivity: One-Half Wavelength Self-Resonant Case

σ_{LF} (S/m)	$\hat{\sigma}$ (S/m)	G_{IN} (mS)	Frequency (MHz)
2.17×10^{-4}	2.40×10^{-4}	0.03	10.45
3.54	3.77	0.035	10.4
5.20	5.43	0.04	10.4
8.54	8.77	0.045	10.4
1.21×10^{-3}	1.23×10^{-3}	0.055	10.4
1.67	1.69	0.07	10.4
2.51	2.53	0.10	10.4
3.47	3.49	0.135	10.4
5.19	5.21	0.19	10.4
7.80	7.82	0.275	10.35
1.08×10^{-2}	1.08×10^{-2}	0.37	10.35
1.53	1.53	0.50	10.35
2.31	2.31	0.745	10.25
3.47	3.47	1.09	10.1
5.47	5.47	1.57	9.7
7.75	7.75	1.86	9.05
1.06×10^{-1}	1.06×10^{-1}	1.86	8.05
1.47	1.47	1.59	7.25
2.01	2.01	1.29	6.83
2.98	2.98	0.94	6.53
5.09	5.09	0.625	6.38
8.45	8.45	0.455	6.32
1.33×10^0	1.33×10^0	0.36	6.32
2.00	2.00	0.315	6.3
2.95	2.95	0.285	6.28
4.80	4.80	0.27	6.28
7.38	7.38	0.27	6.32
$1.18 \times 10^{+1}$	$1.18 \times 10^{+1}$	0.27	6.32

Table C.3 Input Conductance and Resonant Frequency of the Semi-Cylindrical Solenoid versus Target Material Conductivity: One Wavelength Self-Resonant Case

σ_{LF} (S/m)	δ (S/m)	G_{IN} (mS)	Frequency (MHz)
4.24×10^{-3}	4.33×10^{-3}	63.28	21.00
5.56	5.65	52.66	20.98
7.53	7.62	41.03	20.98
9.79	9.88	31.02	20.98
1.28×10^{-2}	1.29×10^{-2}	24.41	20.98
1.63	1.64	19.58	20.98
2.06	2.07	15.84	20.80
2.57	2.58	13.01	20.70
3.30	3.31	10.59	20.55
4.14	4.15	8.93	20.25
5.21	5.22	7.59	19.70
6.83	6.84	6.69	18.50
8.34	8.35	6.26	16.70
1.09×10^{-1}	1.09×10^{-1}	6.46	14.80
1.41	1.41	7.29	13.60
1.77	1.77	8.86	12.95
2.35	2.35	11.24	12.58
3.42	3.42	14.42	12.40
4.41	4.41	18.23	12.30
5.69	5.69	22.98	12.22
7.38	7.38	29.16	12.20
9.27	9.27	35.45	12.19
1.12×10^0	1.12×10^0	41.54	12.18
1.35	1.35	48.40	12.17
1.65	1.65	56.50	12.15
2.07	2.07	65.60	12.14
2.68	2.68	75.90	12.13
3.60	3.60	86.50	12.12
4.99	4.99	95.78	12.12

Table C.4 Input Resistance and Resonant Frequency of the Semi-Cylindrical Solenoid versus Target Material Conductivity: Two Wavelength Self-Resonant Case

σ_{LF} (S/m)	δ (S/m)	R_{IN} (Ω)	Frequency (MHz)
1.80×10^{-4}	5.08×10^{-4}	3.3	39.42
2.64	5.92	3.4	39.40
5.74	9.02	3.9	39.40
7.28	1.06×10^{-3}	4.1	39.40
9.61	1.29	4.5	39.38
1.21×10^{-3}	1.54	4.9	39.38
1.45	1.78	5.2	39.37
1.81	2.14	5.8	39.37
2.15	2.48	6.4	39.35
2.51	2.84	7.0	39.35
2.88	3.21	7.55	39.35
3.28	3.61	8.15	39.34
3.73	4.06	8.85	39.34
4.33	4.66	9.80	39.33
4.90	5.23	10.7	39.33
5.59	5.92	11.9	39.33
6.31	6.64	12.9	39.33
7.23	7.56	14.4	39.33
8.47	8.80	16.3	39.33
1.04×10^{-2}	1.07×10^{-2}	19.2	39.31
1.24	1.27	22.7	39.29
1.53	1.56	26.6	39.27
1.85	1.88	31.5	39.35
2.27	2.30	37.5	39.20
2.80	2.83	45.0	39.13
3.33	3.36	52.5	39.08
3.97	4.00	61.0	38.99
4.78	4.81	72.0	38.87
5.59	5.62	81.5	38.73
6.40	6.43	90.5	38.58
7.32	7.35	101	38.31
8.32	8.35	109	38.02
9.38	9.41	119	37.70
1.07×10^{-1}	1.07×10^{-1}	128	37.26
1.22	1.22	137	36.60
1.37	1.37	143	35.83
1.57	1.57	149	34.81
1.83	1.83	150	33.48
2.13	2.13	154	31.94
2.52	2.52	150	30.33
2.96	2.96	143	29.33
3.54	3.54	132	28.54
4.26	4.26	117	28.15

5.26	5.26	102	27.90
6.62	6.62	85.5	27.76
8.18	8.18	72.5	27.70
1.05×10^0	1.05×10^0	60.0	27.61
1.36	1.36	49.5	27.64
1.69	1.69	43.0	27.63
2.12	2.12	37.5	27.65
2.71	2.71	33.0	27.71
3.39	3.39	30.2	27.73
4.27	4.27	28.4	27.76
5.26	5.26	27.0	27.83
6.45	6.45	26.2	27.88
8.03	8.03	25.4	27.95
9.76	9.76	25.0	28.04
1.11×10^1	1.11×10^1	24.7	28.10

Table C.5(a) Electric Field Strength (Volts/m):
1.0 MHz, X-component

Z \ X	+2	+4	+6	+8	+10	+12	+14
-24	3.8	4.3	3.6	2.7	2.1	1.6	1.2
-22	11.8	9.1	6.1	3.9	2.6	1.8	1.3
-20	38.0	18.6	9.6	5.4	3.3	2.1	1.3
-18	51.2	25.8	12.9	6.6	3.8	2.3	1.4
-16	50.5	27.3	14.4	7.4	4.1	2.5	1.4
-14	48.6	26.2	14.1	7.4	4.1	2.5	1.4
-12	44.3	24.1	13.0	6.9	3.9	2.3	1.4
-10	40.1	21.8	11.5	6.0	3.4	2.1	1.3
-8	37.9	19.2	9.4	4.9	2.8	1.8	1.3
-6	34.1	15.1	6.9	3.5	2.1	1.5	1.2
-4	21.7	8.2	3.7	2.1	1.5	1.3	1.2
-2	5.2	2.4	1.8	1.7	1.5	1.3	1.2
0	3.2	1.9	1.8	1.7	1.5	1.3	1.2
+2	11.9	5.1	2.9	1.9	1.6	1.4	1.3
+4	21.2	9.8	5.3	3.1	2.1	1.6	1.3
+6	26.4	13.9	7.5	4.3	2.8	1.9	1.4
+8	29.3	16.6	9.2	5.4	3.4	2.2	1.5
+10	31.0	18.5	10.6	6.2	3.8	2.5	1.5
+12	33.7	20.0	11.5	6.8	4.1	2.6	1.6
+14	35.8	20.6	11.7	6.9	4.2	2.6	1.6
+16	36.1	20.2	11.2	6.5	4.0	2.5	1.6
+18	35.5	17.4	9.4	5.6	3.6	2.3	1.5
+20	17.7	11.0	6.9	4.4	3.0	2.1	1.4
+22	5.5	5.6	4.4	3.3	2.4	1.8	1.3
+24	2.4	2.9	2.8	2.4	1.9	1.5	1.3

Table C.5(b) Electric Field Strength (Volts/m):
1.0 MHz, Y-component

Z \ X	+2	+4	+6	+8	+10	+12	+14
-24	2.3	1.7	1.3	1.1	1.0	0.8	0.5
-22	1.7	1.3	1.1	1.0	0.8	0.7	0.4
-20	1.0	1.0	0.9	0.8	0.8	0.7	0.4
-18	1.4	1.0	0.9	0.8	0.8	0.7	0.5
-16	2.0	1.3	1.1	0.9	0.8	0.7	0.5
-14	2.2	1.5	1.2	1.0	0.9	0.8	0.6
-12	2.0	1.5	1.2	1.1	1.0	0.9	0.7
-10	2.0	1.6	1.3	1.2	1.0	0.9	0.7
-8	2.1	1.7	1.4	1.2	1.1	1.0	0.8
-6	2.5	1.9	1.5	1.3	1.2	1.0	0.8
-4	2.8	2.0	1.6	1.4	1.2	1.0	0.8
-2	2.9	2.1	1.7	1.4	1.2	1.1	0.8
0	3.0	2.2	1.7	1.4	1.3	1.1	0.9
+2	2.9	2.1	1.7	1.4	1.2	1.1	0.9
+4	2.7	2.0	1.6	1.4	1.2	1.0	0.8
+6	2.5	1.9	1.6	1.3	1.2	1.0	0.8
+8	2.3	1.8	1.5	1.3	1.1	1.0	0.8
+10	2.2	1.8	1.4	1.2	1.0	0.9	0.7
+12	2.3	1.7	1.3	1.1	1.0	0.8	0.6
+14	2.3	1.6	1.2	1.0	0.9	0.8	0.5
+16	2.0	1.4	1.1	0.9	0.8	0.7	0.5
+18	1.7	1.1	1.0	0.9	0.8	0.7	0.4
+20	1.5	1.1	1.0	0.9	0.8	0.7	0.4
+22	2.0	1.4	1.2	1.0	0.9	0.7	0.4
+24	2.5	1.8	1.5	1.2	1.0	0.8	0.5

Table C.5(c) Electric Field Strength (Volts/m):
1.0 MHz, Z-component

Z	X	+2	+4	+6	+8	+10	+12	+14
-24		7.5	3.7	1.9	1.0	0.8	0.8	0.8
-22		14.4	4.8	2.0	1.0	0.8	0.9	1.1
-20		16.2	4.3	1.6	0.9	1.1	1.3	1.5
-18		8.7	2.7	1.3	1.3	1.6	1.9	2.3
-16		6.6	3.0	2.3	2.3	2.5	2.6	2.7
-14		8.3	5.2	4.0	3.6	3.4	3.4	3.4
-12		11.9	7.7	5.9	5.0	4.5	4.3	4.2
-10		14.5	9.8	7.6	6.3	5.6	5.2	5.0
-8		17.1	11.8	9.1	7.6	6.6	5.8	23.3
-6		20.2	14.1	10.6	8.7	7.5	6.8	6.4
-4		24.2	16.2	11.9	9.4	8.1	7.3	6.9
-2		27.0	17.6	12.8	9.9	8.5	7.6	7.2
0		27.0	17.5	12.7	9.9	8.5	7.7	7.2
+2		23.6	15.9	11.8	9.5	8.2	7.5	7.1
+4		19.8	13.8	10.7	8.8	7.7	7.0	6.7
+6		17.1	11.8	9.3	7.9	6.9	6.4	6.1
+8		15.1	10.1	8.1	6.8	6.1	5.6	5.5
+10		13.1	8.5	6.7	5.6	5.1	4.8	4.7
+12		10.8	6.6	5.1	4.4	4.0	3.9	3.9
+14		7.5	4.3	3.4	3.1	3.1	3.1	3.2
+16		6.1	2.2	1.8	2.0	2.2	2.3	2.5
+18		8.1	2.4	1.0	1.1	1.4	1.7	1.9
+20		12.7	4.3	1.5	0.8	1.0	1.2	1.4
+22		11.3	4.2	1.9	0.9	0.8	0.9	1.1
+24		5.6	3.0	1.7	1.0	0.8	0.8	0.9

Table C.6(a) Electric Field Strength (Volts/m):
6.3 MHz, X-component

Z \ X	+2	+4	+6	+8	+10	+12	+14
-24	15.6	17.3	15.4	13.3	9.9	6.8	3.7
-22	32.1	28.2	22.3	16.7	12.6	8.2	4.4
-20	62.1	42.3	29.4	20.9	15.4	9.6	5.0
-18	77.8	51.8	34.9	23.9	16.4	10.8	5.5
-16	78.5	54.6	37.5	25.5	17.4	11.4	5.8
-14	74.5	53.7	37.2	25.4	17.4	11.4	5.7
-12	67.6	49.3	34.6	24.0	16.4	10.6	5.3
-10	59.5	43.4	30.5	21.5	15.4	9.3	4.6
-8	50.0	35.6	25.2	17.8	12.5	7.7	3.6
-6	38.6	27.1	19.1	14.0	9.2	5.5	2.5
-4	24.6	17.5	12.6	8.5	5.4	3.2	1.9
-2	10.0	6.6	4.0	2.7	2.3	2.1	2.0
0	6.2	4.0	2.9	2.6	2.3	2.1	1.9
+2	21.7	15.2	11.1	7.8	5.4	3.7	2.5
+4	34.8	24.9	17.9	13.3	9.1	6.1	3.5
+6	46.7	33.3	23.8	17.0	12.4	8.1	4.6
+8	56.3	40.5	29.0	20.7	15.3	9.8	5.4
+10	63.1	46.6	33.2	23.6	16.5	11.1	6.1
+12	70.0	51.2	36.2	25.4	17.7	12.0	6.5
+14	74.5	54.3	37.8	26.1	18.2	12.2	6.6
+16	77.3	54.1	37.1	25.4	17.6	11.8	6.3
+18	74.3	49.1	33.2	23.2	16.1	10.8	5.8
+20	49.0	36.3	26.6	19.4	14.5	9.3	5.0
+22	22.3	22.8	19.3	15.0	11.6	7.8	4.2
+24	10.7	14.3	13.7	11.5	8.9	6.3	3.5

Table C.6(b) Electric Field Strength (Volts/m):
6.3 MHz, Y-component

Z \ X	+2	+4	+6	+8	+10	+12	+14
-24	6.3	5.0	4.2	3.5	3.1	2.7	2.4
-22	6.2	4.5	3.7	3.1	2.7	2.4	2.1
-20	6.0	3.8	3.1	2.7	2.4	2.2	1.8
-18	3.6	3.0	2.6	2.3	2.1	1.9	1.6
-16	3.5	2.7	2.4	2.1	1.9	1.8	1.4
-14	4.6	3.0	2.7	2.1	1.9	1.7	1.3
-12	4.8	3.7	3.2	2.4	2.1	1.8	1.3
-10	5.9	4.6	3.9	2.9	2.3	2.0	1.4
-8	7.2	5.5	4.5	3.4	2.7	2.2	1.5
-6	8.5	6.4	5.1	3.8	3.0	2.4	1.6
-4	9.2	7.0	5.5	4.2	3.2	2.5	1.7
-2	9.7	7.4	5.8	4.4	3.4	2.6	1.7
0	10.0	7.5	5.9	4.4	3.4	2.6	1.7
+2	9.9	7.4	5.7	4.4	3.3	2.5	1.7
+4	9.2	7.0	5.4	4.1	3.2	2.4	1.6
+6	8.3	6.3	4.8	3.8	2.9	2.2	1.5
+8	7.2	5.4	4.2	3.3	2.6	2.0	1.3
+10	5.6	4.4	3.4	2.8	2.2	1.7	1.2
+12	4.1	3.3	2.7	2.3	1.9	1.5	1.2
+14	2.8	2.5	2.2	2.0	1.8	1.5	1.2
+16	2.3	2.5	2.3	2.1	1.8	1.6	1.2
+18	4.8	3.6	2.8	2.4	2.1	1.8	1.4
+20	7.8	4.6	3.6	2.9	2.5	2.1	1.7
+22	7.6	5.2	4.1	3.4	2.9	2.5	2.0
+24	7.1	5.5	4.6	3.9	3.3	2.8	2.3

Table C.6(c) Electric Field Strength (Volts/m):
6.3 MHz, Z-component

Z \ X	+2	+4	+6	+8	+10	+12	+14
-24	29.3	17.0	8.4	3.7	1.9	2.7	3.5
-22	46.3	21.8	8.8	2.9	2.6	4.3	5.2
-20	48.3	18.6	5.9	2.2	4.7	6.7	7.6
-18	17.1	7.3	2.7	5.8	8.2	9.7	10.3
-16	8.8	8.4	10.0	11.4	12.5	13.1	13.4
-14	25.9	21.1	18.8	17.7	17.3	17.1	16.9
-12	42.1	32.4	27.0	14.7	22.4	21.4	20.7
-10	53.0	41.9	34.5	29.8	26.7	25.0	23.9
-8	62.5	49.8	40.5	34.7	30.9	28.1	26.7
-6	70.7	55.8	45.7	38.5	34.0	31.1	29.2
-4	76.0	60.1	49.2	41.3	36.3	33.0	31.0
-2	78.9	62.5	51.0	43.0	37.5	34.2	32.0
0	80.2	63.4	51.6	43.5	37.9	34.4	32.3
+2	78.4	61.8	50.6	42.6	37.2	33.9	31.7
+4	74.5	58.8	48.2	40.4	35.5	32.4	30.5
+6	68.2	54.3	44.4	37.5	33.0	30.2	28.3
+8	60.4	48.0	39.0	33.4	29.6	27.1	25.8
+10	51.0	40.0	32.9	28.1	25.5	23.8	22.9
+12	40.2	30.9	25.3	22.7	21.0	19.9	19.4
+14	24.2	19.2	16.8	16.2	15.9	15.8	15.7
+16	7.7	6.5	8.3	10.1	11.4	12.1	12.4
+18	22.0	9.0	2.1	4.6	7.2	8.6	9.3
+20	51.5	19.4	6.9	2.0	4.1	5.7	6.8
+22	38.0	19.5	8.7	3.0	2.2	3.7	4.6
+24	23.1	14.1	7.6	3.5	1.9	2.4	3.0

Table C.7(a) Electric Field Strength (Volts/m):
12.8 MHz, X-component

Z \ X	+2	+4	+6	+8	+10	+12	+14
-24	5.9	7.0	6.6	5.5	4.2	2.8	1.5
-22	12.6	12.0	9.9	7.6	5.5	3.6	1.8
-20	26.6	19.7	14.0	10.1	7.0	4.5	2.2
-18	39.8	27.0	18.5	12.6	8.4	5.3	2.5
-16	48.4	32.5	22.0	14.7	9.6	5.9	2.8
-14	55.0	36.1	24.4	16.0	10.3	6.3	2.9
-12	56.1	36.5	24.6	16.3	10.4	6.3	2.9
-10	53.2	35.5	23.5	15.4	9.8	5.9	2.7
-8	47.2	31.4	20.7	13.3	8.5	5.1	2.2
-6	37.9	24.8	16.2	10.4	6.7	3.9	1.7
-4	24.5	16.4	10.5	6.8	4.3	2.4	0.94
-2	9.9	6.4	4.1	2.6	1.5	0.8	0.6
0	6.2	4.1	2.7	1.8	1.2	0.9	0.7
+2	21.3	13.8	9.1	6.0	4.0	2.5	1.4
+4	34.2	22.7	14.9	9.8	6.5	4.0	2.1
+6	44.7	29.6	19.7	12.8	8.3	5.2	2.6
+8	51.3	34.1	22.8	15.0	9.8	6.0	3.0
+10	53.9	36.3	24.3	16.2	10.6	6.5	3.2
+12	54.5	36.5	24.5	16.4	10.7	6.6	3.2
+14	51.1	34.3	23.1	15.6	10.2	6.4	3.1
+16	44.0	30.0	20.5	13.8	9.2	5.8	2.8
+18	35.2	23.8	16.6	11.5	7.8	5.0	2.5
+20	20.0	16.2	12.2	9.0	6.4	4.1	2.1
+22	8.6	9.4	8.2	6.7	4.9	3.2	1.6
+24	3.9	5.4	5.4	4.7	3.7	2.5	1.3

Table C.7(b) Electric Field Strength (Volts/m):
12.8 MHz, Y-component

Z \ X	+2	+4	+6	+8	+10	+12	+14
-24	1.3	1.6	1.4	1.3	1.0	0.8	0.6
-22	2.9	2.5	2.0	1.6	1.2	0.9	0.7
-20	5.7	3.7	2.5	1.8	1.3	1.0	0.7
-18	7.4	4.5	2.8	1.9	1.3	1.0	0.7
-16	7.1	4.3	2.7	1.7	1.2	1.0	0.6
-14	5.5	3.4	2.1	1.4	1.0	0.9	0.6
-12	3.1	2.1	1.4	1.0	0.8	1.0	0.6
-10	1.8	1.6	1.4	1.1	1.0	1.1	0.7
-8	3.8	2.8	2.1	1.6	1.3	1.3	0.8
-6	6.1	4.3	3.0	2.3	1.7	1.6	1.0
-4	7.8	5.5	3.8	2.7	2.0	1.8	1.1
-2	8.9	6.2	4.3	3.1	2.2	1.9	1.2
0	9.2	6.4	4.4	3.1	2.3	1.9	1.2
+2	8.6	5.9	4.1	2.9	2.1	1.8	1.1
+4	7.1	5.0	3.4	2.5	1.9	1.6	1.0
+6	5.1	3.6	2.6	1.9	1.4	1.3	0.8
+8	2.6	1.9	1.5	1.2	1.0	1.0	0.6
+10	0.8	0.7	0.7	0.7	0.7	0.7	0.4
+12	3.3	2.0	1.2	0.9	0.7	0.6	0.4
+14	5.6	3.4	2.1	1.4	1.0	0.7	0.5
+16	7.2	4.3	2.6	1.7	1.2	0.8	0.5
+18	7.3	4.3	2.7	1.8	1.3	0.9	0.6
+20	5.3	3.5	2.4	1.7	1.3	0.9	0.6
+22	2.8	2.4	1.9	1.5	1.2	0.9	0.6
+24	1.7	1.6	1.4	1.2	1.0	0.9	0.6

Table C.7(c) Electric Field Strength (Volts/m):
12.8 MHz; Z-component

Z \ X	+2	+4	+6	+8	+10	+12	+14
-24	11.9	7.4	4.2	2.0	0.7	1.0	1.3
-22	18.5	10.0	4.9	1.9	0.7	1.6	2.1
-20	23.0	10.7	4.5	1.2	1.4	2.6	3.2
-18	18.2	8.3	2.6	1.1	2.9	4.1	4.7
-16	11.7	4.1	1.5	3.5	5.1	5.9	6.4
-14	5.0	4.0	5.7	6.8	7.6	8.0	8.3
-12	11.5	10.8	10.8	10.6	10.6	10.5	10.5
-10	22.0	18.3	16.1	14.5	13.5	12.9	12.6
-8	32.3	25.4	21.2	18.2	16.4	15.2	14.5
-6	42.0	31.8	25.2	21.6	18.8	17.2	16.2
-4	49.6	36.6	28.8	23.8	20.7	18.6	17.5
-2	53.7	39.6	30.8	25.1	21.8	19.5	18.2
0	53.9	40.3	31.2	25.4	22.0	19.7	18.4
+2	52.5	38.6	30.0	24.7	21.4	19.2	18.0
+4	47.0	34.7	27.4	22.9	20.0	18.0	17.0
+6	38.2	29.5	23.7	20.4	17.9	16.4	15.6
+8	28.7	23.0	19.5	17.0	15.3	14.3	13.7
+10	18.7	16.1	14.2	13.2	12.5	12.0	11.8
+12	10.0	9.2	9.1	9.4	9.5	9.6	9.6
+14	6.5	3.6	4.6	5.9	6.8	7.3	7.6
+16	11.4	4.7	1.4	2.9	4.4	5.3	5.8
+18	18.2	8.3	3.0	0.9	2.4	3.5	4.2
+20	22.1	10.1	4.4	1.2	1.2	2.2	2.8
+22	15.6	8.8	4.5	1.8	0.7	1.3	1.8
+24	9.5	6.3	3.6	1.7	0.7	0.8	1.2

Table C.8(a) Electric Field Strength (Volts/m):
27.3 MHz, X-component.

Z \ X	+2	+4	+6	+8	+10	+12	+14
-24	7.0	7.4	6.5	5.3	4.6	2.1	1.4
-22	14.3	11.6	8.5	6.3	4.9	2.2	1.4
-20	31.0	20.6	10.5	7.0	5.0	2.3	1.4
-18	35.1	22.0	10.8	6.9	4.8	2.1	1.3
-16	28.3	18.6	8.7	5.6	4.3	1.6	0.8
-14	16.0	7.4	4.8	2.2	1.5	0.9	0.7
-12	8.5	5.2	2.4	1.5	0.9	0.8	0.7
-10	8.3	13.0	8.5	3.6	2.2	1.2	0.8
-8	32.0	20.7	9.9	6.0	2.8	1.8	0.9
-6	32.1	20.7	9.8	6.0	2.7	1.7	0.9
-4	24.5	16.5	7.6	4.9	2.1	1.4	0.8
-2	10.3	6.4	4.4	1.7	1.0	0.8	0.7
0	15.4	8.7	5.4	2.6	1.2	0.8	0.7
+2	28.9	15.6	8.7	5.3	2.4	1.2	0.8
+4	34.3	22.3	10.6	6.3	2.9	1.7	0.8
+6	33.4	21.6	10.3	6.2	2.8	1.7	0.9
+8	26.8	18.0	8.3	5.2	2.5	1.6	0.9
+10	21.2	15.5	7.2	5.0	2.6	1.9	1.1
+12	26.4	18.9	9.6	6.7	3.7	2.5	1.6
+14	36.2	24.4	13.4	8.5	6.1	3.1	1.9
+16	42.2	27.7	15.8	9.9	6.9	3.6	2.2
+18	43.0	27.3	15.6	10.0	7.0	3.8	2.2
+20	28.8	22.3	13.0	9.0	6.6	3.6	2.2
+22	12.8	16.2	9.7	7.6	6.0	3.1	1.9
+24	6.3	7.6	7.2	6.3	5.2	2.7	1.8

Table C.8(b) Electric Field Strength (Volts/m):
27.3 MHz, Y-component

Z \ X	+2	+4	+6	+8	+10	+12	+14
-24	0.6	0.4	0.0	0.0	0.0	0.0	0.0
-22	0.6	0.5	0.5	0.0	0.0	0.0	0.0
-20	0.8	1.1	0.8	0.6	0.5	0.0	0.0
-18	3.3	2.2	1.3	0.9	0.6	0.0	0.0
-16	4.8	3.6	1.8	1.1	0.7	0.0	0.0
-14	6.0	3.7	2.0	1.2	0.7	0.0	0.0
-12	5.3	3.2	1.8	1.0	0.6	0.0	0.0
-10	3.7	1.9	1.1	0.6	0.5	0.0	0.0
-8	0.7	0.5	0.4	0.0	0.0	0.0	0.0
-6	3.5	1.9	1.1	0.7	0.5	0.5	0.0
-4	5.5	3.5	1.9	1.2	0.7	0.5	0.0
-2	6.9	4.1	2.3	1.3	0.9	0.6	0.0
0	5.9	3.6	2.1	1.3	0.8	0.6	0.0
+2	3.9	2.3	1.3	0.9	0.6	0.5	0.0
+4	1.0	0.7	0.6	0.5	0.5	0.0	0.0
+6	3.2	1.5	0.9	0.5	0.5	0.0	0.0
+8	4.8	2.8	1.5	0.8	0.5	0.0	0.0
+10	5.6	3.3	1.9	1.0	0.6	0.0	0.0
+12	4.4	2.8	1.7	1.0	0.6	0.0	0.0
+14	2.9	1.6	1.2	0.7	0.5	0.0	0.0
+16	1.8	0.6	0.6	0.5	0.5	0.0	0.0
+18	3.0	1.1	0.5	0.5	0.5	0.0	0.0
+20	3.3	1.4	0.6	0.5	0.5	0.0	0.0
+22	2.5	1.3	0.8	0.5	0.5	0.0	0.0
+24	1.8	1.2	0.8	0.6	0.5	0.0	0.0

Table C.8(c) Electric Field Strength (Volts/m):
27.3 MHz, Z-component

Z \ X	+2	+4	+6	+8	+10	+12	+14
-24	8.0	4.1	1.3	0.4	1.1	1.4	1.6
-22	12.7	4.1	0.7	1.1	1.7	2.1	2.2
-20	10.0	1.5	1.6	2.5	2.9	3.0	2.9
-18	7.6	5.6	4.8	4.1	4.1	3.9	3.6
-16	18.8	13.2	8.8	6.2	4.7	4.1	4.1
-14	28.3	14.7	11.5	7.6	5.5	4.4	4.1
-12	29.3	15.2	11.6	7.8	5.7	4.6	4.1
-10	21.7	14.7	9.6	6.7	5.1	4.3	4.1
-8	12.1	8.0	5.7	4.6	4.1	4.1	4.1
-6	4.1	1.3	1.9	3.0	3.6	4.0	4.1
-4	14.7	5.7	1.6	1.6	2.8	3.5	3.9
-2	19.6	9.6	3.8	1.8	2.7	3.4	3.8
0	19.1	9.3	3.9	2.3	3.0	3.7	4.0
+2	14.3	5.8	3.3	3.3	3.8	4.1	4.1
+4	8.0	5.3	4.7	4.3	4.2	4.1	4.1
+6	15.4	12.1	8.7	6.8	5.5	4.8	4.5
+8	27.8	15.4	12.3	8.6	6.6	5.4	4.8
+10	35.4	19.5	14.1	9.6	7.1	5.6	4.8
+12	35.2	19.0	13.7	9.2	6.8	5.3	4.6
+14	26.7	14.7	11.1	7.6	5.6	4.5	4.1
+16	18.1	10.4	6.9	4.9	4.1	4.1	3.9
+18	10.7	4.2	3.1	2.9	3.0	3.0	3.0
+20	17.2	6.7	2.2	1.0	1.5	1.9	2.1
+22	14.7	7.4	3.3	0.9	0.6	1.1	1.3
+24	9.4	5.3	3.1	1.2	0.4	0.5	0.8